

**Tenth United Nations/European Space Agency Workshop  
On Basic Space Science**

**Exploring the Universe – Sky Surveys, Space Exploration and  
Space Technologies**

**Hosted by the University of Mauritius, 25-29 June 2001  
Reduit, Mauritius.**

Papers submitted by the MRT team to the Astrophysics and Space Science  
Special issue on the workshop



# The Pulsar Observing System and Data Analysis Procedure Used at MRT

Nalini H.Issur <sup>1</sup> and Avinash A. Deshpande <sup>2</sup>

1- Faculty of Science, University of Mauritius, Reduit, Mauritius

2- Raman Research Institute, Sadashivanagar, Bangalore 560080, India

## ABSTRACT

The Mauritius Radio Telescope (MRT) was designed to operate mainly as an imaging instrument to carry out a southern sky survey at 150 MHz. However, it has also been successfully used for pulsar observations. In this paper, we give an overview of the pulsar observing system we developed for use at MRT. Our pulsar receiver is of the 'direct-recording' type whereby most of the data processing, including dedispersion is done completely offline. The various steps involved in this data processing are also briefly described.

## 1. Introduction

The radio-emission from pulsars is characterised by its pulsed nature with extremely stable periodicity. The pulse itself is generally confined to a narrow interval compared to the pulsar period. Each pulsar has its own characteristic period and pulse shape. 'Normal' and 'millisecond' pulsars have periods of the order of the second and a few seconds respectively. The pulse shape and intensities evolve with radio frequency making it important to observe at various frequencies to try to understand these objects. Southern Pulsars have however not been well studied at low frequencies.

The Mauritius Radio Telescope (MRT) (Golap et al., 1998), is a T-shaped array of helices, located in Mauritius ( $lat = -20.5^{\circ}$ ). It is essentially an imaging instrument, designed to carry out a southern sky survey. We developed a set-up suitable for pulsar observation with MRT, in an attempt to further exploit this existing facility. The new set-up would also be useful for other studies requiring a single-beam mode of observations. Our aim was to demonstrate the capability of the MRT set-up for reasonably sensitive pulsar observations and study the observational properties of some Southern Hemisphere pulsars at our low observing frequency.

## 2. New Set-Up for Pulsar Observations

For pulsar observations, we need to be able to study the time-structure in a periodic signal which is not only weak (typically 10 mJy at 400 MHz) but has also undergone distortions due to propagations through the interstellar medium (ISM). While observing pulsar signals at a frequency

$f_0$ , over a finite bandwidth  $\Delta f$ , the dispersive ionized ISM in fact causes a smearing over a time  $t_{smear}$  given by ( Huguenin )

$$t_{smear}[\text{secs}] = 8.29 \times 10^3 DM (\Delta f / f_0^3) \quad (1)$$

where the dispersion measure DM is the column density of electrons along the line of sight, expressed in  $pc.cm^{-3}$  and frequencies are in MHz. As can be seen, the effect is more severe for high DM pulsars and when large bandwidths are employed, specially at low radio frequencies.

Dispersion smearing can be reduced by using a small bandwidth or dividing the total observing bandwidth into a number of narrow frequency channels. The intensity outputs from the various channels are added after incorporating suitable delays as given by eq 1. This process is known as *incoherent dedispersion* (Huguenin; Hankins *et al.*, 1975).

We deduce that the maximum bandwidth  $\Delta f$  (MHz) that can be employed to obtain a time resolution  $t_{res}$  (secs) is given by

$$\begin{aligned} \Delta f[\text{MHz}] &= 1.205 \times 10^{-4} t_{res} (f_0^3 / DM) \\ &= 1.205 \times 10^{-4} (t_{res} / P) (P / DM) f_0^3 \end{aligned} \quad (2)$$

where  $t_{res} / P$  corresponds to the fractional time-resolution.

For short period pulsars of large DM, the demands for high resolution profiles introduce another limitation. We need to use smaller  $\Delta f$ , but then the time interval ( $1/\Delta f$ ) between independent samples increases. This puts a limit to the time-resolution that can be achieved. In incoherent dedispersion, the optimum time-resolution is therefore obtained when  $t_{smear} = 1/\Delta f$  (Deshpande, 1989). Using Eq. 1, this corresponds to

$$t_{res}[\text{sec}] = 9.1 \times 10^{-2} DM^{1/2} f_0^{-3/2} \quad (3)$$

with an optimum choice for the bandwidth given by

$$\Delta f_{opt}[\text{KHz}] = 10^{-2} \times f_0^{3/2} \times DM^{-1/2} \quad (4)$$

where DM is in  $pc.cm^{-3}$  and  $f_0$  in MHz.

In practice therefore, for pulsar observations there is an obvious need for a pulsar receiver with dedispersing capability. Some tracking capability is also required, at least to allow the integration of the weak signals over a certain time interval.

Our set-up for pulsar observations was successfully tested and installed in July 1996. It includes

- A tracking system, allowing observation of a source over a span of 2 degrees around its meridian transit i.e.  $8sec(\delta)$  mins of time.
- A 'Portable Pulsar Receiver (PPR)'

- a GPS receiver linked to the observatory clock and the above units.
- a Pulsar Processor (PP) from the ATNF was also temporarily available.

### The Tracking System

For pulsar observations only the East-West (EW) array is used. This has 1024 helices which are divided in 32 groups of 32 helices each. The helices respond to Right Circular Polarisation and have a HPBW of  $\approx 60^\circ$ . They are tilted such that the maximum response is towards  $\delta = -40.5^\circ$ . In this direction, the effective collecting area is  $\approx 4096 \text{ m}^2$ .

The tracking system consists of 32 phase-shifters with 4 phase-shifter sections each. They are connected in the lab in the 1st IF path of the 32 EW groups. With a beam flipping time of about 3 secs for  $\delta = 0$ , the pointing accuracy lies within the 90% gain points of the combined EW beam. ( 1 EW group beam  $\approx 2^\circ$ , while the combined EW beam  $\approx 4'$ ). The whole tracking system is controlled from a PC, through 32 phase-shifter drivers. Each driver also has 4 pairs of LEDs to indicate the status of the phase-shifters during tracking.

### The Portable Pulsar Receiver

The portable pulsar receiver (PPR) is a 'direct recording' device, incorporating a Fast Data Acquisition System. Signal voltages are sampled at Nyquist rate ( $\approx 2.1 \text{ MHz}$ ). These are quantised with 2 bits/sample. The data is recorded on a HD after bit-packing.

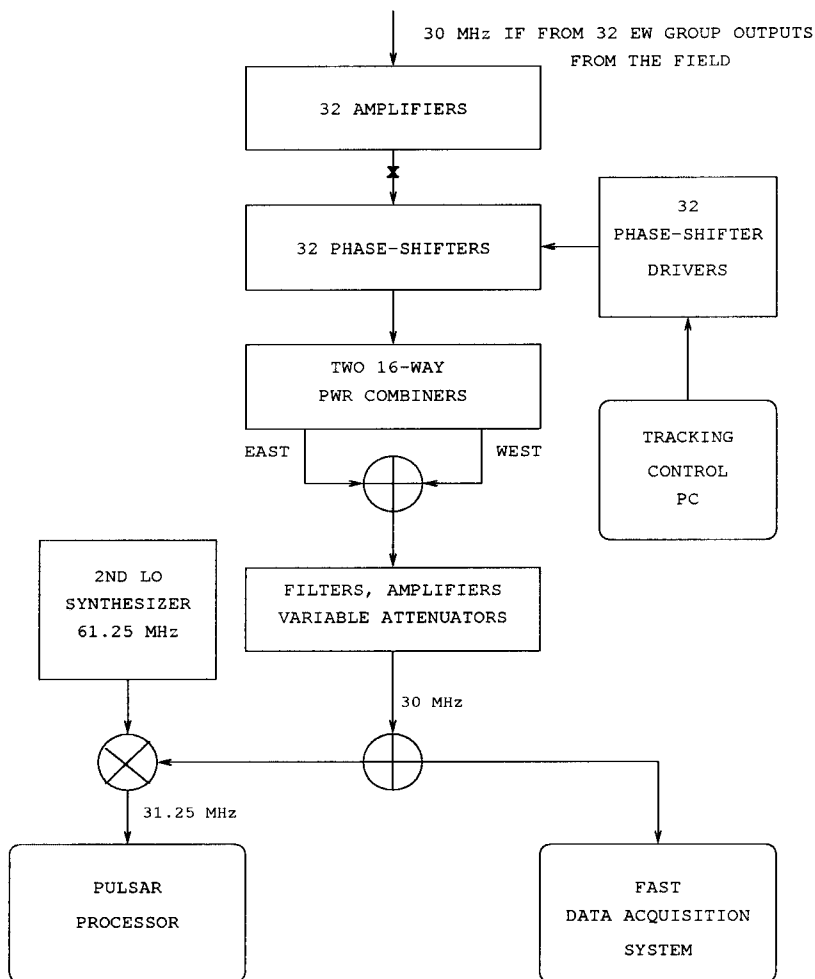
The system has the advantage of being relatively simple and leaves a lot of flexibility in the data processing. The post-processing, including dedispersion is done completely offline and can therefore be optimized for each case.

### Sensitivity

The minimum detectable average flux density  $S_{av,min}$  corresponding to optimum smoothing (i.e. of the order of the pulse width  $W$ ) and folding the data obtained in a total time  $\tau$ , over the pulse period  $P$  can be expressed as below ( Vivekanand *et al.*, 1982 )

$$S_{av,min} = \frac{\beta(2kT_{sys}/A_e)}{\sqrt{\Delta f_T \tau}} \times \sqrt{W/(P - W)} \text{ where}$$

$\beta$  is the desired signal-to-noise ratio,  $k$  is the Boltzmann constant,  $T_{sys}$  is the system temperature,  $A_e$  is the effective collecting area and  $\sqrt{\Delta f_T}$  is the total observing bandwidth used.



SIGNAL PATH FOR PULSAR OBSERVATIONS AT MRT

Fig. 1.— The signal path inside the receiver room - the part before the point marked 'x' is common with that used for the imaging observations.

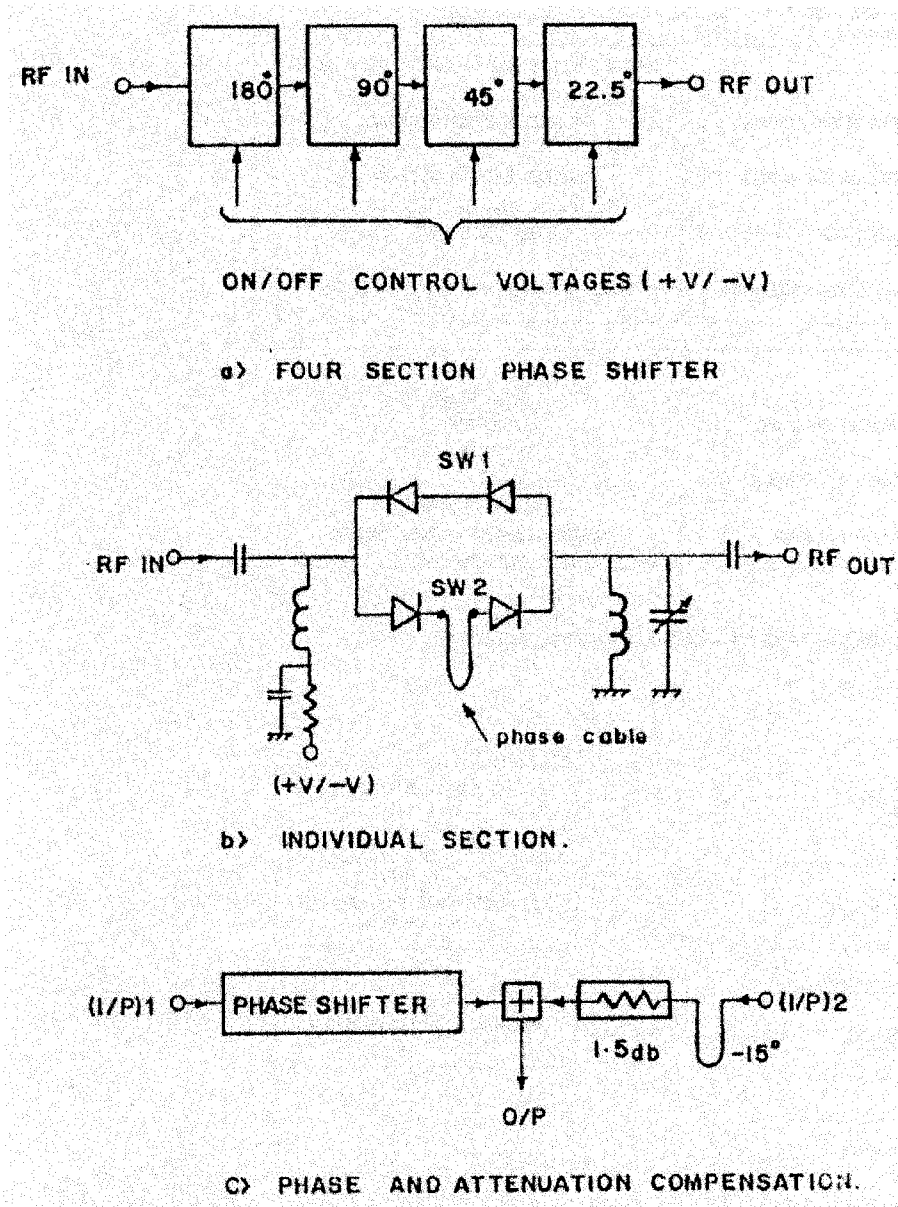


Fig. 2.— The phase-shifter module

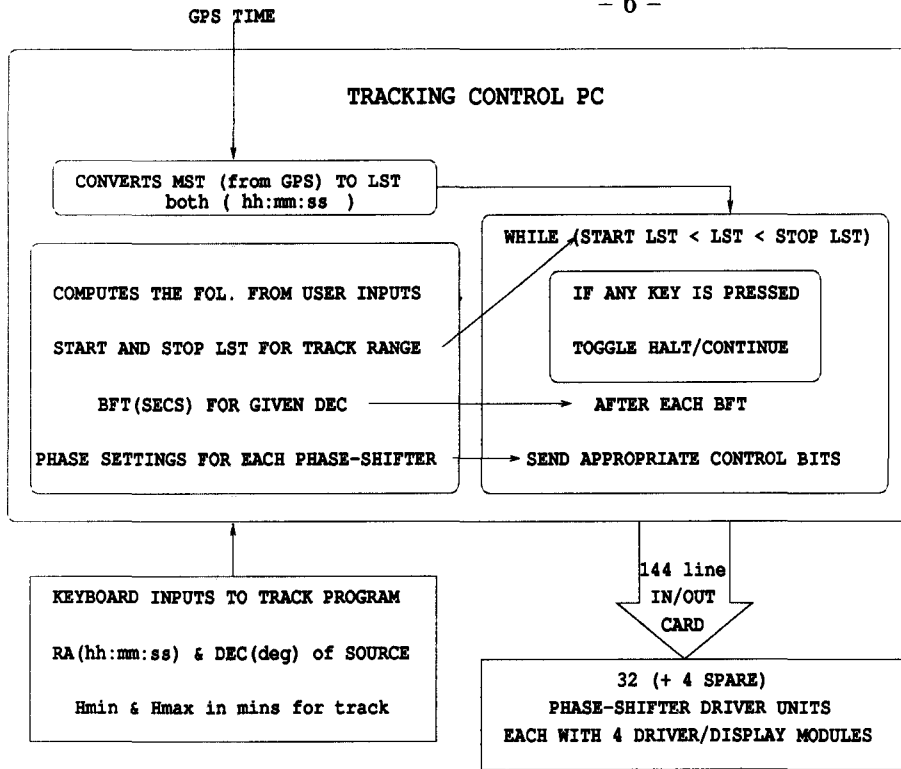
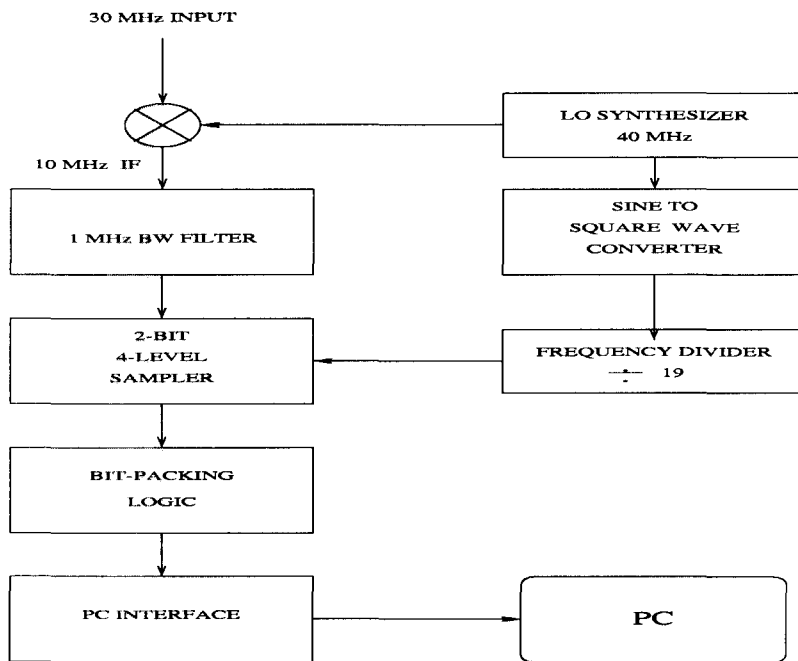


Fig. 3.— chart illustrating the PC based control system



SIGNAL FLOW IN THE FAST DATA ACQUISITION SYSTEM

Fig. 4.— Block diagram of the Portable Pulsar Receiver used at MRT.

With the pulsar observing system described in the previous section, we can expect therefore to detect a typical pulsar having an average flux density of about 100 mJy, with a signal-to-noise ratio of  $\approx 25$ . This is for a pulsar with a 5% duty cycle at the centre of our primary beam ( $\delta = -40.5^\circ$ ), when a total predetection bandwidth of 1 MHz is used and the average system temperature is about 600 K. About 30 pulsars fall within the expected sensitivity range and could be selected for observations. Sources are generally tracked within the HPBW of an East-West group ( $2^\circ$ ).

### 3. Data Processing

We have used an incoherent dedispersion scheme so far to process the PPR data. The main steps involved in producing the dedispersed output are as follows:

1. *Producing spectrometer data.* Successive stretches of data with  $2N$  samples each are Fourier transformed to get the equivalent outputs of  $N$  frequency channels.  $N$  is chosen such that the time-resolution is near optimum for the DM of the pulsar. With  $\Delta f_{opt} \propto DM^{-1/2}$ , for the lowest DM of  $2.65 \text{ pc.cm}^{-3}$ , we use  $N = 64$ , and achieve a time-resolution of  $60.8 \mu\text{s}$ .
2. *Determination of gain variations and interference detection.* The spectrometer outputs are analysed to look for gain variations which occur during tracking, interference spikes in time as well as narrow-band interference across frequency channels.
3. *Dedispersion and removal of spurious periodicities.* Corrections for the gain variations are applied at this stage and bad spectral channels as well as interference time-sections are discarded. This makes use of the information recorded in step 2. The corrected outputs are added together after suitable time-shifting to take into account the delay due to dispersion as given by eq. 1.

The  $DM = 0$  fluctuation spectrum is also produced to look for spurious periodicities in the data, such as the 100 Hz produced by the a.c. mains. Such periodicities as well as their harmonics can then be removed from the dedispersed output.

The dedispersed time-series can then be resampled and 'folded' over the apparent pulsar period (P) to produce an average profile. This is used to study the general pulse morphology, estimate the pulse width and scatter broadening when possible, and also to determine flux densities. The flux calibration is based on an estimate of the system temperature, which includes a contribution of 300 K from the receiver noise. We assume that the collecting area is equal to its theoretical value - this may be in error by  $\approx 20\%$ . The effective sky background temperature at our observing frequency is estimated by extrapolating from the 408 MHz values of Haslam et al. (1982), using a spectral index of -2.5 and taking into account the response of our tracking beam towards the source of interest.

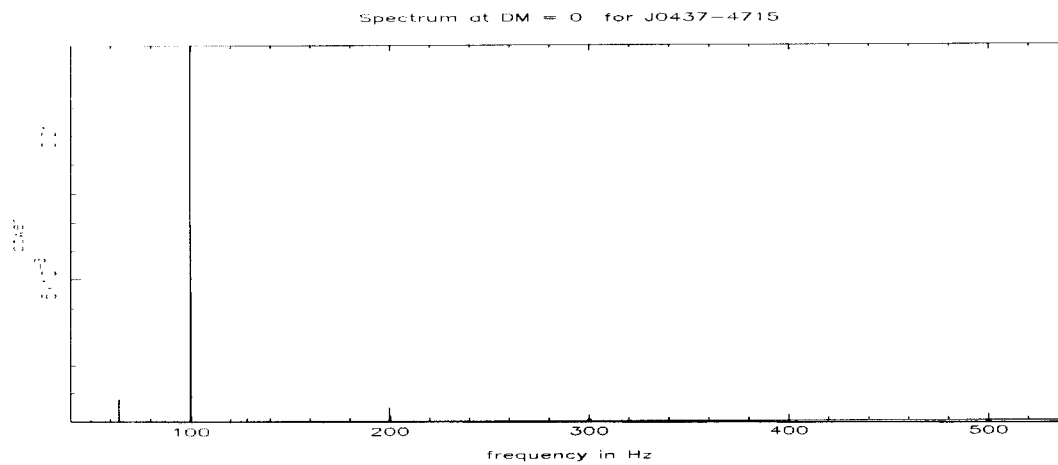


Fig. 5.— A fluctuation spectrum showing spurious periodicities.

The plot shows a typical fluctuation spectrum from a  $DM = 0$  time-series. The feature near 100 Hz is by far the most prominent and due to the 50 Hz AC mains. A few (much weaker) harmonics of the 100 Hz feature are also apparent. The other weaker spurious feature seen is around 64.5 Hz.

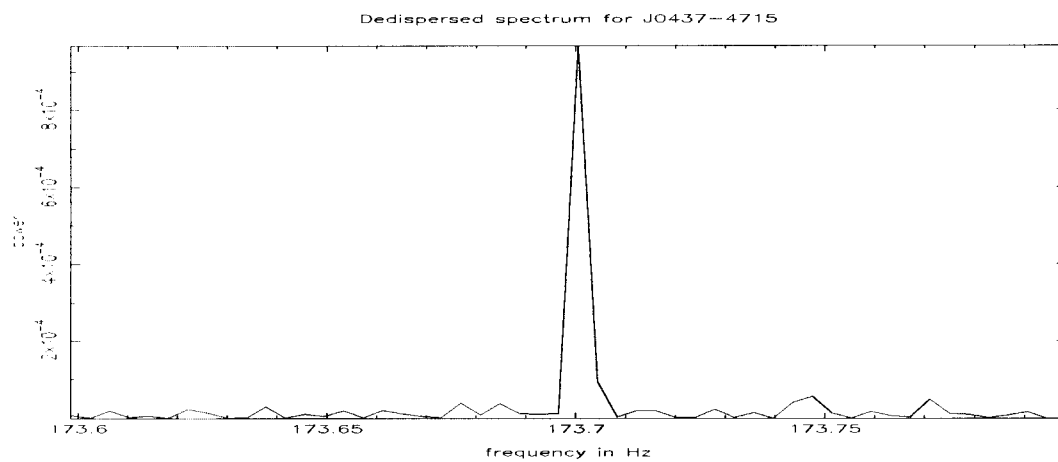


Fig. 6.— Dedispersed fluctuation spectrum of a time-series showing a pulsar signal.

The pulsar frequency corresponds here to that of the millisecond pulsar J0437-4715 and is near 173.69 Hz.

The dedispersed time-series can also be used to extract a train of single pulses for single-pulse analysis. This provides a powerful tool for probing into the details of the radio-emission process. The single-pulse analysis we use here makes use of the SPULSES package of Deshpande (1998). Several functions are available for different types of analysis.

The data processing described above has led to the detection of ten pulsars, including a millisecond pulsar. Some of the results based on the various types of analysis mentioned here will be discussed in another paper in the same issue.

### Acknowledgements

MRT is an Indo-Mauritian facility operated by the University of Mauritius and the Raman Research Institute, India. The design and fabrication of both the tracking system and the PPR were done at RRI.

### REFERENCES

- Golap K., Udaya Shankar N., Sachdev S., Dodson R., Sastry Ch. V., 1998. “A Low Frequency Radio Telescope at Mauritius for a Southern Sky Survey” *J. Astrophys. Astr.*, **19**, 35.
- Huguenin G.R., Methods in Experimental Physics, volume 12,-Part C.
- Hankins, T.H., Rickett, B. J., in Experimental Physics, volume 14, Chapter Pulsar Signal Processing. 1975.
- Deshpande A.A., Technical report, Raman Research Institute, 1989.
- Vivekanand, M., Narayan, R., Radhakrishnan, V., 1982. *J. Astrophys. Astr.*, **3**, 237.

# Low Frequency Observations of Pulsars at MRT - Results on a few 'normal' pulsars and a 'millisecond' pulsar

Nalini H.Issur

Faculty of Science, University of Mauritius, Reduit, Mauritius

## ABSTRACT

The MRT pulsar observing system set-up in July 1996 has been used to observe about 30 pulsars at our low observing frequency of 150 MHz. From the data considered so far, we have detected 10 pulsars, including the bright millisecond pulsar (MSP) J0437-4715. This is the only MSP observable at such a low frequency making its study specially interesting and more so that it has some apparently unusual properties. In this paper, we discuss some of our main results obtained on the MSP J0437-4715 and on the 'core-single' normal pulsars J1453-6413 and J1752-2806. Our results are also compared with those obtained at other frequencies.

## 1. Introduction

The MRT pulsar observing system (Issur 2000, 2001) set-up in July 1996 has been used to observe about 30 pulsars at our low observing frequency of 150 MHz. From the data considered so far, we have detected 10 pulsars, including the bright millisecond pulsar (MSP) J0437-4715 which we could sometimes see very clearly. This allowed us to undertake a fairly detailed study. The 'core-single' pulsars J1453-6413 and J1752-2806 could always be seen clearly at MRT. We undertook a fairly detailed study of these two pulsars as well, comparing our data with those obtained at other frequencies. The other pulsars we have detected are J0630-2834, J0738-4042 (a relatively high DM pulsar with  $DM = 160.8 \text{ pc.cm}^{-3}$ ), J0953+0755 (a northern pulsar), J1057-5226, J1456-6843, J1751-4657 and J1900-2600. The signal-to-noise ratios we obtain for these do not however allow a very detailed study. In the following sections we discuss some of the main results obtained on the MSP J0437-4715 and on the 'core-single' normal pulsars J1453-6413 and J1752-2806, all three of which were observed quite frequently from July to December 1996.

## 2. The millisecond pulsar J0437-4715

Because of its very low dispersion measure ( $DM = 2.65 \text{ pc.cm}^{-3}$ ), J0437-4715 is the only millisecond pulsar ( $P = 5.75 \text{ ms}$ ) which can be observed at very low frequencies. Dispersion and scatter broadening makes all others difficult to observe at frequencies below about 200 MHz. Since MSPs and normal pulsars are thought to form distinct classes of objects, a study of this bright and

nearby MSP is specially interesting as it provides a unique opportunity to investigate the properties of a millisecond pulsar over a very wide frequency range.

Fig 1 shows an observation of J0437-4715 at MRT when the pulsar is bright. In fact, we found the observed intensity of the pulsar to vary by a factor of about 20, similar to that noted at 327 MHz (Ables et al. 1997). This is likely to be due to diffractive scintillations over time-scales somewhat larger than the duration of each observation (8-12 mins). Our results, based on the average profiles from our best observations, are summarised in table 1. We obtain a very broad pulse profile, with significant emission over  $\approx 200^\circ$  of longitude. The profile is dominated by 2 peaks of comparable strength, at longitudes  $\approx -55^\circ$  and  $0^\circ$  ('core' component) respectively. The core width is estimated to be around  $35^\circ$ . Visual impressions indicate the presence of 1 or 2 more outer features. The peak flux density is found to be  $\approx 2.5$  Jy while the 'average' flux density is  $\approx 600$  mJy (upper limit). We note that the spectral index of this pulsar is  $-1.5$  at intermediate frequencies with perhaps a steepening at higher frequencies. Our flux estimate indicates either a turn-over or flattening in the spectrum at low frequencies.

#### Profile evolution with frequency

An alignment of the 150 MHz profile with some higher frequency ones, with respect to the 'core' component shows that it fits into the general trend observed at higher frequencies (fig 2). The amplitude ratio between the outer (conal) components and the core component increase from less than 0.1 at 2320 MHz to about 0.9 (component at  $-55^\circ$ ) at 150 MHz. The outer components on BOTH sides of the main peak are seen to shift to earlier longitudes towards lower frequencies. The resulting separation of 'conal' components and total extent of the pulse appear however essentially constant. Navarro et al. (1997) had noted a frequency dependent lag of the total intensity profile with respect to the polarisation profile - perhaps indicating a frequency dependent beam direction. The 'shifts' we find are compatible with their observations, indicating a 'lag' of  $\approx 20^\circ$  at 150 MHz. Such a frequency dependent beam direction, with the main part of the central beam missed at lower frequencies, is perhaps the cause for a possible turn-over in the spectrum at low frequencies and the observed 'unusual' spectral differences between the core and 'conal' components.

Peak flux density (highest peak)	$2.5 \pm 1.0$ Jy
Average flux density	$600 \pm 100$ mJy
Separation of main peaks	$55 \pm 5^\circ$
Rel.intensity of left peak w.r.to 'highest' peak	0.7 to $\approx 1$
Pulse width at outer half-power points	$120 \pm 10^\circ$
Pulse width at outer one-tenth points	$170 \pm 10^\circ$
Estimated half-width of main ('core') component	$\approx 35^\circ$

Table 1: Average properties of J0437-4715 at 150 MHz.

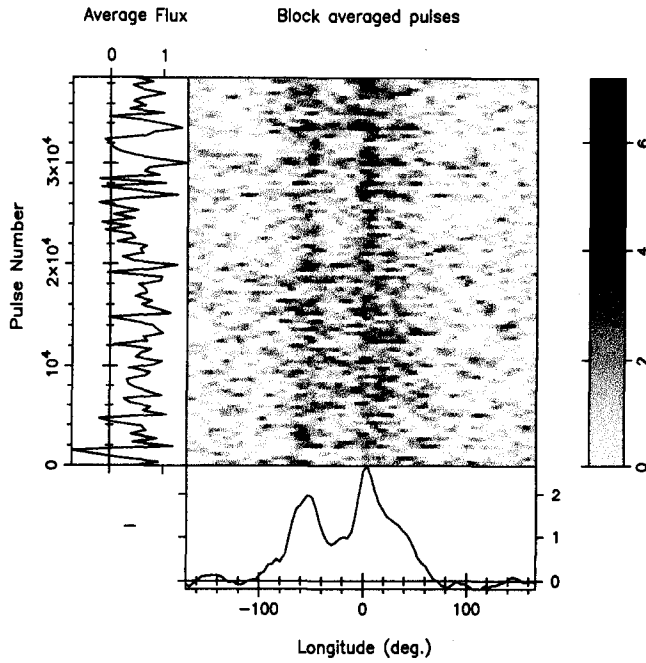


Fig. 1.— Observation of J0437-4715 when the pulsar is bright  
Grey scale shows 39000 pulses (averaged over 390 pulses). 95 bins are used across one period and smoothed over a 3-bin window.

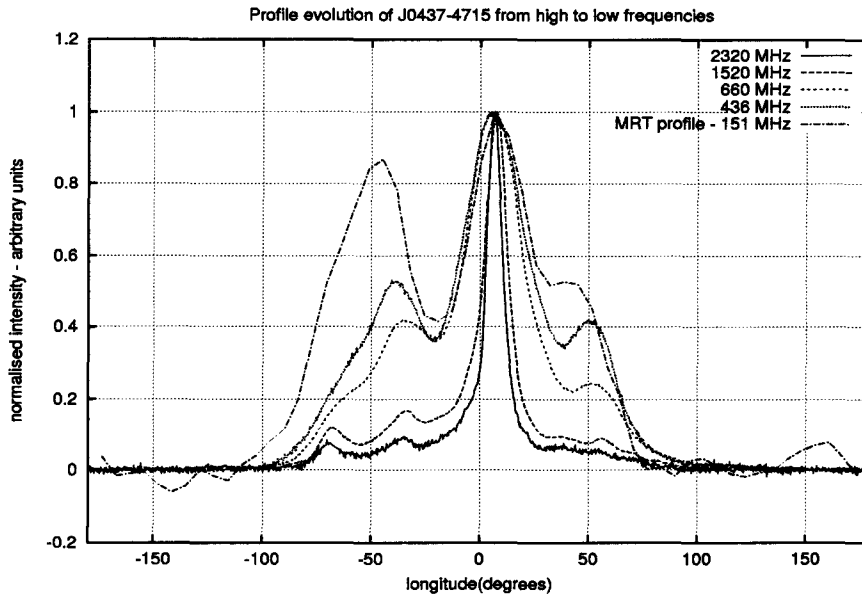


Fig. 2.— Profile evolution of J0437-4715 from high to low frequencies.  
The high frequency profiles are taken from the EPN data base (Bell et al. 1997). The highest peaks have been normalised to one and aligned. The outer components on both sides of the main peak become relatively stronger at lower frequencies and are seen to shift to earlier longitudes.

### Correlation analysis and pulse components

The complex shape of the J0437-4715 profile has been noted by several authors. Gil and Krawzyck's (1997) find 7 components in the profile, but up to 12 components have been quoted. It is therefore particularly interesting to try to identify *physical components* in the profile, using a correlation technique on single-pulse sequences. Using the LCORR function of the SPULSES software (Deshpande, 1998), we compute the longitude-longitude correlation in the fluctuations at zero period delay on a good set of 39,000 pulses, using subfolds with progressively longer integration. With 500 subfolds, the correlation map begins to suggest  $\approx 7$  features of slightly enhanced correlation (more than  $3\sigma$ ) around the noise diagonal (fig 3, left).

We attempted a similar analysis on 327 MHz data made available to us from the Ooty radiotelescope as this data has better signal-to-noise on single pulses. The correlation map in figure 3 (right) reveals 7 well defined components, compatible with Gil and Krawzyck's (1997) model. In addition we find a weak but significant correlation between the 'core' beam and one side of the 'conal' beam (around long.  $\approx -100^\circ$ ). Overall, the correlation shows a rather complex variation with pulse period delay across the longitude range. We find time-scales of the order of 10-20 P (associated mostly with the central component) and 4 P (associated mostly with the left conal region between  $\approx -40^\circ$  to  $\approx -80^\circ$ ).

### 3. PSRs J1453-6413 and J1752-2806

Both these pulsars happen to be of the 'core-single' type, following Rankin's (1983a) classification scheme. While J1752-2806 ( $P = 0.563$  s,  $DM = 50.9$  pc.cm $^{-3}$ ) has been well studied at various frequencies, J1453-6413 ( $P = 0.179$  s,  $DM = 71.1$  pc.cm $^{-3}$ ) has not been well studied earlier because of its very southern declination.

For J1453-6413, we obtain an average flux density of  $\approx 300$  mJy with an upper limit less than 500 mJy. This may indicate a turn-over from the spectral index of  $-1.9$  applicable at higher frequencies, but should be treated as rather tentative given the short time-span of our observations compared to the expected refractive scintillation time-scale of the pulsar. For J1752-2806, we obtain an average flux density of  $\approx 600$  mJy. The calibration error may here be up to  $\approx 30$  %, given that the sight-line is towards the galactic centre region where the sky brightness temperature increases sharply. Our flux density is significantly smaller than the values of Slee et al. (1986) at 160 MHz, and likely to be due to long term variations caused by refractive scintillations. In any case, there is a clear turn-over from the spectral index of  $-2.6$  applicable at higher frequencies.

### Spectral evolution of pulse width

We investigated the evolution of pulse width with frequency for both these pulsars, using data available at all frequencies, including our data. The profiles in both cases had earlier been shown to exhibit a narrowing in the intermediate frequency range, appearing to regain their broader widths by 150 MHz (Rankin 1983b). When we take into account more recent and better quality data, we find that the trend observed earlier may not hold true.

In the case of J1453-6413, we obtain a pulse half-width of about 7.0 deg on the average, while an earlier value quoted at 170 MHz was 9.0 deg (McCulloch 1982). Comparing our measurements at 150 MHz with recent measurements at other frequencies, we find that the pulse-width remains practically constant below 1 GHz, up to at least 150 MHz, in spite of the relatively high DM of the pulsar (fig 4).

In the case of J1752-2806, we find that the width does NOT regain its 'extrapolated' width by 150 MHz (fig 5). We obtain a pulse half-width of about 6.5 deg on the average, while an earlier value quoted at 170 MHz (McCulloch 1982) was 8.2 deg. The trends we note in the spectral evolution of pulse widths for these two 'core-single' pulsars may be of significance, specially with respect to the mechanism associated with the emission of a core beam.

### Correlation analysis and pulse components

We have used our best observations to try to investigate the behaviour of these two pulsars on a single-pulse basis. In particular, the correlation analysis we attempted (using the same procedure as mentioned for J0437-4715) to try to identify 'physical components' in the profiles yielded interesting results.

In the case of J1752-2806, the correlation map at zero period delay (fig 6, right) surprisingly reveals quite clearly two components in the profile. The fluctuation spectrum is featureless as would be expected for 'core-single' pulsars. However, the variation of amplitude for the pulsar harmonics in the 'raw fluctuation spectrum' also indicates the presence of two components. Both analyses indicate a separation of about 7 to 8 degrees in longitude between the two presumably 'core' components.

In the case of J1453-6413, the single-pulse correlation analysis usually showed one dominant component as would be expected for a 'core-single' pulsar. However, here too we found a slight suggestion for two close components within the pulse, in some observations, after using the data in subfolds (fig 6, left). We note that the measured pulse widths of this pulsar appear to show slight variations between different observations, beyond the expected accuracy of each measurement. This may be due to some kind of modal behaviour with variations in the relative intensities of the two 'core' components.

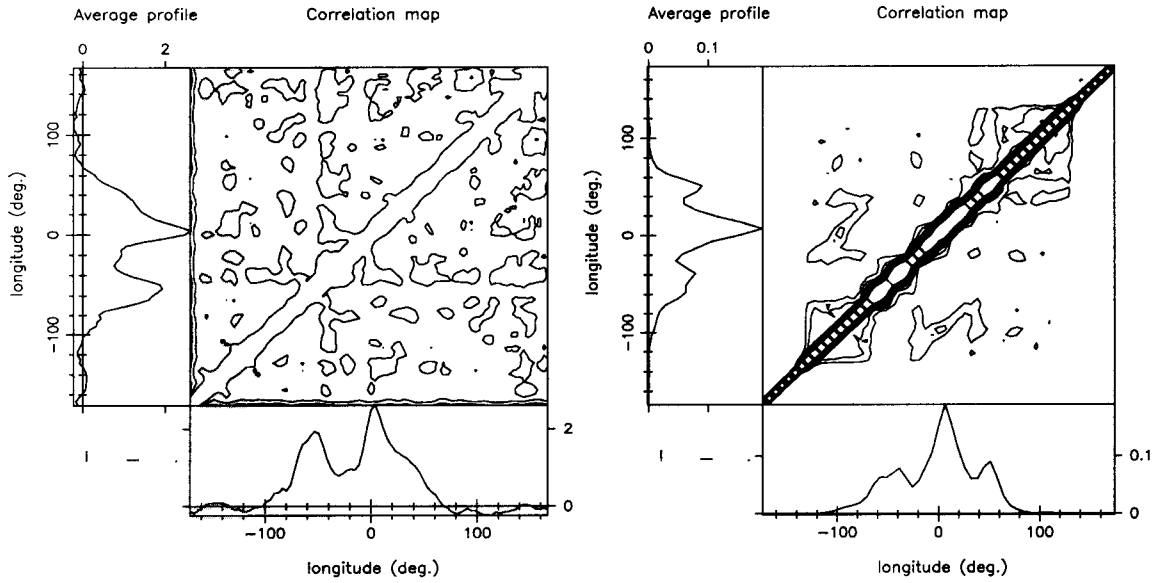


Fig. 3.— Correlation maps for J0437-4715 .

Left: Using 39000 pulses from MRT 150 MHz data in a sequence of 500 subfolds. Right: Using a sequence of 6040 single pulses from Ooty 327 MHz data. The correlations in the fluctuations are performed at zero period delay.

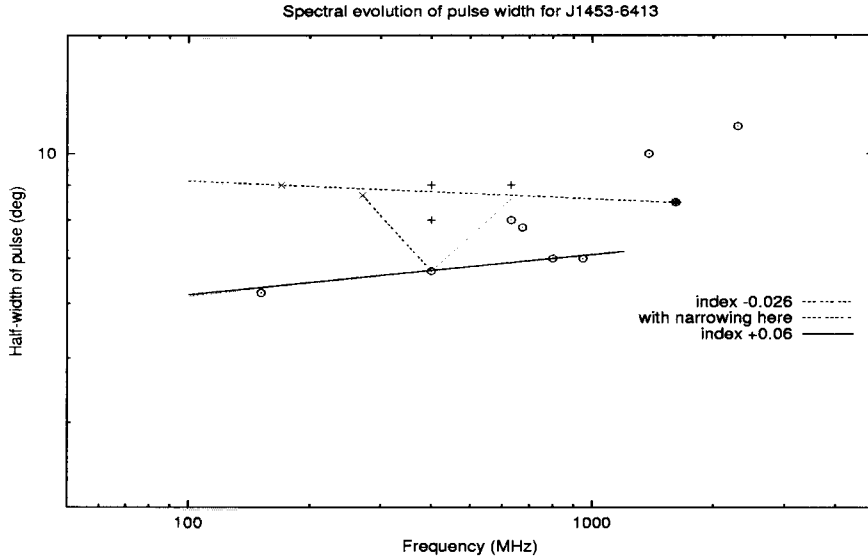


Fig. 4.— Spectral evolution of the 3 dB pulse-width for J1453-6413

Symbols: '+' & 'x' correspond to values quoted in the literature & taken from Rankin (1983b) respectively. 'o' are new estimates from original profiles. The dotted lines correspond to the fit previously found by Rankin, with a narrowing region. The solid line shows another possible fit with a positive index.

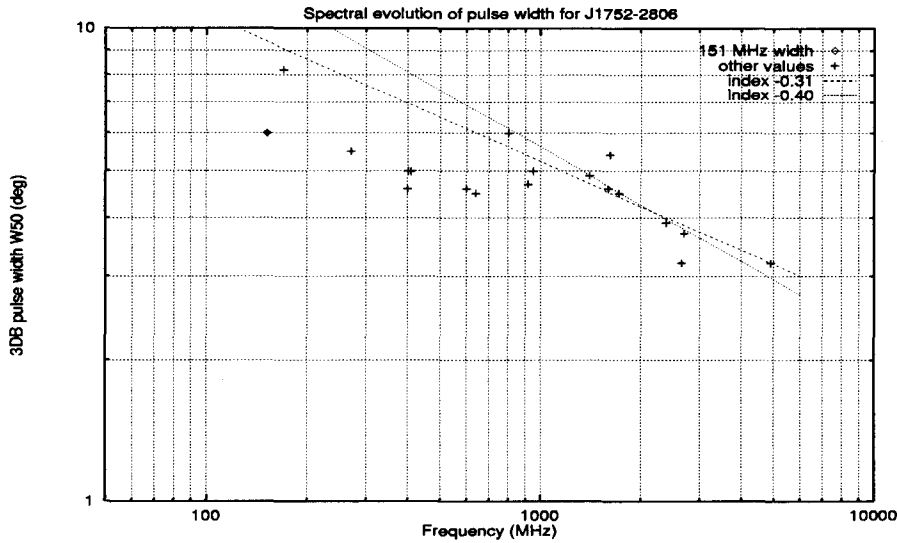


Fig. 5.— Spectral evolution of the 3 dB pulse-width for J1752-2806. The 151 MHz width we obtain is marked with a 'o'. The dashed line corresponds to a power law index of -0.31 as found by Rankin. Presently available data seem to indicate an even steeper power law (index of -0.4) for the high frequency behaviour. The low frequency widths remain well below the extrapolated lines.

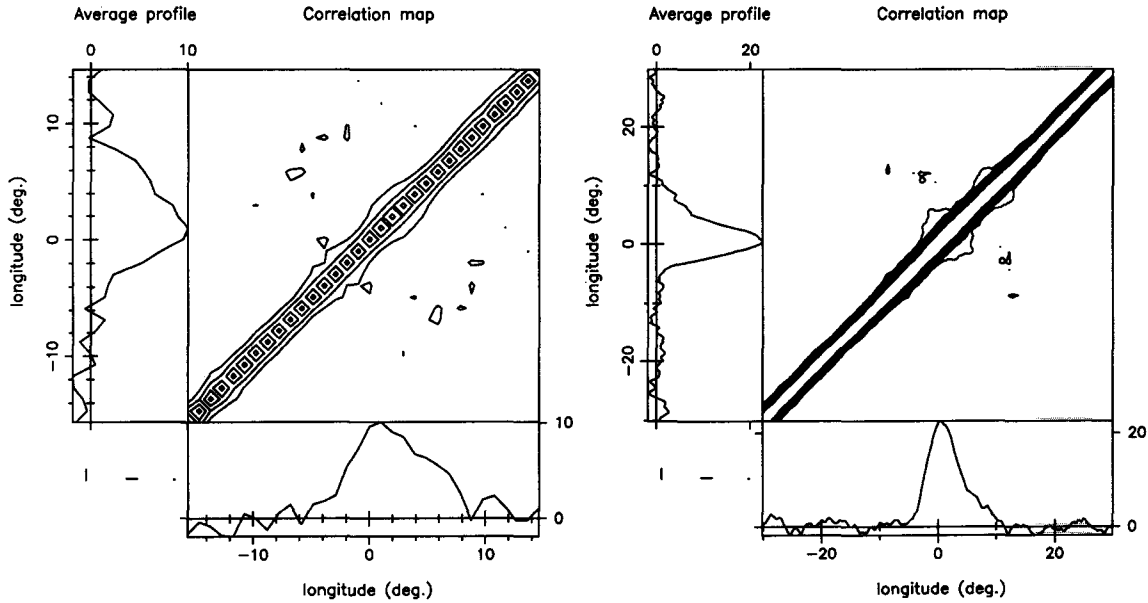


Fig. 6.— Correlation maps for J1453-6413 and PSR J1752-2806  
Left: Using a set of 2048 pulses in 256 subfolds for J1453-6413. Right: Using a set of 800 single pulses for J1752-2806. In both cases the correlation is performed at zero-period delay.

To summarise, our single-pulse analysis have revealed the somewhat unexpected presence of structure within the ‘core’ beam while these are not obvious as seen in the average profiles.

## REFERENCES

- Ables J.G., McConnell D., Deshpande A.A., and Vivekanand M. *ApJ. Lett.*, 475, L33, 1997.
- Bell J.F., Bailes M., Manchester R.N., Lyne A.G., Camilo F., and Sandhu J.S. *MNRAS*, 286: 463, 1997.
- Deshpande A. A. *SPULSES Manual*, 1998.
- Gil J. and Krawczyk A. *MNRAS*, 285: 561–566, 1997.
- Issur N.H. *PhD Thesis, Univ. of Mauritius*, 2000.
- Issur N.H. The Pulsar Observing System and Data Analysis Procedure Used at MRT. *Ap & SS*, this Vol, 2001a.
- McCulloch P.M., Hamilton P.A., and Manchester R.N. (MHMb). *Unpublished*, 1982.
- Navarro J., Manchester R.N., Sandhu J.S., Kulkarni S.R., and Bailes M. *ApJ*, 486: 1019–1025, 1997.
- Rankin J.M. *ApJ*, 274: 333–359, 1983a.
- Rankin J.M. *ApJ*, 274: 359–368, 1983b.
- Slee O.B, Alurkar S.K, and Bobra A.D. *Australian Journal of Physics*, 39: 103–14, 1986.

# **A New Tracking System for the MRT**

U. Chummun and G. K. Beeharry

Department of Physics, University of Mauritius, Reduit, Mauritius

## **1. Abstract**

A new tracking system is being designed at the Mauritius Radio Telescope(MRT). The current setup is that of a transit instrument and this limits the integration time-on-object to eight minutes. The sensitivity will be significantly improved as the integration time is increased to 60 minutes at zenith. The new setup will allow more sensitive observations of weak pulsars, transient phenomena like coronal mass ejections, radio recombination lines, interplanetary scintillation and VLBI.

## **2. Introduction**

Since the Mauritius Radio Telescope(MRT) has come into operation, continuum observation has been carried out mostly in the transit mode. Observing in transit mode implies that the telescope has an integration time of 16 seconds, which is too small for the detection of faint sources (Kraus 1980). In 1996 an electrical tracking system was set up (Issur, 1997). Some modifications were made on the existing setup of the MRT so as to be able to do both continuum and pulsar observation. This modified setup enabled the observation of pulsars for an eight-minute period (at local zenith). However, this time period is too short for the observation of weaker signals.

A pioneering survey of the radio sky in the southern hemisphere has been carried out from  $-10^{\circ}$  to  $70^{\circ}$  in declination at a frequency of 151.5 MHz. However, the first round of survey lacked the desired resolution; of the predicted number weak sources only few were detected (Golap 1998).

We are investigating the possibility of increasing the tracking period to one hour while observing in continuum mode or in pulsar mode. Our aim is to obtain a phased array facility so that we can improve the sensitivity of observations. Moreover, the study of transient phenomena, like bursts, is difficult with the present tracking time. Increasing the tracking time will increase the probability for the MRT to observe these phenomena. Furthermore, the time variability of sources can be studied if they are being tracked for a longer period of time. At present we are limited by the integration time.

## **3. Description of the MRT**

The Mauritius Radio Telescope (MRT), operating at 151.5 MHz, is essentially a meridian transit telescope (Golap 1998, Sachdev 1999). It consists of 1088 antennas in the form of a tee.

The basic element is a helical antenna having a gain of 11 dB and a bandwidth of 120 MHz (from 80 to 200 MHz). The East-West (EW) array consists of 1024 helices which are arranged in 32 groups of 32, while the North-South (NS) array consists of 64 antennas arranged in 16 groups of 4. The local coordinates are U, in East-West direction, and V in South direction.

The antennas in the NS arm are placed on movable trolleys. The different trolley positions are called allocations in the MRT jargon. On the existing rail the trolleys cannot approach the centre of the EW arm nearer than 11 m. This has been designed in order to avoid cross-talk between antennas. A 15 m North extension with 1 trolley which can approach the EW arm down to 2 m has been built and is used to measure the lowest spatial frequencies. The U-V coverage is completed in one year, because of the motion of the Sun.

Along the 2 km long EW arm, the land is rocky and uneven, with height differences of up to 35 m between some groups. In order to minimise the problem of non-coplanarity, each group of the EW arm is built on a horizontal wall which then ensures that at least each group is on one level. The height differences from group to group is less marked in the eastern arm than in the western arm.

With these dimensions for the EW and NS arms, in the pencil beam mode of the array, the resolution obtainable is  $4' \times 4.6' \sec(ZA)$  where ZA is the zenith angle. The point source sensitivity is expected to be about 200 mJy at  $3\sigma$  level.

### 3.1. The Helical Antenna

The primary element used at the MRT is a peripherally fed monofilar axial-mode helix of 3 turns with a diameter of 0.75 m and a height of 1.75 m. This is mounted above a stainless steel reflector mesh of grid size  $2'' \times 2''$ . The helix is wound using a 1.5 cm diameter round aluminium tubing supported with a central UV (UltraViolet) stabilised light weight PVC (PolyVinylChloride) cylinder and radial PVC rods. The axial mode provides maximum radiation along the helix axis. It responds to frequencies between 80 and 200 MHz with right circular polarisation (Kraus 1988). A quarter-wave transformer used in the feed network optimises the VSWR to 1.5 around 150 MHz. The helical antenna has a collecting area of about  $\lambda^2$  ( $4\text{m}^2$  at 150 MHz) with a half power beam width (HPBW) about  $60^\circ \times 60^\circ$ . The helices are mounted with a tilt of  $20^\circ$  toward the south to get a better coverage of the southern sky ( $-70^\circ$  to  $-10^\circ$  dec.), including the southernmost part of the galactic plane. The HPBW of the primary beam of each EW group is  $2^\circ \times 60^\circ$  and allows observation of a source for roughly  $8 \times \sec(\delta - 20^\circ)$  minutes of time, where  $\delta$  is the declination. In each group four helices are combined using hybrids and the output is pre-amplified by a low noise amplifier (MCL Chip). The eight amplifier outputs are further combined through a 8:1 power combiner to form a group output. This arrangement repeats in each EW group.

Table 1: MRT Specifications

Observation frequency	151.5 MHz
Basic Element	helical antenna
No. of helices	
East-West arm	1024
North-South arm	64
EW arm length	2088 m
NS arm length	880 m
Polarisation	Right Circular
HPBW of helix	60° × 60°
Collecting area of helix	4 m <sup>2</sup> at 150 MHz
Declination coverage	-10° to -70°
first IF	30 MHz
second IF	10.1 MHz
Instrumental bandwidths	0.15, 1, 1.5 MHz
Correlation receiver	32x16 complex channels
Collecting area per baseline	90 m <sup>2</sup>
Sensitivity per baseline	30 Jy (for 1s integration, 1 MHz bandwidth)
No. of baselines measured per day	32x16
Synthesised beam width	4' × 4.6' sec(ZA)
Expected Point source sensitivity	200 mJy (3σ)

### 3.2. The Field Setup

Figure 1 describes how the signal is collected in an EW group. This arrangement is different from the NS group. In the NS group, signal is collected using a set of four antennas. They are connected through a 4:1 power combiner and the output is the NS group output. The group output (for EW as well as NS) is heterodyned with a local oscillator (LO) signal of frequency 121.5 MHz. This gives a down converted intermediate frequency (IF) signal of 30 MHz. This IF signal is further amplified by 36 dB using a MHW590 Chip and is sent to the lab through a 1 km RG213U cable.

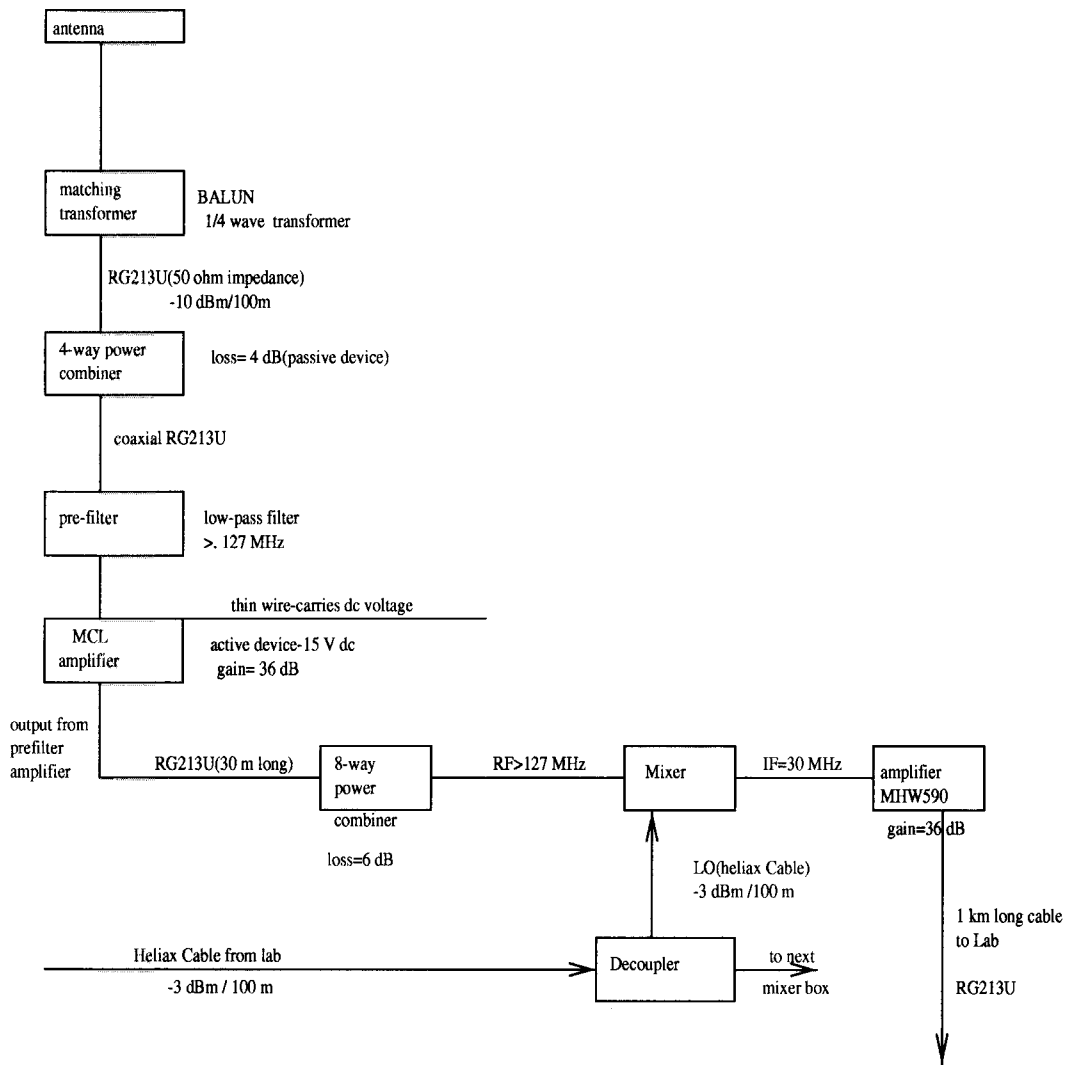


Fig. 1.— Overview of the Field

#### 4. The Existing Tracking System

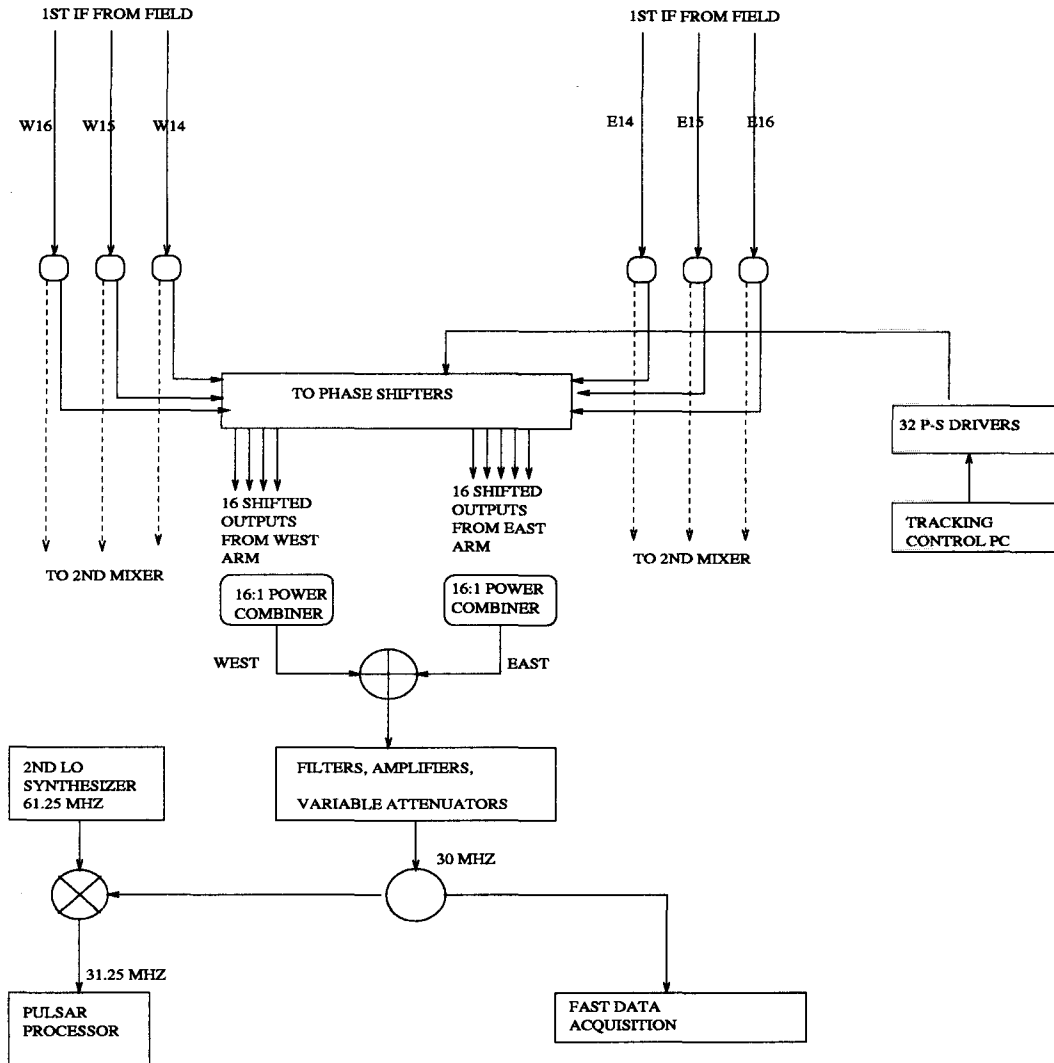


Fig. 2.— The 8-minute tracking system

##### 4.1. The Signal Path

Figure 2 is a schematic of the present tracking system used in the study of pulsars. The first IF (30 MHz) signal from the field reaches the laboratory through 1 km long RG213U cables. In the lab, these signals are split through 1:2 power splitters. One signal goes to the second mixer and finally reaches the correlator after passing through the sampler. The other signal is sent to

a phase shifter module. The phase shifted signals of the East and West arms are combined using 16:1 power combiners. The total output of the West arm from the power combiner is summed with the total output of the East arm. The output of the 2:1 power combiner is filtered, amplified and the output is again split. One signal is heterodyned with a LO of 61.25 MHz and the heterodyned signal is sent to the pulsar processor(ATNF Processor). The other output is sent to the fast data acquisition system (FDAS).

In this scheme, both pulsar and continuum observations can be done simultaneously. It should be noted that the implementation of the tracking system has been largely simplified since all the electronic modules for controlling the phase shifters and the phase shifters themselves are found in the laboratory. Moreover, the advantage of carrying out both observations simultaneously is possible because the split first IF signal can be run to the second mixer and to the phase shifters using small lengths of BNC cables.

#### 4.2. Minimum Detectable Flux with the East-West array

An increase in the observation time increases the sensitivity of the array as per the equation 1 below

$$S_{min} = \frac{Qm'(2kT_{sys})}{A_e\sqrt{(Bn_{samp}\tau)}} \quad (1)$$

where  $S_{min}$ =minimum detectable flux in Jy

Q=a constant

m'=receiver dependent constant

k=Boltzmann's constant

$T_{sys}$ =system noise temperature

$A_e$ =effective aperture area

B=pre-detection bandwidth

$\tau$ =post-detection integration time

$n_{samp}$ =number of independent samples averaged after post-detection integration.

#### 4.3. Pulsar Observation with the Existing System

The existing tracking system consists of a Portable Pulsar Receiver (PPR) and a GPS linked to the observatory clock also. Both the tracking system and the PPR have been specially designed and built at the Raman Research Institute(India) for use at the MRT. This system has allowed the observation of pulsars having an average flux density of about 100 mJy, with a signal to noise ration of  $\approx 25$ . This is for a pulsar with a 5% duty cycle at the centre of our primary beam ( $\delta = -40.5^\circ$ ),

when a total predetection bandwidth of 1 MHz is used and the average system temperature is about 600 K.

## 5. Design Criteria for a New Tracking System

### 5.1. Sensitivity Considerations

An increase in the tracking time will undeniably increase the sensitivity of the telescope. With this enhanced sensitivity, deeper observations can be carried out in this part of the southern sky, namely that of weak pulsars, interplanetary scintillations. We will also be able to feed group outputs phased over a longer span of time to the correlator.

### 5.2. Using a Survey Instrument for Tracking

Although the MRT was primarily designed to conduct the 151.5 MHz survey, it has also been used for pulsar observations. During pulsar observations, only the East-West arm is used. The group outputs are added together, with a tracking capability of about  $2^\circ$  for a source transiting at meridian. This corresponds to eight minutes for an equatorial source. The data is recorded at a fast rate over a band width of 1 MHz. The data processing is done to produce a dedispersed output in the desired format, including the pulsar profile unique to each pulsar.

### 5.3. Different Possible Tracking Schemes

In designing an electrical steering system, it would have been interesting to introduce phase shifting at the level of the individual helix element. As already mentioned in section 3.1, this element has a HPBW of  $60^\circ$  in sky. This would have enabled the tracking time to be extended to four hours. Table 2 summarises the different tracking schemes which are possible and their relative merits and demerits.

Table 2: Tracking schemes with relative normalised survey sensitivity

Type	Tracking time	Normalised sensitivity	Remarks
Individual antenna	4 hour	1	best
Group of 4 antennas	1-hour	2	simpler
Group of 32 antennas	8-minute	5-6	existing

We are designing the one-hour tracking as it is a simpler system to implement, for the time being. We will not have to disturb the physical setup, as in the case of four-hour tracking. Since

the MRT has been primarily designed as a survey tool, priority was given to the continuum mode of observation. The eight-minute tracking system was implemented to test whether the MRT could be used to observe pulsars without modifying the field setup. Since a group of four helices within each group in the East West is available in the field, we don't need to dismantle any existing setup for the one-hour tracking. Therefore, we have used the subgroup of 4 antennas as our building block for a simpler tracking system.

#### 5.4. Present Practical Limitations on Four Hour Tracking

A tracking system which uses the full capacity of the antenna setup would lead to 4-hour tracking time at zenith. Evidently, with that system, the number of pulsars that can be observed will increase largely. However, the implementation of such a system would also involve changing the way the cabling is done. A christmas tree setup could be used. However, with this scheme, it would be difficult to carry out continuum observation simultaneously.

#### 5.5. One Hour Tracking

##### 5.5.1. *The one-hour phase shifter module*

Figure 3 shows a possible implementation of the tracking system for one hour of observation. Our aim is to track sources for one hour at zenith. This is possible if phase shifters are placed at the output of the 4-way combiners (Figure 3). The beam of a 4-antenna subgroup has a half power beam width of  $15^\circ$  in the E-W direction. We have decided to sweep the sky with contiguous EW beams having an overlap of at least 95%. The beams will be flipped to a new position, through 0.42 arc minutes, every 2 sidereal seconds (Figure 14).

A six-bit phase shifter has been designed for this purpose and is currently under test. The phase shifter is expected to give phase shifts of  $5.6^\circ$ ,  $11.2^\circ$ ,  $22.5^\circ$ ,  $45^\circ$ ,  $90^\circ$  and  $180^\circ$  at an operating frequency of 150 MHz. With such a phase shifter, we can introduce a phase as accurate as  $\pm 2.8^\circ$ . This will give a pointing error of  $\Delta\theta \approx 6.68'$  when two adjacent EW subgroups are considered. Since such phase errors will be randomly distributed for the 256 EW subgroups, the pointing error is reduced by a factor of  $16(\sqrt{256})$  on average. This gives  $\Delta\theta \approx 0.42'$  and it lies well within the 95% gain points of the full EW beam.

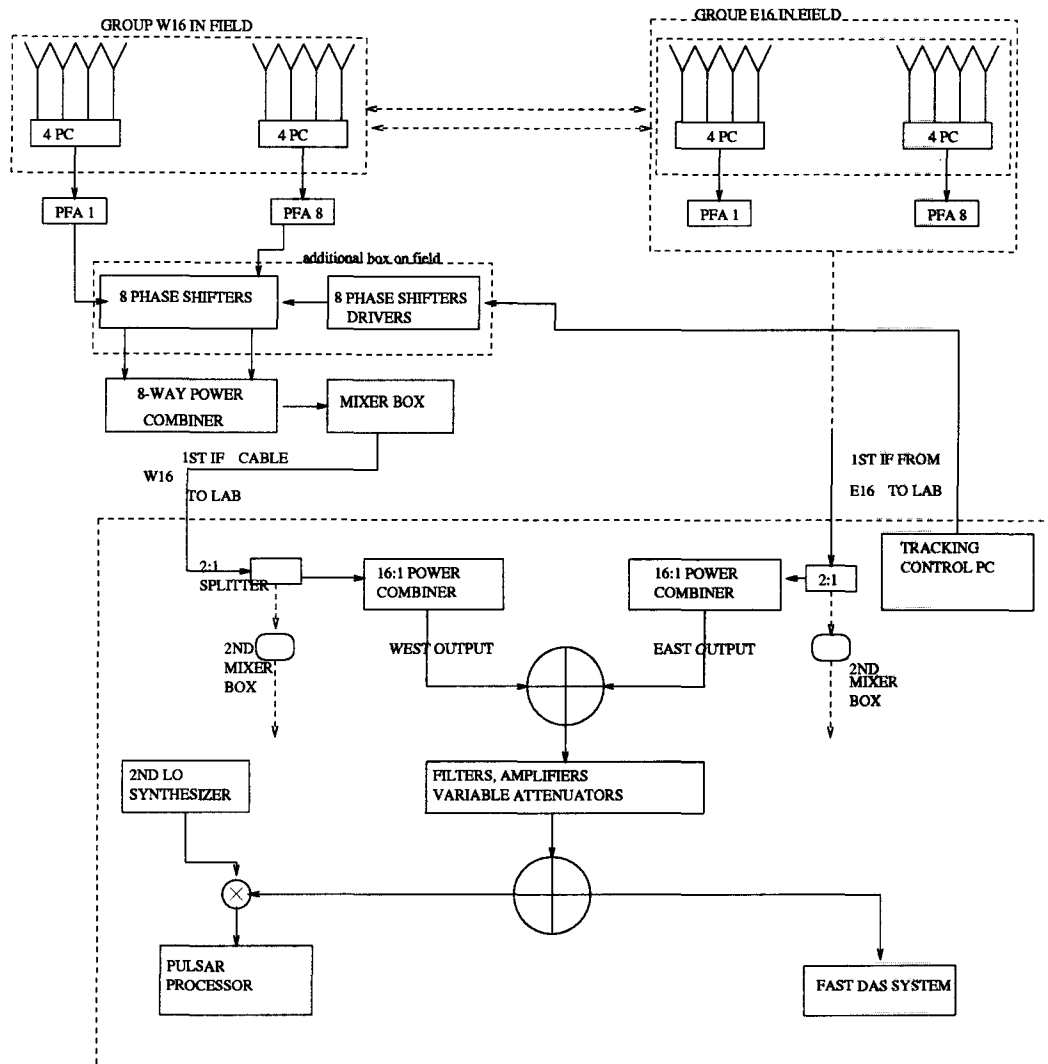


Fig. 3.— The proposed 60-min. tracking system (overview)

Microstrip transmission lines of different lengths are used for the delay lines. This technique has been adopted instead of using RGU cables for the delay lines so as to minimise the weight as the phase shifters will be placed outside in boxes. Moreover, the soldering might break under the tensile stress of the cables. Using microstrip transmission line ensures longevity of the phase shifter under our climatic conditions. The telescope is 1 km away from the sea and we are in the direct path of perennial trade winds.

A phase shifter circuit has been thus produced using plain double-sided PCBs, whereby the artwork is etched onto the board manually. We are also working on photo-resist double-sided PCBs. The plain double-sided PCBs are cheap but working with them proves to be tedious. The photo-

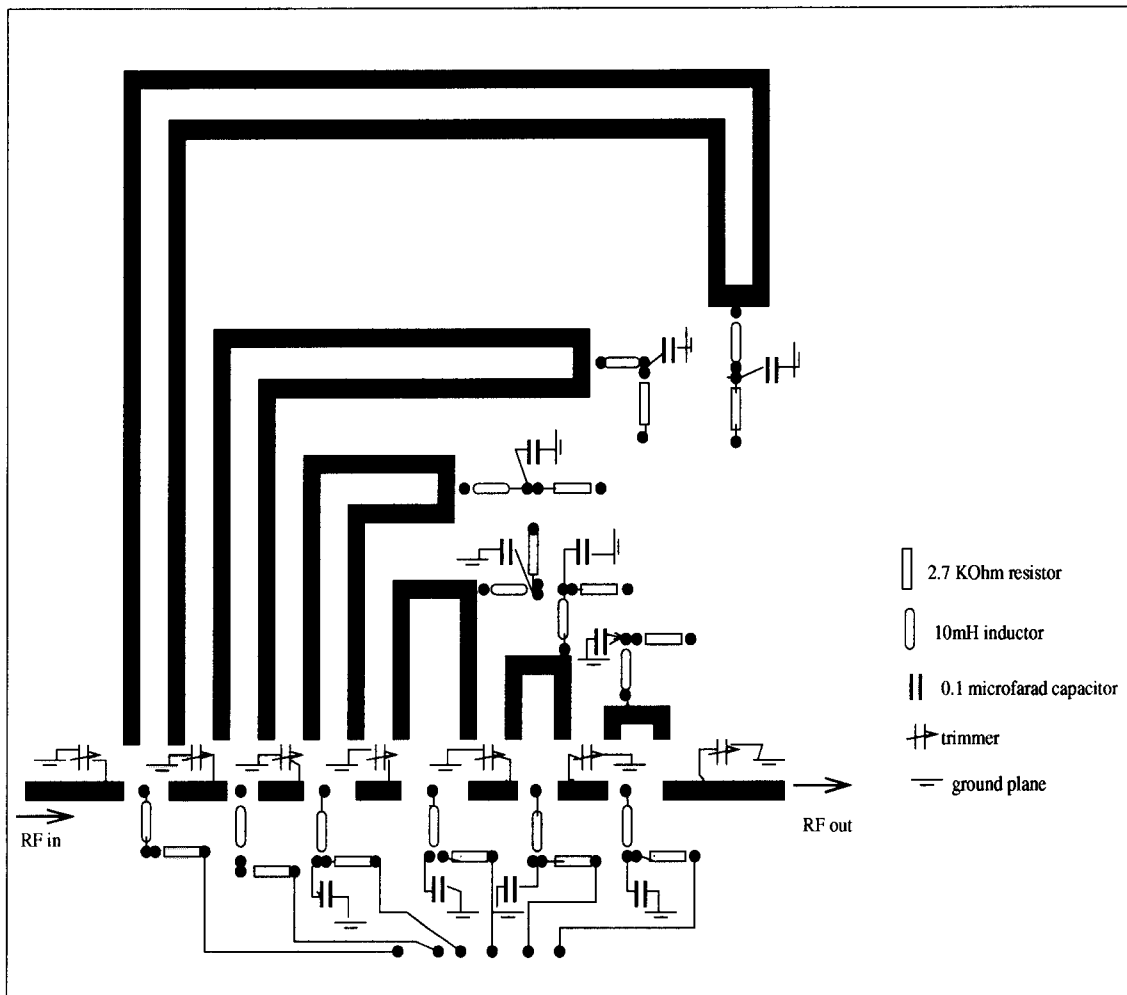


Fig. 4.— The phase shift circuit (delay side).

resist double-sided PCBs are costly but replications of circuits is very easy, quick and accurate. We are trying to minimise the insertion loss of the circuit. The strips are designed to minimise reflection loss at the corners. Figures 4 and 5 show the delay part on one side of the circuit and the DC control on the other side. Figure 6 shows the circuit used.

Figure 7 shows the phase shift introduced in practice. As can be seen it gives a performance close to that predicted in theory. Figure 8 details the corresponding loss in dB for each combination which is quite satisfactory.

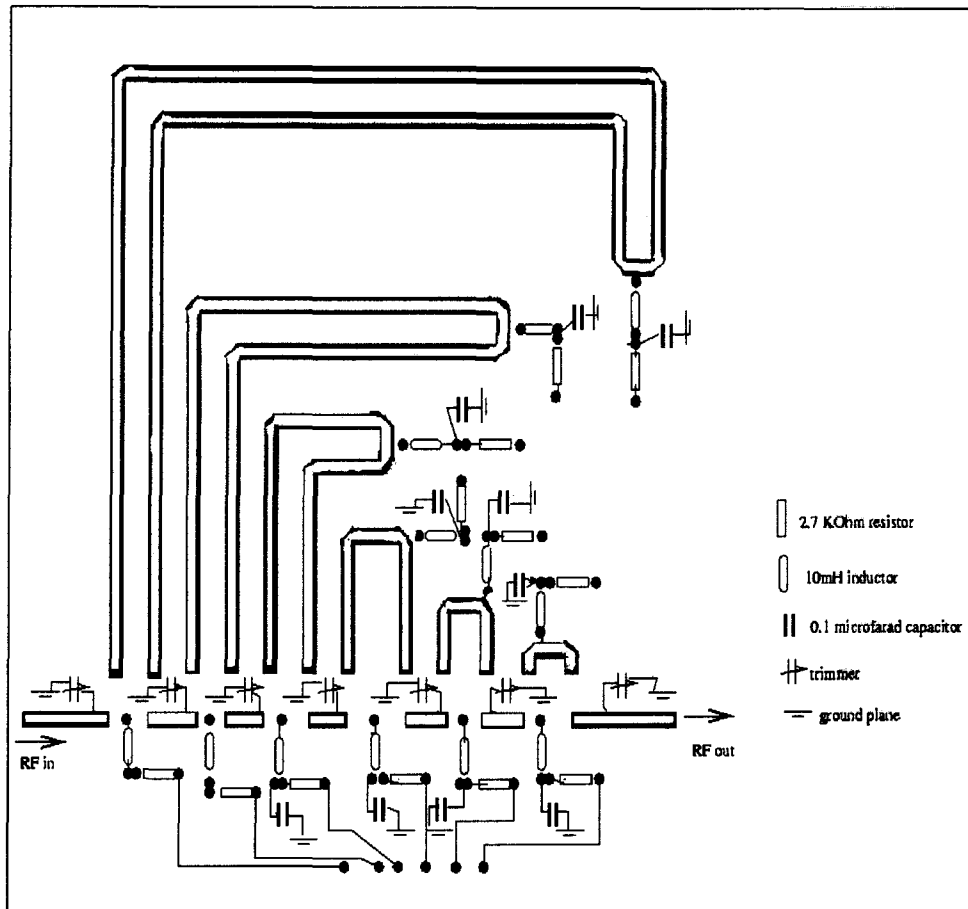


Fig. 5.— The phase shift circuit (DC side). The hollow lines show the delay circuit on the other side of the board.

### 5.5.2. The usage of the existing tracking system

After having phased the outputs from the different subgroups within a group in the field, the signals are summed into one through the 8:1 power combiner. This signal is down-converted and sent to the laboratory. Now this signal, also known as the first IF, was previously being phased with its adjacent neighbours to enable 8-minute tracking. This time it will compensate for phase differences between individual groups which are otherwise difficult to compensate using the RF phase shifters located in the field. No major change is required in that part of the setup as the system has been verified to be working smoothly.

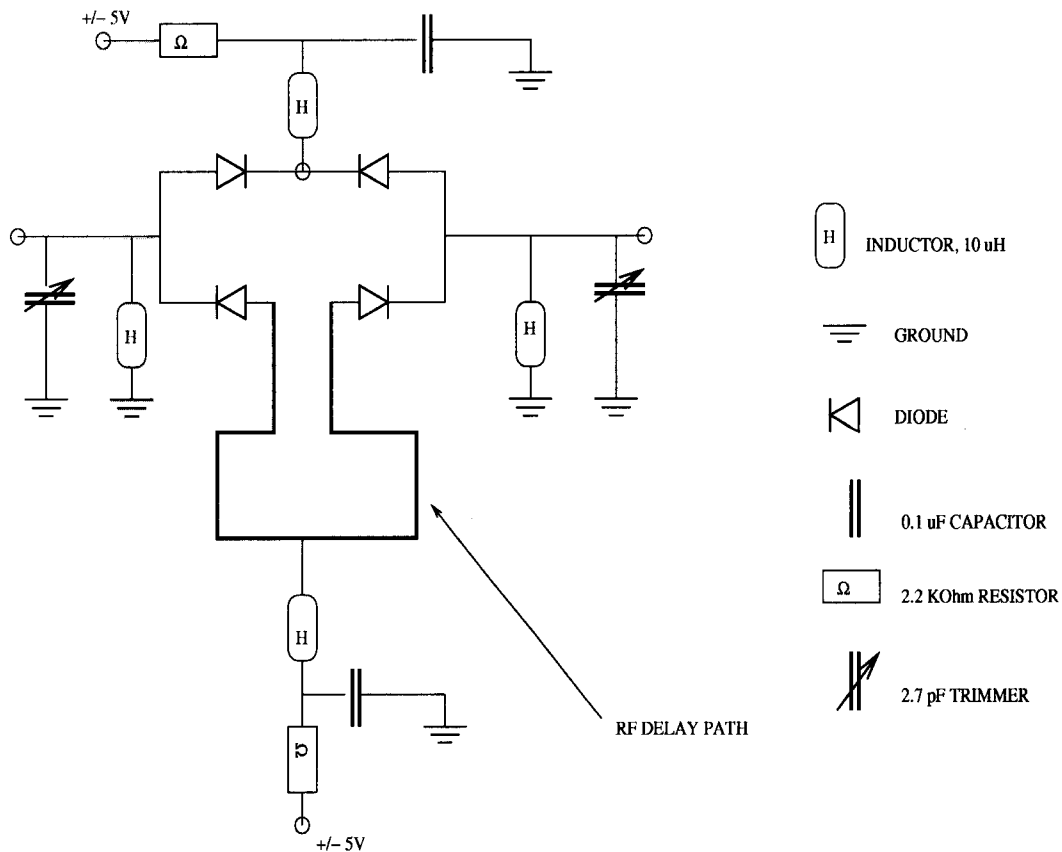


Fig. 6.— A schematic of the phase-shifter circuit diagram

### 5.5.3. The delay system

On top of the doubled-layered phase-shifter system, we need a delay system. After phasing the EW beam in field and in the laboratory, we need to add a delay gradient module. The purpose of this delay gradient module is to minimise the effect of bandwidth decorrelation which are significant at this stage.

### 5.5.4. Bandwidth Decorrelation Effects

Decorrelation results from delays in signal arriving across each individual sub-array and from errors in delay compensation in the signal paths from the arrays.

The following formalism follows von Arx et al (1978) on the Clarke Lake receiver system which has been adapted for use at the MRT. Errors in delay compensation will be considered first . Consider the monochromatic response of a single sideband interferometer consisting of two isotropic

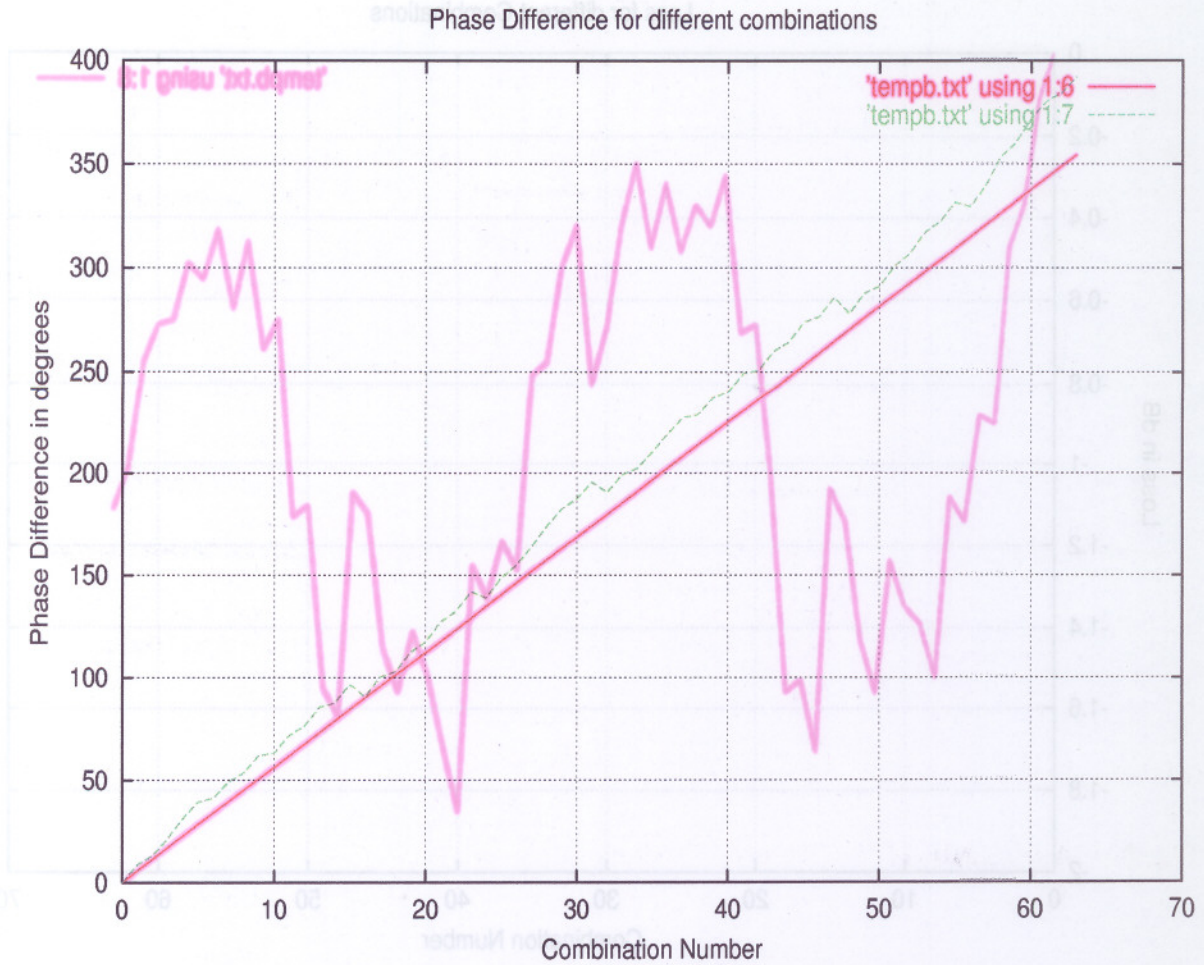


Fig. 7.— A datasheet of the performance of the device

elements separated by a distance  $L$ . If the angle between the wavefront and the line joining the elements is  $\alpha$ , the response is:

$$\cos\left(\frac{2\pi\nu L \sin\alpha}{c}\right) = \cos(2\pi\nu\Delta t) \quad (2)$$

where  $\Delta t = \frac{L \sin\alpha}{c}$  = the time delay between signal arriving at the two elements. We compensate  $\Delta t$  with an inserted incremental delay,  $\tau$ , and  $\Delta\tau = \Delta t - \tau$  is the error in delay compensation. Then the monochromatic response is  $\cos(2\pi\nu\Delta\tau)$ .

To obtain the response over a uniform bandwidth,  $\Delta\nu$ , centered at  $\nu_0$ , we must integrate the monochromatic response. The wideband response is then:

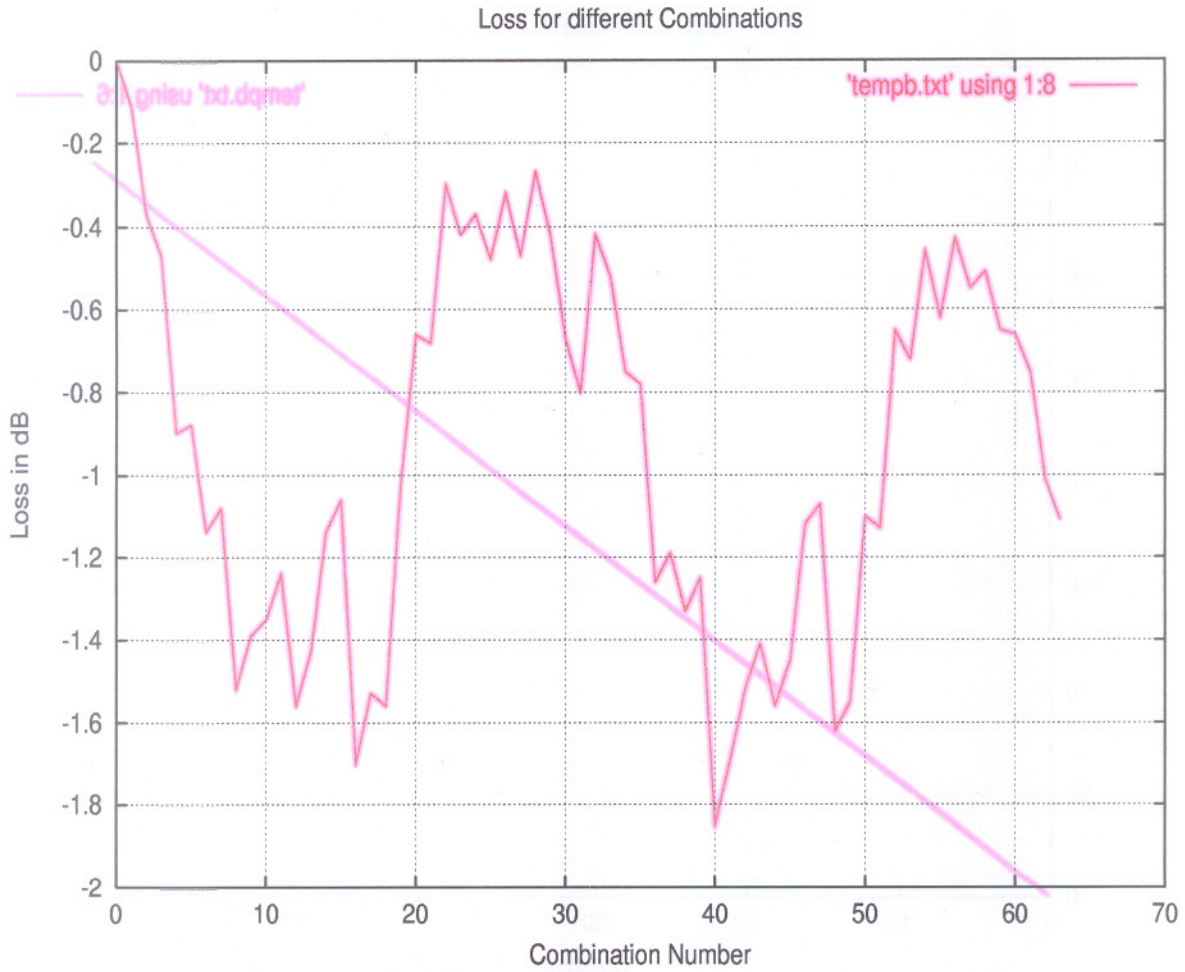


Fig. 8.— A datasheet of the transmission performance of the device

$$\begin{aligned}
 R &= \frac{1}{\Delta\nu} \int_{\nu_o - \frac{\Delta\nu}{2}}^{\nu_o + \frac{\Delta\nu}{2}} \cos(2\pi\nu\Delta\tau) d\nu \\
 &= \frac{1}{2\pi\Delta\nu\Delta\tau} [2\cos(2\pi\Delta\tau\nu_o) \sin(\pi\Delta\tau\Delta\nu)] \\
 &= \cos(2\pi\Delta\tau\nu_o) \text{sinc}(\Delta\tau\Delta\nu)
 \end{aligned} \tag{3}$$

The first factor only represents the phase shift introduced by  $\Delta\tau$ . The second factor is the fringe washing function and its departure from unity represents the decorrelation caused by delay compensation errors.

The standard bandwidth of our system is 1 MHz. We sample at 2.1 MHz and compensate

delays in digital delay line with the corresponding delay increments of  $(2.1 \text{ MHz})^{-1} = 476.19 \text{ ns}$ . Therefore, the delay errors should not exceed 238.09 ns. Using this value of  $\Delta\tau$ , the maximum decorrelation is given as  $\text{sinc}(\Delta\nu\Delta\tau) = 0.9588$ . Hence we are losing about 4% in sensitivity.

In addition to the effects of incremental delay errors, the radiation received by the antenna groups themselves will suffer from partial coherence effects when we observe away from the zenith. Consider a linear array of length  $l$  phased in a direction  $\gamma_0$  where  $\gamma_0$  is the angle between the incoming wavefront and the normal to the array axis. The impressed phase gradient will be  $\Delta\phi$  wavelengths/unit length with  $\sin\gamma_0 = \lambda\Delta\phi$ .

At a monochromatic frequency  $\nu_0 = \frac{c}{\lambda_0}$  the normalised response pattern about the direction  $\gamma_0$  is:

$$P(\gamma - \gamma_0) = \text{sinc}\left[\frac{l}{\lambda_0}(\sin\gamma - \sin\gamma_0)\right] \quad (4)$$

Consider the response in the direction  $\gamma_0$  at a wavelength  $\lambda = \lambda_0 + \Delta$  and note that  $\sin\gamma = \lambda\Delta\phi$ . Then:

$$P(\gamma - \gamma_0) = \text{sinc}\left[\frac{l}{\lambda_0}(\lambda\Delta\phi - \lambda_0\Delta\phi)\right] = \text{sinc}\left[\frac{l}{\lambda}\lambda\Delta\phi\right] \quad (5)$$

To get the broadband response we must integrate  $P(\lambda - \lambda_0)$  over the wavelength interval corresponding to  $\Delta\nu$ . The signal from the array is

$$V(\gamma_0) = \frac{1}{\Delta\lambda} \int_{-\frac{\Delta\lambda}{2}}^{\frac{\Delta\lambda}{2}} P(\gamma - \gamma_0) d\lambda = \frac{1}{\Delta\lambda} \int_{-\frac{\Delta\lambda}{2}}^{\frac{\Delta\lambda}{2}} \text{sinc}\left(\frac{l\Delta\phi\delta}{\lambda}\right) d\delta \quad (6)$$

For  $\delta \ll \lambda_0$  we can let  $\lambda = \lambda_0$  in the argument of the sinc function. This only neglects the fact that the resolution of the array is proportional to  $(l/\lambda)$ .

## 6. The Control System

### 6.1. The Control System Specifications

For the implementation of the tracking system discussed above, a suitable tracking control system is needed to generate the appropriate control signals. It is wiser to build a separate system which will help send/monitor the control signals to the phase shifter modules. We already have such a controller for the existing tracking system. We are designing a controller, partly based on the existing system, for the one hour tracking. We discuss below a description of the control system.

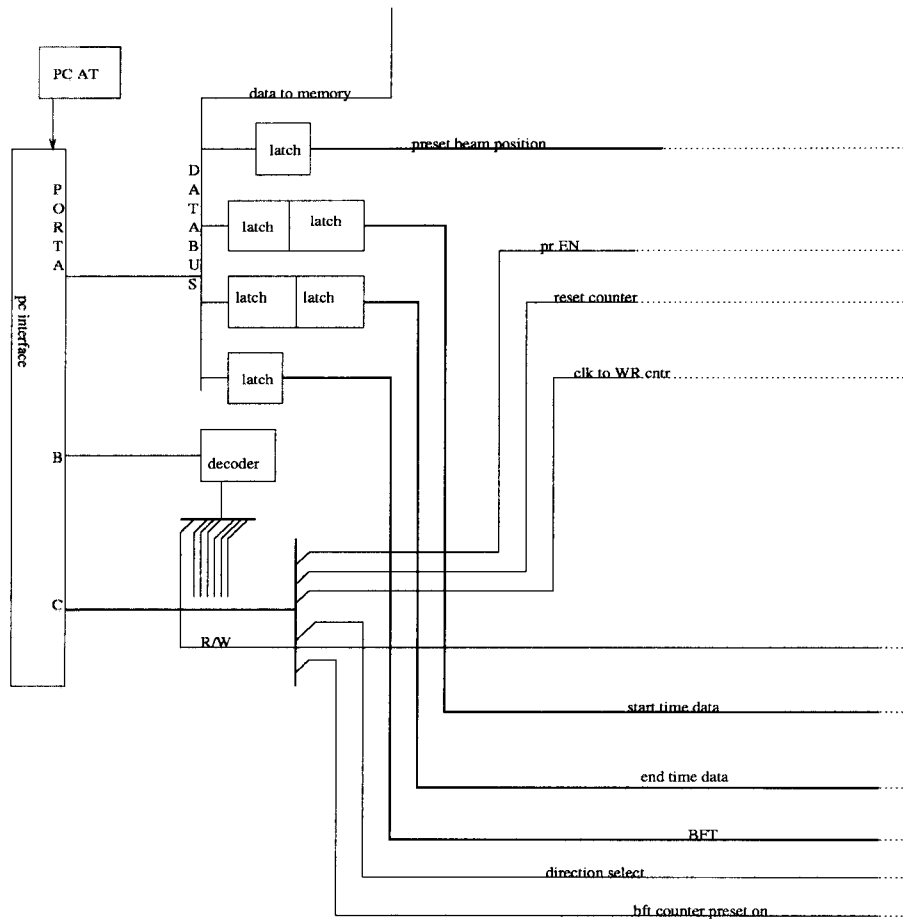


Fig. 9.— The memory modules, start/end times comparator and the beam flipping counter (field modules) of the 60-min. tracking system

Figures 10, 9, 11 show the block diagram of the proposed tracking/monitor system. It is divided into three parts as follows:

1. Personal computer (PC) interface(in laboratory)
2. Memory modules, start/end times comparator and the beam flipping counter (in field modules)
3. Control signals/voltages monitoring(in field and back to laboratory)

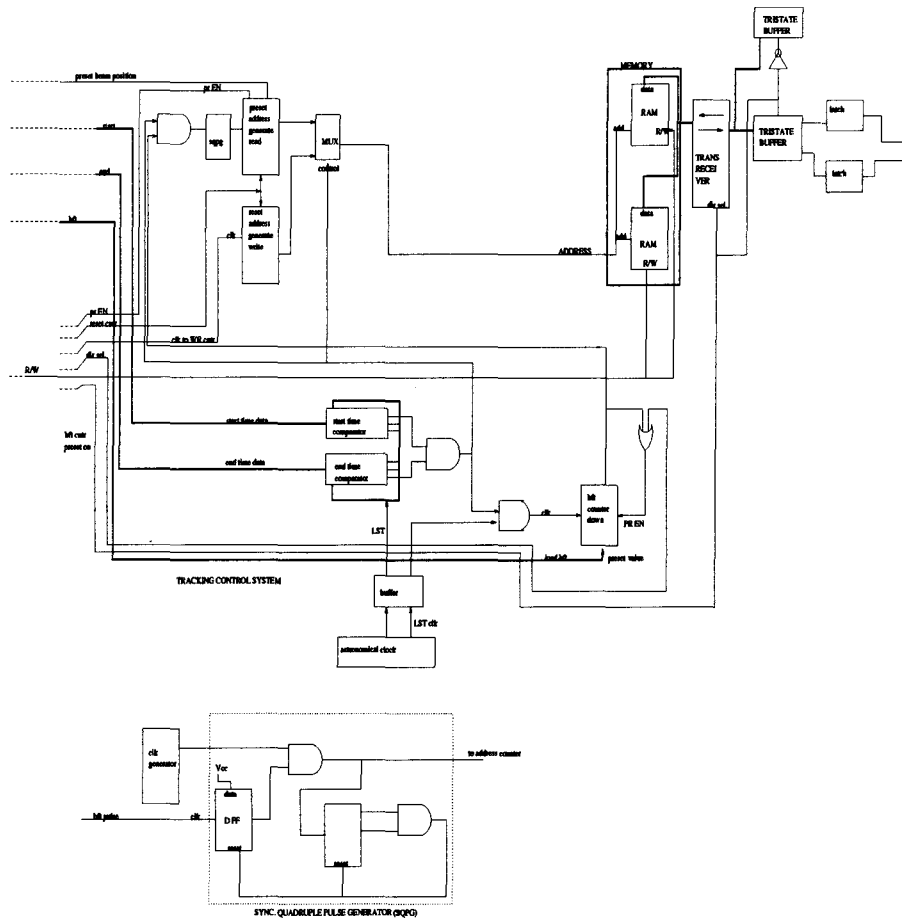


Fig. 10.— The proposed PC interface of the 60-min. tracking system

## 6.2. PC interface

This unit (Figure 10) is used to download the control bits information to the memory modules from the pc. These bits are calculated by the software, which on getting the right ascension (RA) and declination (DEC) of the source to be tracked, from the user, estimates the bits for all the beam positions. The software also estimates the START and END times of observation and the Beam Flipping Time(BFT) and downloads into appropriate counters in the tracking/control monitor(TCM). This interface is also used to indicate the status of the control bits in the monitoring mode of operation of the TCM.

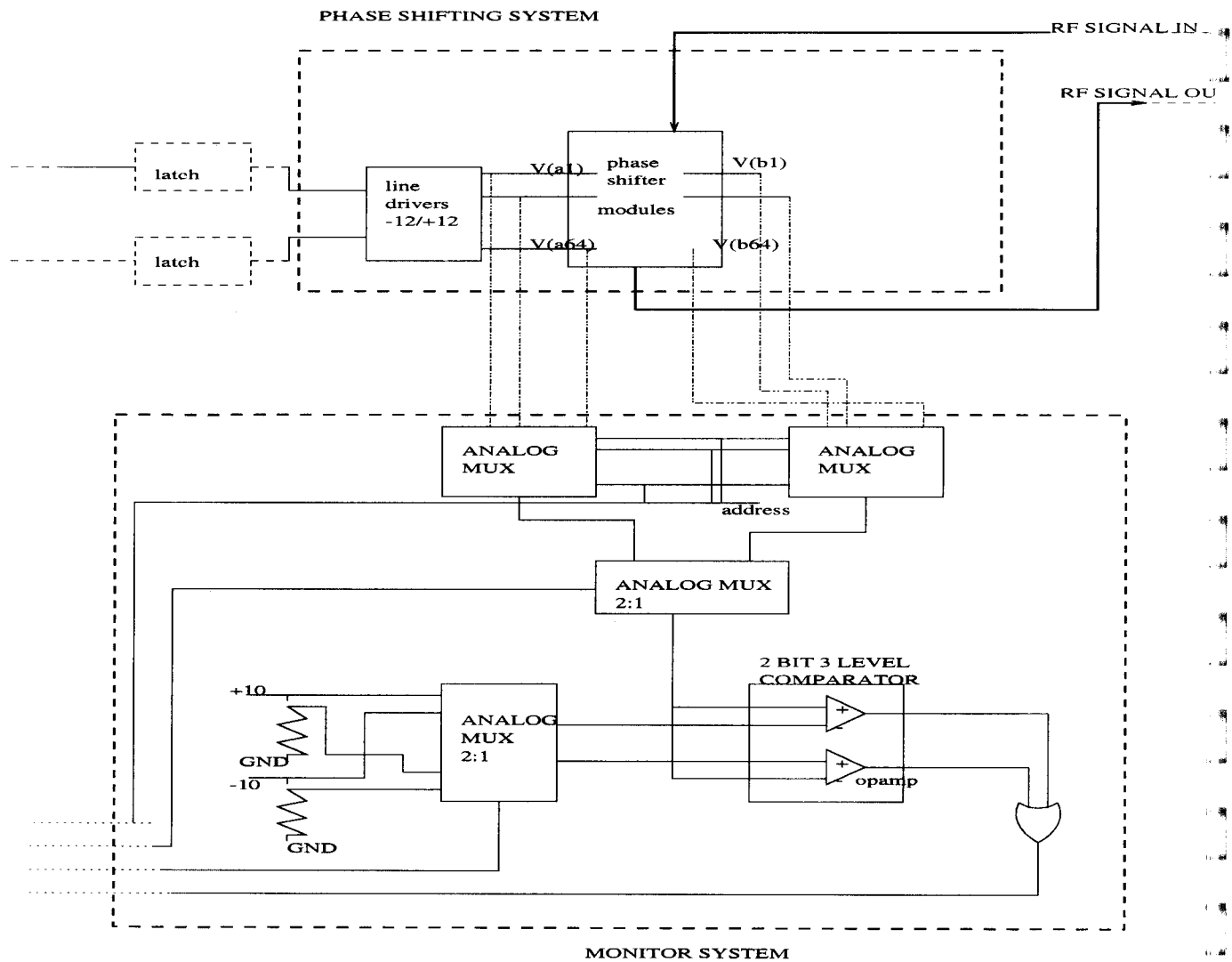


Fig. 11.— The phase shifter module control signals/voltages monitoring of the 60-min. tracking system

### 6.3. Memory modules, start/end times comparator and the beam flipping counter (field modules)

This logical block consists of the RAM memories wherein the control bits are stored (Figure 9). The driver modules convert the digital control bits from the RAM memory to the corresponding analog voltages (+12 V, -12 V) in order to switch on/off the control bits in the phase shifter module (PSM). This section also consists of a comparator logic for the START/END time and the BFT

counter.

#### 6.4. PSM control signals/voltages monitoring

This section basically monitor/check the voltages which are sent to the PSM (Figure 11). A comparator is used to determine the voltage levels both at the “send end” and the “load end”. The principle of operation of the TCM is now explained.

As described above, there are two modes of operations:

##### 1. Phase shifter setting

This is the normal mode of operation and the user is provided with the option of setting the phase shifter values of all the subgroups. The choice of selectively setting the phase shifter values of any subgroup is also provided. In this mode, the PC accepts the RA and DEC values of a particular source to be tracked and calculates the necessary control signals for all the beam positions. A source at a declination  $\delta$  takes  $4 \times \sec(\delta - 20^\circ)$  sidereal seconds to cross 1 arcmin of a beam. This time interval is called the Beam Flipping Time (BFT) for 1 arcmin and corresponds to the observing time in each of the 256 beams. Since we have chosen to flip the beam each 0.42 arcmins the the BFT becomes  $2 \times \sec(\delta - 20^\circ)$  sidereal seconds.

Given the RA and DEC of a source, the start time ( $T_s$ ) and end sidereal times ( $T_e$ ) of tracking are downloaded to the RAM memories in the TCM.

When the  $T_s$  equals the local sidereal time(LST), obtained from the astronomical clock, the tracking operation starts. The counter which is set to beam flipping time(BFT) starts counting down from a maximum value. The counter reads the new phase shifter control signal/voltages from the memory. When the LST equals to the stop time,  $T_e$ , the tracking is stopped.

These control bits which are TTL logic levels (0V, 5V) are then transferred to +12/-12 V by the “Driving Modules” which control the switching on/off of the phase shifter modules.

##### 2. Monitoring the status of the control signals/voltages

This option is included to monitor the proper functioning of the individual subgroup phase shifter modules. The control signals being sent to the phase shifter modules are being monitored at two points, namely at the system end and at the (load) phase shifter end.

The control signals/voltages (driver outputs), which are fixed at +12 V, are determined by taking into account wire losses and the minimum voltage of +10 V required to control the diode.

The DC current drawn by each control bit is measured as follows. It is estimated by measuring the voltages both at the TCM end and the load end using another comparator. This will directly indicate the user whether the control signals sent to the phase shifter modules are functioning properly. Different options are provided in the control programs to monitor the control voltages

either sequentially or selectively.

### 7. Results Expected

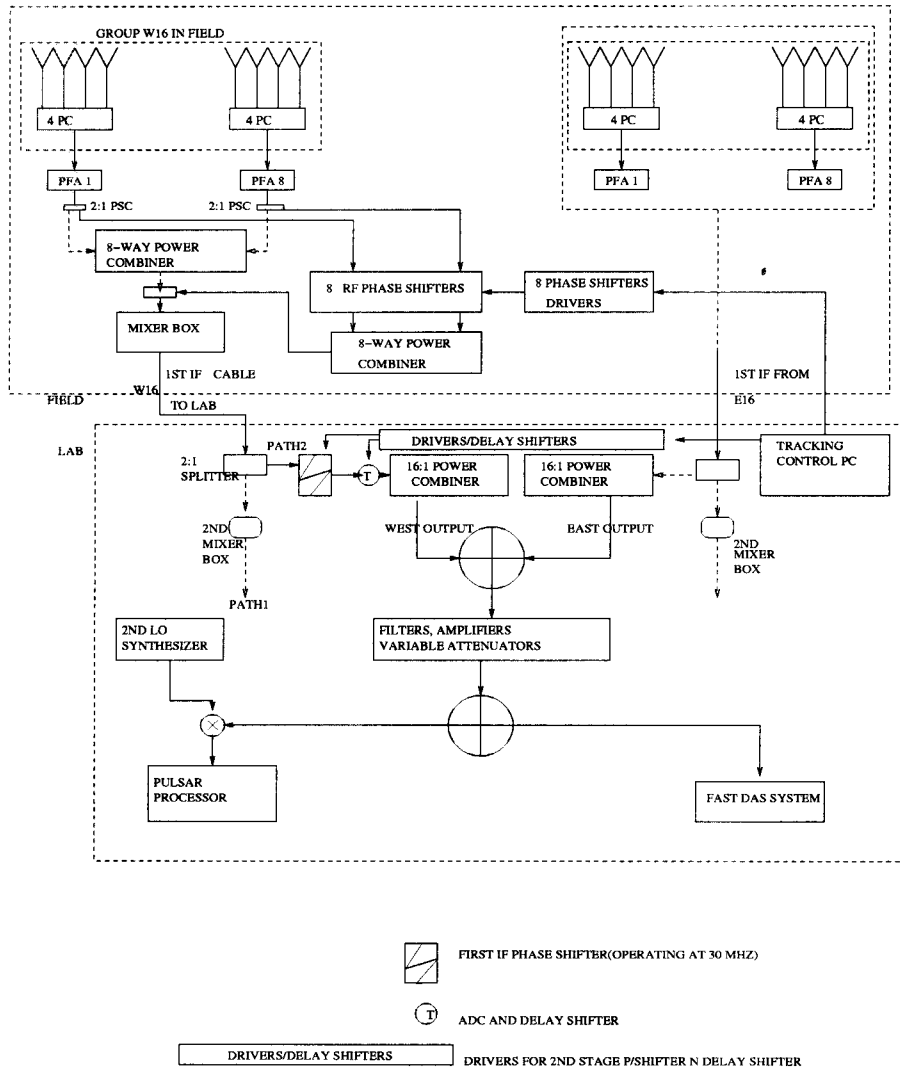


Fig. 12.— The whole tracking system

Figure 12 shows the final setup after the RF phase shifter modules have been placed. We have already produced prototype phase shifters using the scheme described in the section on phase shifters. Laboratory tests are being conducted on them. Then, we will test them, using the control system being developed, on an array of 4 EW groups. We will investigate their performance by tracking known pulsars. This exercise will also allow us refine our product.

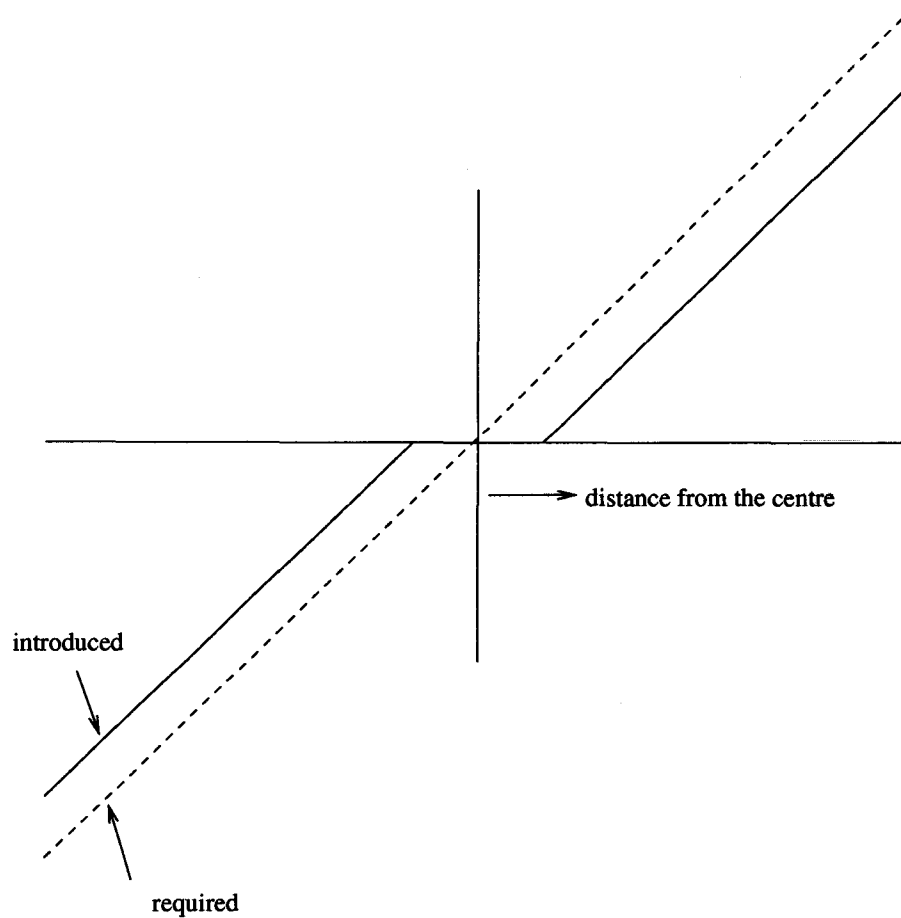


Fig. 13.— The phase gradient along the EW array

After the successful implementation of the phase shifters, the telescope (main beam) is expected to be able to track a source for 1 hour at local zenith (figure 14). This will facilitate the observation of weak pulsar signals, low frequency recombination lines and interplanetary scintillation (Verschuur & Kellermann 1988, Christiansen & Högbom 1987). Moreover, the amount of time over which a point source can be integrated will be increased by tracking that particular source as it moves. This will increase the sensitivity of the telescope by a factor of four compared to eight-minute tracking at local zenith.

- *Weak Pulsar.*

Pulsars are generally very weak sources of electromagnetic radiation. As stated above, increasing the sensitivity of the telescope will enable us to detect weaker pulsars and to extend our studies in the southern part of the sky at radio frequency 151.5 MHz. We will then be able to investigate the pulse shapes, flux densities, variability, scattering and possibly micro

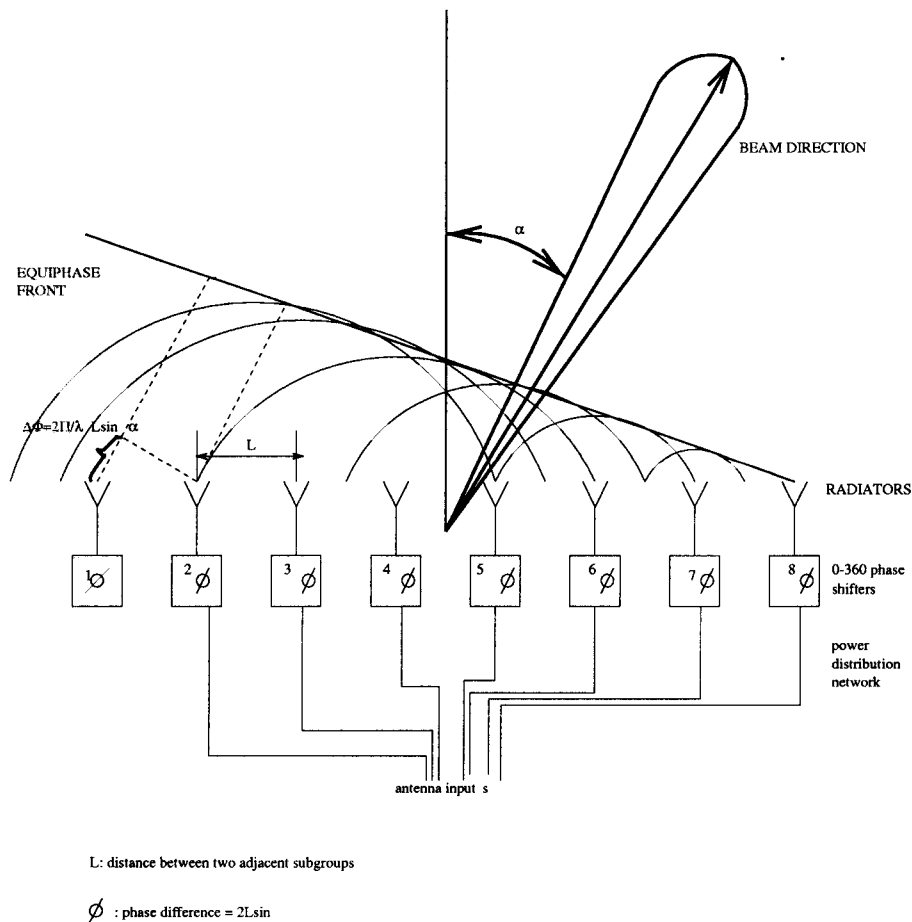


Fig. 14.— The beam of an EW group being parked in the east direction

structure. We will be able to study variations of period longer than the actual 8-minute limit (at zenith). We can then compare our results with those obtained in other parts of the sky at other frequencies (Issur 1997).

- *Radio Recombination Lines.*

An increase in the sensitivity will help in the survey of radio recombination lines (RRLs) from starburst galaxies at low frequencies. Up to now, RRLs have been detected in fourteen galaxies which are not within our field of view (they are found in the northern celestial hemisphere). Moreover, these observations were made at very high frequencies, in the order of GHz (Kantharia et al 1998).

- *Interplanetary Scintillation.*

Radiation coming from a distant source is usually diffracted by objects found in the inter-

planetary medium. This diffraction gives rise to scintillations which can help us investigate the nature of the interplanetary medium. It can further help us in designing future radio telescopes bearing in mind that the radiation we receive is usually affected by solar wind which induces irregular effects (Thompson et al 1986).

- *VLBI*.

It is important to consider the use of MRT as a VLBI element as it is at a crucial geographic location. It can probably be used with Indian radiotelescopes operating at similar wavelengths, like the Great Metre Wave Radio Telescope (GMRT).

The authors would like to express their deep thanks to Prof. N Udaya Shankar for fruitful discussions. They would also like to thank the other members of the MRT team. U. Chummun is supported by a TEC grant.

### References

1. Ables, T.G., McConnell, D., Deshpande, A.A. & Vivekanand, M., 1997 ApJL **475**, L33.
2. Chandrasherakan, S.D., 1993, *A Single Beam Forming Receiver For MRT*, Raman Research Institute, Bangalore.
3. Cornwell, T.J. & Perley, A. Editors, 1991, *Radio Interferometry: Theory, Techniques and Applications*, **19**.
4. Christiansen, W.N. & Högbom, J.A., 1987, *Radiotelescopes*, Cambridge University Press.
5. Deshpande, A.A., Ramkumar, P.S. & Chandrashekar, S., 1997.
6. Golap, K., 1998, *Ph.D. Thesis*, University of Mauritius (submitted).
7. Issur, N.H., 1996 *Tracking at the MRT*.
8. Issur, N.H., 1997, Bull. Astr. Soc. India, **25**, 541-548.
9. Kantharia, N.G. & Anantharamaiah, K.R. & Goss, W., 1998, *VLA observations of Hydrogen and Carbon recombination lines towards W3A at 1.4 GHz*, ApJ, **504**, 375.
10. Kraus, J.D., 1986, *Radio Astronomy*, 2nd ed., Cygnus-Quasar.
11. Kraus, J.D., 1988, *Antennas*, McGraw-Hill.
12. Mailloux, R.J., 1994, *Phased Array Antenna Handbook*, Artech House.
13. Roshi, A.D. & Anantharamaiah, K.R., 1997, *Hydrogen and carbon recombination lines towards the Galactic Centre near 328 MHz*, MNRAS, **292**, Issue 1, 63-70.
14. Sachdev, S., 1999, *Ph.D Thesis - Wide Field Imaging at The MRT*, University of Mauritius.
15. Sethuraman, R. & Balakrishnan, N., 1983, *Radiation & Propagation*, IIT-Madras, Khanna Publishers.
16. Swarup, G., 1984, *The Ooty Synthesis Radio Telescope: First Results*, *Journal of Astrophysics & Astronomy*, **5**, 139-148.
17. Thompson, A.R., Moran, J.M. & Swenson Jr., G.W., 1986, *Interferometry and Synthesis in Radio Astronomy*, Wiley Publications.

18. Verschuur, G.L. & Kellermann, K.I. Editors, 1988, *Galactic & Extragalactic Radio Astronomy*, Springer-Verlag.
19. von Arx, B., Caflich, M., Erickson, W.C., *The TPT Electronics System*, AP78-027.

# **Tenth United Nations/European Space Agency Workshop On Basic Space Science**

**Exploring the Universe - Sky Surveys , Space Exploration and  
Space Technologies**

**Hosted by the University of Mauritius , 25-29 June 2001  
Reduit, Mauritius.**

## **List of papers submitted by the MRT team to the Astrophysics and Space Science Special issue on the workshop**

1. **Imaging With The Mauritius Radio Telescope- Challenges and Results.**  
*N.Udaya Shankar, K.Golap, S.Sachdev, R.Dodson, M.Katwaroo,  
Ch.V.Sastry*
2. **Full Resolution Images From The Mauritius Radio Telescope.**  
*V.N.Pandey , Radhakrishna Somanah, N.Udaya Shankar*
3. **Limitations Of The Tangent Plane Approximation For Wide-Field  
Imaging Using The Mauritius Radio Telescope**  
*N.Oozeer and N.Udaya Shankar*
4. **Study Of Extended Radio Galaxies At 151.6 MHz Using The Mauritius  
Radio Telescope.**  
*Radhakrishna Somanah and N.Udaya Shankar*
5. **The Pulsar Observing System And Data Analysis Procedure Used At  
MRT.**  
*Nalini H. Issur and Avinash A. Deshpande*
6. **Low Frequency Observations Of Pulsars At MRT – Results On A Few  
'Normal ' Pulsars and a 'Millisecond' Pulsar.**  
*Nalini H.Issur*
7. **A New Tracking System For The MRT.**  
*U.Chummun and G.K.Beeharry*

# Imaging With The Mauritius Radio Telescope Challenges and Results

N. Udaya Shankar<sup>2,1</sup>, K. Golap<sup>1</sup>, S. Sachdev<sup>2,1</sup>, R. Dodson<sup>2,4</sup>, M.Katwaroo<sup>1</sup>, Ch. V. Sastry<sup>3,1</sup>

<sup>1</sup>*Department of Physics, University of Mauritius, Reduit, Mauritius*

<sup>2</sup>*Raman Research Institute, Sadashivanagar, Bangalore 560080, India*

<sup>3</sup>*Indian Institute Of Astrophysics, Koramangala, Bangalore 560034, India*

<sup>4</sup>*Physics Department, University of Durham, Durham, U.K.*

## ABSTRACT

The Mauritius Radio Telescope (MRT) has been built with the main objective of surveying the southern sky at meter wavelengths. MRT is a Fourier synthesis, T-shaped non-coplanar array. It consists of a 2048 m long East-West arm with 1024 fixed helices and a 880 m long South arm with 15 trolleys. Each trolley has four helices. A 512 channel, 2-bit 3-level complex correlation receiver is used to process the data from the EW and S group outputs. At least 60 days of observing are required for obtaining the Fourier components of the brightness distribution of the sky required to complete the survey. The MRT survey will be one of the most extensive survey at low frequencies providing a moderately deep radio catalog reaching a source density of about  $2 \times 10^4 \text{ sr}^{-1}$  over most of the sky south of south of  $\delta = -10^\circ$  with an angular resolution of  $4' \times 4.6' \text{ sec}(\delta)$  and a limiting flux density of 200 mJy ( $3\sigma$  level) at 151 MHz. This paper will describe the telescope, the observations carried out so far, challenges of imaging with the data acquired over a period exceeding four years with a non-coplanar array, and summarises the results obtained so far.

## 1. Introduction

The primary task of observational radioastronomy is the measurement of intensities and direction of arrival of radiation from cosmic objects, in those portions of the spectrum which lie in the radio range. The first systematic survey of the radio universe was carried out by Grote Reber (1944) using a backyard telescope with a resolution of  $12^\circ$  operating at a frequency of 160 MHz. With the quest for higher angular resolution the exercise of surveying soon shifted to higher frequencies. Even so, many low frequency surveys were carried out after Reber's survey. See Golap et al (1998) for details. Most of these surveys are in the northern hemisphere. 6C survey (Baldwin *et al* 1995) is by far the most extensive survey of the northern sky at low frequencies. This survey provides a moderately deep radio catalog reaching a source density of about  $2 \times 10^4 \text{ sr}^{-1}$  over most of the sky north of  $\delta = +30^\circ$  with an angular resolution of  $4.2' \times 4.2' \text{ cosec}(\delta)$  and a limiting flux density of 120 mJy at 151 MHz. An equivalent of the 6C survey for the southern sky does not exist. Since

the survey of Mills *et al.* (1958) at 80 MHz there has not been much effort at low frequencies to map the southern sky. Thus there is an obvious need to survey the southern sky at a frequency around 150 MHz. At this frequency synchrotron sources show up much better than at higher frequencies, such as 408 MHz, due to their spectra. Sources also show up better at 150 MHz than at lower frequencies since the absorption due to the interstellar gas is much less than at deca-meter wavelengths. For this purpose a radio telescope operating at 150 MHz has been constructed at Bras d'Eau, Mauritius. Mauritius was chosen as the site for the new telescope due to its strategic geographic location (latitude =  $-20.14^{\circ}$ ), where the Galactic Centre is almost overhead.

## 2. Mauritius Radio Telescope

**Design Criterion** The MRT is designed based on the technique of using small movable antennas to synthesise the measurements of a much larger telescope, called aperture synthesis. This technique was pioneered at Cambridge in England. In this technique a telescope pair is configured in a manner that is best described as an interferometer in the ordinary optical sense and measures the fringe contrast, which is in general a complex number. The radio astronomers call this complex visibility. Filled as well as unfilled apertures can be synthesised by moving a pair of telescopes to obtain interferometers of different spacings and adding appropriately the visibilities obtained.

The visibilities measured by an interferometer of baseline  $\vec{b} \equiv (u, v, w)$  is given by Thompson *et al* (1986):

$$\tilde{V}(u, v, w) = \int \int \frac{A(l, m)B(l, m)}{\sqrt{1-l^2-m^2}} \exp(-i(lu + mv + nw)) dl dm. \quad (1)$$

where  $A(l, m)$  is the amplitude response of the array,  $B(l, m)$  is the sky brightness distribution and  $l, m, n$  are the direction cosines.

Let  $B'(l, m) \equiv \frac{B(l, m)A(l, m)}{\sqrt{1-l^2-m^2}}$ . Then the above equation becomes

$$\tilde{V}(u, v, w) = \int \int B'(l, m) \exp(-i(lu + mv + w\sqrt{1-l^2-m^2})) dl dm. \quad (2)$$

where  $B'(l, m)$  is the modified brightness distribution. For planar arrays this relationship can be simplified to a 2-dimensional Fourier transform. Thus, a radio astronomer measures the Fourier components of the brightness distribution of the sky by using pairs of telescopes rather than the image of the sky directly as done by optical astronomers. In radio astronomy this techniques is also referred to as Fourier synthesis and indirect imaging.

With an objective of synthesising roughly an aperture of dimensions  $1Km \times 1Km$ , a T-shaped configuration with a 2 Km long EW arm and a 1 Km long S arm, was chosen for its simplicity. Aperture synthesis with fixed antennas in the EW arm and movable elements (trolleys) in the S arm were chosen to minimize the hardware required. An abandoned old railway line running

North-South was rebuilt for use as the South arm. This restricted the length of the S arm to 880m. On this rail the trolleys cannot approach the EW arm nearer than 11 m. To ensure that the array responds to structures of all sizes in the sky, the array should provide all spacings available in a square aperture. To meet this requirement, a 15 m North extension with one trolley almost touching the EW arm has been built and is used to measure the visibilities at short baselines. However, this trolley cannot approach the EW array nearer than 2 m. Hence baselines with 1 m spacing in the S direction are not measured.

The local terrain is rocky and very uneven, especially along the EW arm with height differences of up to 35 m. To minimize the problems of non-coplanarity, it was decided to level the EW arm in multiples of 64 m ( $32\lambda$ ) so that the antennas in each group will be at the same height.

After the closure of the Clark Lake Radio Telescope (CLRO) the two-bit three-level 512 channel complex correlation receiver was kindly donated to the MRT. The MRT was designed by considering the availability of the 512 channel CLRO correlator system (Erickson *et al* 1982 ), the constraints due to the available terrain and the presence of man-made interference. For optimal use of the 512-channel complex correlation receiver, several schemes were considered before arriving at a configuration consisting of 16 movable trolleys in the NS arm and 32 groups in the EW arm. Details of these considerations are given by K. Golap (1998).

**Description Of MRT** The MRT is a T-shaped non-coplanar array consisting of a 2048 m long EW arm and a 880 m long south arm. In the EW arm 1024 fixed helices are arranged in 32 groups and in the NS arm 16 trolleys with four helices on each. The primary beams of the helices have a full width at half maximum (FWHM) of  $60^\circ$ , and they are mounted with a tilt of  $20^\circ$  toward the south, i.e., the peak of the primary beam is at  $\delta = -40^\circ$ . This leads to a declination coverage of  $-70^\circ$  to  $-10^\circ$  allowing a better coverage of the southern sky including the Galactic plane. The outputs of the EW and the south groups are heterodyned to an intermediate frequency (IF) of 30 MHz in the field, and are brought to the observatory building through coaxial cables. In the observatory, these outputs are further amplified and down-converted to a second IF of 10.1 MHz. These are then quantized to 2-bit 3-levels and sampled at 12 MHz. These are further processed in a 512-channel digital complex correlation receiver to measure the visibility function. The 512 complex visibilities are integrated and recorded at intervals of 1 second. At the end of 24 hours of observations the trolleys are moved to a different position so as to sample the NS baselines with a spacing of 1m and new visibilities are recorded. Allocation refers to the placement of the trolleys on a given sidereal day. A minimum of 60 days of observing are needed to obtain the visibilities up to the 880 m spacing. The Fourier transform of the phase corrected visibilities obtained after the complete observing schedule produces a map of the area of the sky under observation with a synthesized beam of width  $4' \times 4.6' \text{ sec}(\delta + 20.14^\circ)$ . The phase corrections mentioned above take into consideration the non-coplanarity of the baselines. The expected root mean squared (RMS) values of the background in the synthesized images, arising from the system noise with a 1 MHz bandwidth and an integration time of 8 seconds is expected to be around 200 mJy ( $3\sigma$ ).

Observing frequency	151.5 MHz
Telescope configuration	T shaped 2048 m EW arm and 880 m NS arm
Basic element	helical antenna
Polarization	Right Circular
HPBW of helix	$60^\circ \times 60^\circ$
Declination coverage	$-70^\circ$ to $-10^\circ$
Collecting area of helix	$4 \text{ m}^2$ at 150 MHz
East-West arm	32 groups with 32 helices each
North-South arm	15 trolleys each with 4 helices
1 <sup>st</sup> IF frequency	30 MHz
2 <sup>nd</sup> IF frequency	10.1 MHz
Instrumental bandwidths	0.15,1.0,1.5,3.0 MHz
Digitization before correlation	2-bit 3-level
Correlation receiver	$32 \times 16$ complex channels
No of baselines measured per day	$32 \times 16$
Minimum and maximum baselines	0, 1024 $\lambda$
Time to get full resolution image	60 days
Synthesized beam-width	$4' \times 4.6' \text{sec}(\delta + 20.14^\circ)$
Point source sensitivity	200 mJy ( $3 \sigma$ )

Table 1: MRT Specifications

A detailed description of the telescope is to be found in Golap *et al* (1998). Table 1 summarizes the MRT specifications. The Figure 1 shows an aerial view of the Mauritius Radio Telescope.

### 3. Challenges

#### 3.1. Installation

The 1088 helices, the field electronics consisting of 272 low-noise amplifiers, 48 super-heterodyne receivers, IF system consisting of more than 50 Km of transmission lines, the IF pre-processors in the observatory and the back-end including the modifications to the CLRO correlator system to adapt it for use at the MRT, were designed, assembled and tested at the Raman Research Institute. These were transported to Mauritius and installed. In-house and external interference were the main sources of problems while installing.

We found the oscillators in switch mode power supplies of Personal Computers to be the main source of Radio Frequency Interference (RFI) emanating from the observatory building. These and the other parts of the receiver system were shielded by putting them in grounded Faraday cages.



Fig. 1.— The figure shows an aerial view of the Mauritius Radio Telescope (MRT).

The analog and digital parts were grounded separately.

The observatory building was not built with shielding. We reduced the effect of interference from the observatory by covering it with grounded stainless steel mesh.

To reduce the effect of common-mode interference picked up by the first IF cables and by the second IF signal lines, phase switching of the LO was implemented. We were also faced with the noise generated by the LO generator at 30 MHz, the first IF frequency. This leaked to the IF port of the first mixer and produced high correlations in some of the baselines. To reduce this, we used a band elimination filter centered around 30MHz in the path of the Local Oscillator (LO).

The first IF at 30 MHz, is heterodyned with an LO of 40 MHz. In this conversion, stray

signals centered around 50 MHz, picked up by long cables carrying the first IF to the observatory building, gets into the observing band. This gives increased noise in the observing band. To reduce their effects, we introduced sharp cut-off band-pass filters centered around 30 MHz just before heterodyning.

The interference in Mauritius is predominantly due to local television transmission and other communication facilities operating around 150 MHz. The receiver system design was basically targeted to suppress interference from the radio broadcast and other communication channels around 10 MHz. Modifications to the design to adapt to the local interference environment was carried out on site.

### 3.2. Wide-field Imaging With the MRT

During the installation stage of the Mauritius Radio Telescope we identified the need for wide field imaging with this telescope to make it an efficient surveying instrument. Although the use of larger bandwidths results in a better sensitivity (for continuum observations) of a telescope, it restricts the field of view of the image if the relative delays between the signals being correlated are not compensated. The loss in sensitivity at the edges of the field is appreciable if delays ( $\tau$ ) are comparable to the inverse of the bandwidth. This effect is known as bandwidth decorrelation.

To obtain interference free observations, we restrict the observing bandwidth to 1 MHz. This bandwidth does not pose a problem for synthesizing the primary beam in the RA direction which is  $2^\circ$  wide. However both the EW and the NS groups have wide primary beams in declination extending from  $-70^\circ$  to  $-10^\circ$ . We will, therefore, be concerned with compensating geometric delays for zenith angles along the meridian  $z_{a_0}$ . It can be shown that for a given delay compensation, we will be able to observe only a part of the sky with small decorrelation (less than 20 %). This is referred to as the delay zone around the point at which the geometrical delay has been compensated and is around  $15^\circ$  wide. To image the declination range  $-70^\circ \leq \delta \leq -10^\circ$ , using a 1 MHz band keeping the bandwidth decorrelation to less than 20 % even on the longest NS baseline, requires visibility measurements with four delay settings.

The existing system measures visibilities with only one delay setting. Thus one has to collect data for different delay zones on separate days. A minimum of 60 days of observing are needed to obtain the visibilities up to the 880 m spacing. We measure the visibilities on a given allocation for about 3 sidereal days to ensure interference free data. It therefore takes 180 days to obtain data for all the baselines. However, during this time the Sun moves through half the sky (12 hours in right ascension) thereby preventing full sky coverage with the 6 month data. We therefore carry out the observations in two rounds. In the second round we observe the same NS baselines after about 6 months interval. This ensures that we have night time observations for all the NS baselines. Measurement of visibilities with four different delay settings on separate days makes the total time required for acquiring data for the survey to be of the order of four years. This would make the

MRT a very inefficient surveying instrument.

We designed and built a recirculator system which allows us to measure visibilities with different delay settings in one observation schedule using the existing correlator. In the recirculator the digitised data is sampled at a slower rate (2.65625 MHz) stored in a dual buffer memory and the correlations are measured at four times this rate (10.625 MHz) using the existing correlator. To program the correlator system and the recirculator boards, and also to acquire data from the correlators, we designed and built a new data acquisition and a control system (DAS). This data acquisition system comprises of a double bank of memories shared by two PCs running on DOS. Details of the system design, installation, observations and imaging using the recirculator data are described in Sachdev (1999) ; Sachdev & Udaya Shanker (2001).

### 3.3. Observations

During the period from May 1994 to March 1999 more than 20,000 hours of astronomical observations have been carried out for the survey ( $\approx 2$  Tera-bytes of data). We have completed two rounds of observations on all the baselines. Analysis shows that we have 10,000 hours of observations, which we call class I data. This covers almost all allocations for all the 24 hours of sidereal time, when the Sun is at least 6 hours away from the meridian. Interference is found to be minimum during this time. This indeed shows that we have enough data for the completion of the survey. Details of data archiving are given in the contribution entitled full resolution images from the MRT in this volume.

### 3.4. Interference

Apart from its strategic geographic location, Mauritius was chosen as the site for the new telescope as the island was also considered a paradise for low frequency astronomy due to its interference-free environment. Due to the industrial growth in Mauritius it is no more an interference-free site. This has confirmed the general belief that totally interference-free site may be a thing of the past, especially at low frequencies. In Mauritius the band around 150 MHz is not a primary allocation for radio astronomy. The Government of Mauritius has allocated only a 1 MHz band from 150 MHz to 151 MHz and not the band from 150.05 to 153 MHz, generally allocated to radio astronomy ( Handbook On Radio Astronomy,1995). Emission from a new communication facility operating at 149 MHz, spills into the protected band making it unusable for radio astronomy. There is also interference from unidentified satellite(s) in this band. The front end of the receiver system has been built with sufficient bandwidth so that the observing frequency can be shifted (within 145-155 MHz) to an interference free zone by tuning the LO. The 1 MHz band around 151.5 MHz has been found to be relatively quiet and is therefore presently used for observations. Since this is not a protected band in Mauritius, an application for protection of this frequency has been made

to the Government of Mauritius.

We measure the visibilities on a given allocation for about 3 sidereal days to ensure interference free data for the survey. In addition a technique to detect man-made interference in the visibility data has been developed. This technique is based on the understanding that the interference is generally 'spiky' in nature and has Fourier components beyond the maximum frequency which can arise from the radio sky and therefore can be identified. We take the sum of magnitudes of visibilities on all the baselines measured at a given time. This gives a single time series to detect interference in the place of 512 visibilities measured. Assuming that the interference affects all the baselines similarly, the incoherent summation of the visibilities also improves the detectability of the interference. The sum of the visibility magnitudes is then high-pass filtered to get a time series from which the contribution of the sky is removed. Interference is detected in the high-pass data using an iterative scheme. In each iteration, interference with amplitudes beyond a certain threshold are detected. These points are then removed from the original time series and the resulting data is high-pass filtered and the process repeated. The raw data is not modified by the interference detection programs. The right ascension of the detected points are stored in a file and this information on interference is used in the subsequent calibration and imaging programs. We have also studied the statistics of the strength, numbers, time of occurrence and duration of the interference at the MRT. They indicate that most of the interference have strengths less than  $100\sigma$  ( $\approx 85\%$ ). The interference is largely during the day (MST 8-15 hours) and is linked to the local industry. A large fraction  $\approx 80\%$  of the interference occur for durations less than 6 seconds. There are generally less than 20 instances in the full 24 hours when the interference lasted 6 consecutive seconds. This indicates that very often the interference excision can be carried out while post integrating the visibilities by giving a zero weighting to the interference points. The level of undetected interference is of the order of the noise in the final image. This, in terms of flux density is  $\approx 100$  mJy.

### 3.5. MARMOSAT

The visibilities measured are processed off-line using MARMOSAT, the MAuRitius Minimum Operating System for Array Telescopes ( Dodson 1997) . This is designed in-house to transfer the visibilities to images which can be ported to standard astronomical image processing softwares such as AIPS. The programs in MARMOSAT cater to the following needs: gives an on-line view of the data recorded and offers facilities to view phase, magnitude, closure errors, fringe frequencies, signal-to-noise ratio, mean and scatter of the visibilities measured. This helps to detect gross errors quickly. The programs also cater to the determination of complex gain of the antennas, position calibration of the antennas, combining data of different days, transforming the visibilities to get brightness distribution. Further details of these programs are given by R. Dodson ( Dodson 1997). In its configuration, the method of observation and data analysis, the MRT cannot be categorised as one belonging to the telescopes else where in the world. This partly compelled us to take up the development of programs in-house. This resulted in a number of simple innovations which have

helped in improving the quality of the images. Antenna calibration is one such crucial area and is described in the next subsection.

### 3.6. Antenna calibration

The complex gains of the antennas are estimated using the measured visibilities for the sources MRC0915-119, MRC1932-464 and MRC2211-173. The sensitivity per baseline is 30 Jy for an integration time of one second. In the  $2^\circ$  (approximately 8 minutes of time) EW-group primary beam, the above sources are observable in each baseline with a minimum Signal to Noise Ratio (SNR) of about 35. There is a paucity of strong sources in the southern sky required for reliable calibration. This leaves us with a situation where we can calibrate the array only a few times in a sidereal day. Thus it is important to ensure that the receiver system has good phase stability. The instrumental phase is estimated by taking the difference between the phase of the observed visibilities and the expected phase due to the point source calibrator (or calibrators). The instrumental gain is estimated by measuring the relative amplitudes of the fringes on different baselines. We have found that the day-to-day RMS variation per baseline in phase is about  $\pm 7^\circ$  and the RMS amplitude variation is about  $\pm 0.1$  dB. The RMS variation of phase from one calibrator to another (eg. MRC1932-464 and MRC0915-119) is about  $\pm 10^\circ$ .

The following steps taken in the calibration process have enhanced the quality of the images.

- The last group of the East array (E16) is fed to the correlator in the place of the 16<sup>th</sup> trolley. This gives a set of baselines formed between E16 and the E-W array on all observing days. This helps to check the repeatability of data. These baselines with each trolley give 31 independent closure information which are used in the calibration. This mode of observing reduces the number of usable trolleys to only 15.
- Satisfactory calibration cannot be obtained for short baselines, where there are less than two fringes in the EW-group beam due to the calibrator. This is tackled at MRT by calculating 47 antenna complex gains from the measured complex visibilities. At this stage we reject those baselines with short EW components (essentially the first four E and W group outputs with the S array) and input the closure information obtained from the step 1.
- The recirculator system can configure the correlator in the  $(E + W) \times E$  and  $S \times S$  modes for one integration time (roughly 100 ms in every second of data collection). Since both EW and S arrays are linear, this mode provides visibilities on several redundant baselines to calibrate the array using the Redundant Baseline Calibration technique. Software development to take advantage of observations carried out in this mode is under development.
- Instead of using a single source calibration we need to do a 'field of view' calibration which would take into consideration contribution of several sources in the field of view. The paper on Full resolution images from MRT in this volume (Pandey *et al*) touch upon this aspect.

- Due to paucity of strong sources we have not been able to calibrate the visibilities measured with different delay settings. Using the receiver configuration we have devised a procedure (Sachdev 1999; Sachdev & Udaya Shanker 2001) for estimating the instrumental phase in the four delay zones using a calibrator in only one of the delay zones. This needs information about the centroids of the bandpasses of each baseline. We measured the bandpasses and estimated the variation in the centroids of the bandpasses of the 512 baselines used for imaging. We have established that variation causes only a 5 degree RMS error in the instrumental phase calibration. Thus the hardware at MRT allows high dynamic range imaging ( $\approx 1000$ ).

### 3.7. Transforming Visibility To Brightness distribution

The sampling of the visibilities on the EW grid is at intervals equal to the size of each EW group. This gives grating responses which fall on the nulls of the primary beam while synthesizing on the meridian. For synthesis away from the meridian, one of the grating response starts moving into the main lobe of the primary beam. This leads to the synthesized beam being a function of the hour angle. To simplify matters, imaging is presently done on the meridian only. The scanning in right ascension is provided by the motion of the earth.

The  $u, v$  coverage of MRT (EW and the NS components of the baseline) can be thought of as a pleated sheet, extended in both  $u$  and  $v$ , with discrete steps in  $w$  (height) as we move from one EW group to the one at a different height. As we are imaging a very large field of view ( $60^\circ$  field), the approximate coplanar approach, wherein the phase term due to the heights is assumed to be a constant over the synthesized field of view, is invalid. Thus for MRT, an equivalent of a 3D imaging method is required.

At MRT we transform the measured visibilities using a Fast Fourier Transform (FFT) along the regularly sampled  $v$  axis, apply a Direct Fourier Transform (DFT) along the  $w$  axis and finally sum along  $u$  to obtain the image on the meridian. A DFT on  $w$  is required as the sampling in  $w$  is not uniform. The direct transform corrects every term along the zenith angle on the meridian for the group heights. This is equivalent to declination dependent phasing of the groups to a common (and artificial) 2D plane. A detailed discussion on the problem of non-coplanarity specific to MRT is described else where in this volume (N.Oozeer & Udaya Shankar 2001).

Imaging on the meridian permits a maximum integration time of 16s, with one observation schedule. This is not enough to achieve the confusion limit. To improve the sensitivity, so that the noise in the images can reach the confusion limit, we need to image the full  $2^\circ$ , the FWHM of the beam of east-west groups. Imaging away from the meridian would require a deconvolution scheme to take into account the variation of the synthesized beam with hour angle. Software development to carry out two dimensional synthesis using MRT data is under progress.

## 4. Results

### 4.1. A Low Resolution Survey

We are processing the available data to make a low resolution survey of the sky. Observations, up to a baseline of 178 m along the S arm, do not require the recirculator. We have taken this as a natural cutoff and have made low resolution images using only the eight central groups of the EW arm and trolley positions up to 178 m in the S arm. A part of the survey covering the RA range 18:00 to 24:00 hrs and 00:00 to 05:00 hrs has been completed.

The survey has a resolution of  $13' \times 18' \sec(\delta + 20.14^\circ)$ . MRC1932-464, with a flux density of 81 Jy/beam was used as the primary flux calibrator (Golap, 1998). The expected RMS noise in the images due to contributions from the confusion and receiver noise (for a 1 MHz bandwidth with an integration time of 19 seconds) are expected to be 0.7 Jy. The noise seen on the map is 0.8 Jy and is very close to the expected value.

This survey has a resolution comparable with the 408 MHz survey of Haslam et al. (1982) and the 34.5 MHz survey of the GEETEE (Dwarakanath and Udaya Shankar, 1990). Hence this will provide a valuable data base to study the spectral indices of the Galactic radio continuum emission between 408 MHz, 150 MHz and 34.5 MHz. Most Supernova remnants in our Galaxy have been discovered from their radio emission and for majority of them this remains the only means of studying them. This survey can contribute in the identification of large diameter faint SNRs, especially far from the Galactic plane. We also hope to identify a few new Galactic loops.

We have detected around 900 sources with flux densities above 3Jy/beam level in the low resolution survey. Many of them have been identified with Molongolo (Large *et al* 1981) and Culgoora sources (Slee 1977).

Apart from the scientific motivation, one of the main reasons for making low resolution images is to develop techniques for imaging with a non-coplanar array like MRT. The main outcome of the low resolution survey is the development of an algorithm for deconvolving the MRT images. The Point Source Function (PSF) of a non-coplanar array like MRT is declination dependent. We have developed an algorithm to transform the PSF estimated at one declination to the PSF at any other declination. This has enabled us to deconvolve the MRT images made by restricting ourselves to simple cleaning algorithms.

### 4.2. SNRs associated with young Pulsars

A group of known supernova remnants which are possibly associated with pulsars were selected as one of the most interesting studies which could be done with the MRT. The MRT with its completely filled  $uv$  coverage, low frequency of operation, and its southern declination is ideally suited to investigate the associations. The filled  $uv$  coverage gives it a much higher large scale surface brightness sensitivity. The lower frequency results in higher sensitivity to

non-thermal radiation. It's southern declination is an ideal location for observing the direction towards the Galactic centre where the majority of these associations are to be found. The associations of G5.4-1.2 with PSR 1758-23, G8.7-0.1 with PSR 1800-21, G315.4-2.3 with SN 185, G320.4-1.2 with PSR 1509-58, G343.1-2.3 with PSR 1706-43 were investigated. In combination with the images made by MRT the publicly available X-ray data and published images with other frequencies conclusion about associations were drawn. The study indicate that the most of the supernova remnants studied are associated with the pulsars or the proposed associations can be maintained . Details are given in Dodson (1997).

### **5. A Study Of The Low Spatial Frequency Response Of MRT**

Radio images made with the aperture synthesis telescope often do not contain low spatial frequencies. This is because short baselines suffer from problems of mutual coupling and do not get calibrated correctly. In addition short baselines also respond to extended emissions around the calibrators, there by violating the assumption that the calibrators are point sources. At MRT the array and receiver system have been designed to measure base lines down to zero spacing (except one metre and two metre along north-south) and the calibration scheme avoids the short baseline visibilities to derive antenna phases. In order to check the calibration of the low spatial frequency of MRT the region around the galactic centre was imaged at 150MHz using one of the GMRT dishes. GMRT is an aperture synthesis array consisting of 30 fully steerable parabolic dishes of 45m diameter each (Swarup *et al* 1991). The idea was to compare the images at the same frequency made with the MRT array and a single dish which does not suffer from the problem of mutual coupling. The study indicated that the calibration of the low spatial frequencies at MRT is satisfactory. This demonstrated the effectiveness of the antenna calibration scheme used at MRT. The study also led to the development of a procedure to generate a composite map in which the low spatial frequency information from GMRT can be fused with high spatial frequency measurements from MRT. See Katwaroo (1997) for details. The procedure developed for fusing the low spatial frequency data from a single telescope with the high spatial frequency data from a synthesis telescope will enable us to carry out a survey using MRT with a proper calibration of all the spatial frequencies.

### **6. Present Status**

The present status of the survey and other observational programmes at the observatory are described in other contributions on MRT in this proceedings.

## 7. Acknowledgments

We thank V. Radhakrishnan for his interest and encouragement from the initial stages of the project. We also thank N. Kumar, RRI and Mohammedbhai, UOM and R.Cowsik, IIA for their continued support. We gratefully acknowledge M. Modgekar, C.M. Ateequlla and H.A. Aswathapa from the Raman Research Institute, R. Somanah and N. Issur from the University of Mauritius and G.N. Rajashekar from the Indian Institute of Astrophysics for their efforts in this project. We thank all those from the Raman Research Institute, Indian Institute of Astrophysics, and the University of Mauritius who have contributed towards this project.

## REFERENCES

- Baldwin, J. E., Boysen, R. C., Hales, S. E. G., Jennings, J. E., Waggett, P. C., Warner, P. J., and Wilson, D. M. A., 1985, *MNRAS*, **217**, 717.
- Dodson, R.G., "*The Mauritius Radio Telescope And A Study Of Selected Supernova Remnants Associated With Pulsars*". PhD thesis, University of Durham, 1997.
- Dwarakanath, K.S., Udaya Shankar, N., 1990, *J. Astrophys. Astr.*, **11**, 323.
- Erickson, W. C., Mahoney, M. J., and Erb, K., 1982, *ApJS*, **50**, 403.
- Golap, K., "*Synthesis Imaging at 151.5 MHz using the Mauritius Radio Telescope*". PhD thesis, University of Mauritius, 1998.
- Golap, K., Udaya Shankar, N., Sachdev, S., Dodson, R., Sastry, Ch. V., 1998, *J. Astrophys. Astr.*, **19**, 35.
- Handbook On Radio Astronomy, 1995, Radiocommunication Bureau, Geneva.
- Haslam, C.G.T., Salter, C.J., Stoffel, H., Wilson, W.E., 1982, *Astron. Astrophys. Suppl. Ser.*, **47**, 1.
- Katwaroo, M., "*A study of the low spatial frequency response of the Mauritius Radio Telescope and a test for isothermality in a few HII regions*". M.Phil thesis, University of Mauritius, 1997.
- Large, M. I., Mills, B. Y., Little, A. G., Crawford, D. F., and Sutton, J. M., 1981, *MNRAS*, **194**, 693.
- Mills, B.Y., Slee, O.B., Hill, E.R. 1958, *Aust. J. Physics.*, **11**, 360.
- Oozeer, N., Udaya Shankar, N., 2001. *Submitted to UN-ESA proceedings, 2001.*
- Pandey, V.N., Somannah, R., Udaya Shankar, N., 2001. *Submitted to UN-ESA proceedings, 2001.*
- Reber, G. 1944, *Astrophys. J.*, **100**, 279.
- Sachdev, S., "*Wide field Imaging with the Mauritius Radio Telescope*". PhD thesis, University of Mauritius, 1999.

Sachdev, S., Udaya Shankar, N., 2001. *J. Astrophys. Astr.*, **22**, 229.

Slee, O.B., 1977, *Aust. J. Physics. Suppl*,**43**, 1.

Swarup, G., Ananthkrishnan, S., Kapahi, V.K., Rao, A.P., Subrahmanya, C.R., Kulkarni, V.K., 1991, *Current Science*,**60**, 95.

Thompson, A. R., Moran, J. M., Swenson, G. W. Jr. "*Interferometry and Synthesis in Radio Astronomy*". John Wiley and Sons, 1986.

# Full Resolution Images From The Mauritius Radio Telescope

V.N.Pandey<sup>1</sup>, Radhakrishna Somannah<sup>2</sup>, N. Udaya Shankar<sup>1,2</sup>

<sup>1</sup>*Raman Research Institute, Sadashivanagar, Bangalore 560080, India*

<sup>2</sup>*Department of Physics, University of Mauritius, Reduit, Mauritius*

## ABSTRACT

The first set of full resolution images have been made using the Mauritius Radio Telescope (MRT) for the Right Ascension range 18:00 to 19:00 hours and the declination range  $-70^\circ$  to  $-10^\circ$ . This is a part of the southern sky survey at 151.5 MHz being carried out using the MRT. To minimise the effect of bandwidth decorrelation, the images are made from the visibilities recorded with four different delay settings. This paper discusses three key issues of data analysis for the survey: Selection of good data for the survey, detection and removal of interference in the images and, preliminary analysis of these images.

## 1. Introduction

Very few surveys of the southern sky exist at frequencies below 1 GHz, and none which are as deep as the 6C survey of the northern sky (Baldwin *et al.* 1985). The MRT was built to fill the gap in the availability of deep sky surveys of the southern sky at low frequencies. It is a T shaped Fourier synthesis instrument operating at 151.5 MHz and is situated in the north-east of Mauritius at a southern latitude of  $20^\circ.14$ . The main objective of a survey using the MRT is to contribute to the database of southern sky sources in the declination range  $-70^\circ \leq \delta \leq -10^\circ$  covering the entire 24 hours of Right Ascension (RA), with a resolution of  $4' \times 4'.6 \text{ sec}(\delta + 20^\circ.14)$  and a point source sensitivity of  $\sim 200 \text{ mJy}$  ( $3\sigma$  where  $\sigma$  is the RMS noise in the image). This telescope is also expected to image large scale structures and low-surface brightness features in the southern sky, with its coverage of short baselines down to zero-spacing. The details of the telescope can be found in Golap *et al.* 1998; Udaya Shankar 2001.

### 1.1. Imaging with the MRT

To obtain maximum interference free observations at MRT, we use a bandwidth of 1 MHz. Although the use of larger bandwidths results in better sensitivity of a telescope, it restricts the angular range over which an image can be made if the relative delays between the signals being correlated are not compensated. To keep the bandwidth decorrelation for a bandwidth of 1 MHz to less than 15% even for the longest baselines for the entire declination range  $-70^\circ$  to  $-10^\circ$ , baselines

longer than 178m in the North South (NS) direction are measured with a maximum of four delay settings (Sachdev 1999; Sachdev and Udaya Shankar 2001). Each delay setting is most suitable for imaging a different range of declination, known as zones which are given in Table 1.

Zone I	$-10^\circ < \delta < -26^\circ$
Zone II	$-22^\circ < \delta < -38^\circ$
Zone III	$-34^\circ < \delta < -54^\circ$
Zone IV	$-46^\circ < \delta < -70^\circ$

Table 1: Declination zones used at MRT

The visibilities measured are processed off-line using the MAuRitius Minimum Operating System for Array Telescopes (MARMOSAT) (Dodson 1997). This is designed in-house to transfer the visibilities to images which can be ported to Astronomical Image Processing System (11) (AIPS)<sup>1</sup>.

The programs in MARMOSAT cater to the following needs: Selection of good data for the survey, detection of interference, calibration of the array, position calibration of antennas, transforming the visibilities measured to get a dirty image which is the true brightness distribution convolved with the Fourier transform of visibility sampling function also called the Point Spread Function (PSF), combining different day's of images taking into consideration the relative antennae gains on different days, the analysis of dirty images and their deconvolution. At MRT presently we carry out imaging restricted to the meridian. The two-dimensional image is the time stack of one-dimensional images on the meridian.

The present paper focusses on the following data processing steps.

- (a) Selection of good data for the survey.
- (b) Analysis of one day's images, which includes, detection of interference not detected in the first round and estimating the relative antennae gains on different days.
- (c) Preliminary analysis of the Images.

The steps (a) and (b) have been refined recently to make data processing more efficient and step (c) describes the new results.

## 2. Selection of good data for the survey

### 2.1. Data Organisation

During the period from May 1994 to March 1999 more than 20,000 hours of astronomical observations have been carried out for the survey. At MRT we have 1024 fixed helices in the

---

<sup>1</sup>The AIPS is a software package for calibration, data analysis, image display, plotting, and a variety of ancillary tasks on Astronomical Data. It comes from the National Radio Astronomy Observatory.

East-West (EW) arm which are arranged in 32 groups of 32 helices each. The south (S) arm consists of 15 movable trolleys each having 4 helices, which move on a 880m long rail. To measure visibilities up to 880m spacing, with a 1m spacing we require 60 allocations. Allocation refers to the placement of the 15 trolleys on a given sidereal day. In each allocation observations are carried out for a minimum period of three days (Sachdev 1999; Sachdev and Udaya Shankar 2001). This ensures that we have good data, sufficient for imaging even if one has to discard data due to several factors such as man made interference, Sun affecting the observations and unexpected instrumental failures. At MRT to facilitate data handling, and automation of data processing, the data is organized in hourly (Local Sidereal Time - LST) files.

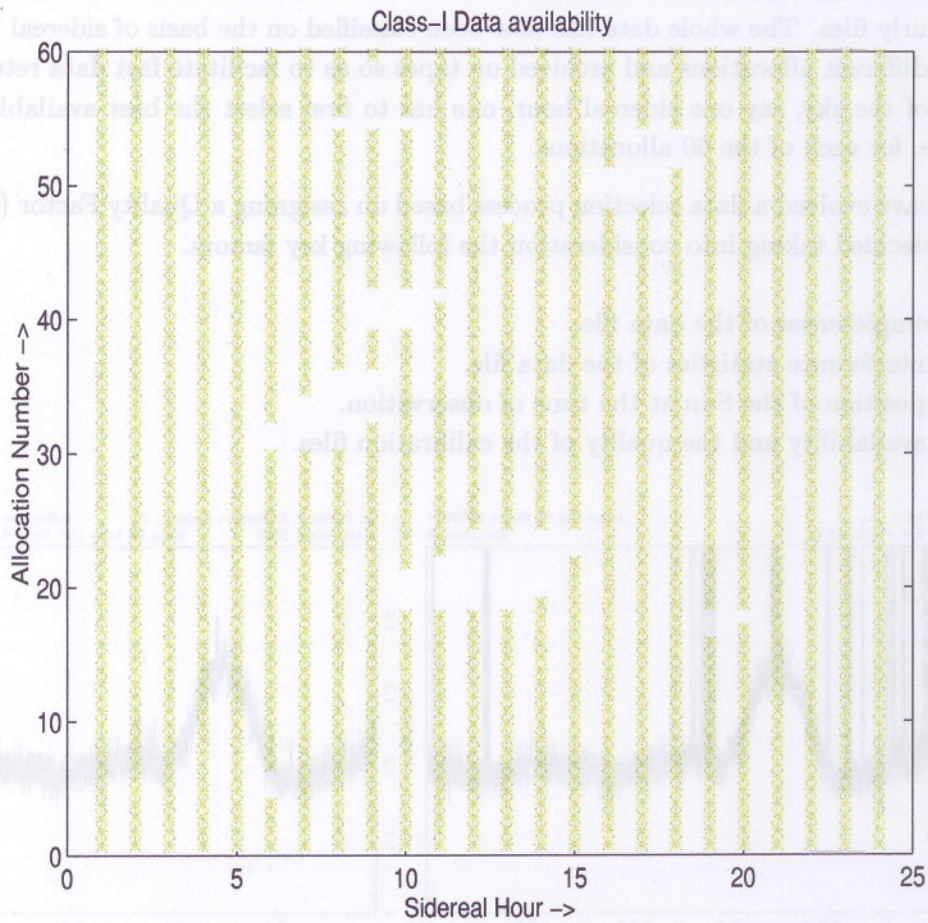


Fig. 1.— The figure shows the availability of Class-I data for different allocations & sidereal hours (denoted by a \*). There are a few gaps which can easily be filled by Class-II data.

A simple statistical analysis was carried out on the available data to get an estimate of the quality of data. Since night time observations are generally found to be interference free and also have minimum interference from Sun, it is classified as Class-I data. Class-I refers to a data file

observed when the Sun's Right Ascension is 6 hours farther than the Local Sidereal Time. Figure 1 shows the result of the analysis. It is clear that there is at least one Class-I data file, for most of the 60 allocations for each sidereal hour. There are very few gaps which can be easily filled by the Class-II data, where Class-II refers to a data recorded when Sun's RA is 3 to 6 hours away from the LST. Similarly we have Class-III and Class-IV data which refer to data recorded when Sun's RA is 2 to 3 hours and less than 2 hours away from LST respectively. The figure 1 indicates that data set for the survey is indeed complete.

## 2.2. Data selection

Data base for 20,000 hours of observations are stored as and when the observations are carried out in hourly files. The whole data has now been classified on the basis of sidereal hour of observations for different allocations and archived on tapes so as to facilitate fast data retrieval. To image a region of the sky, say one sidereal hour, one has to first select the best available data from the data base, for each of the 60 allocations.

We have evolved a data selection process based on assigning a Quality Factor (QF) to the data which is decided taking into consideration the following key factors.

- (i) The completeness of the data file.
- (ii) The interference statistics of the data file.
- (iii) The position of the Sun at the time of observation.
- (iv) The availability and the quality of the calibration files.

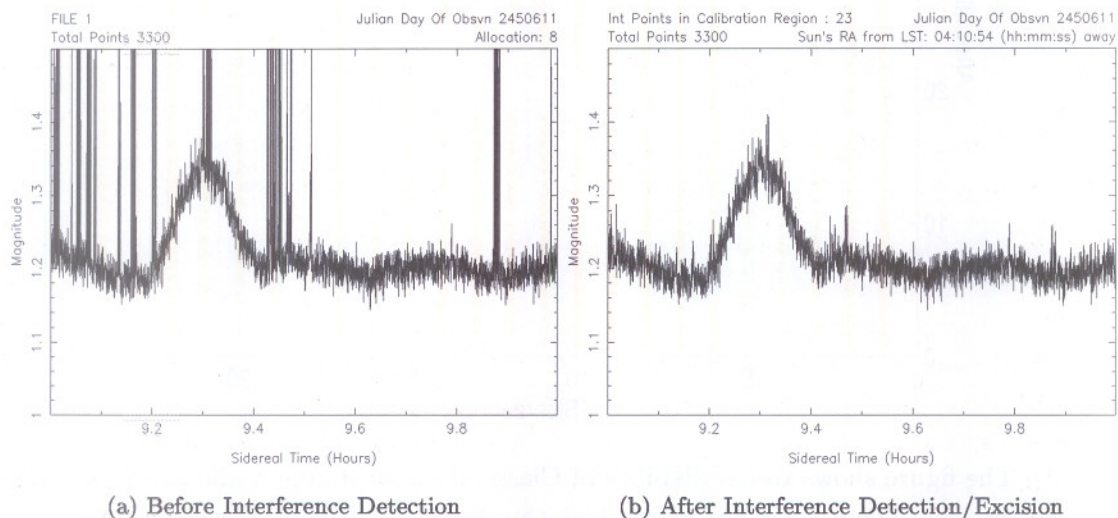


Fig. 2.— This figures 2(a) and 2(b) show the sum of magnitudes of visibilities on all the baselines for a given allocation plotted versus Sidereal Time, before and after detection/excision of interference. There are 155 interference points in this observation file having 3300 points. The interference points are a few, and are of short duration. This is an example of an acceptable data file for imaging.

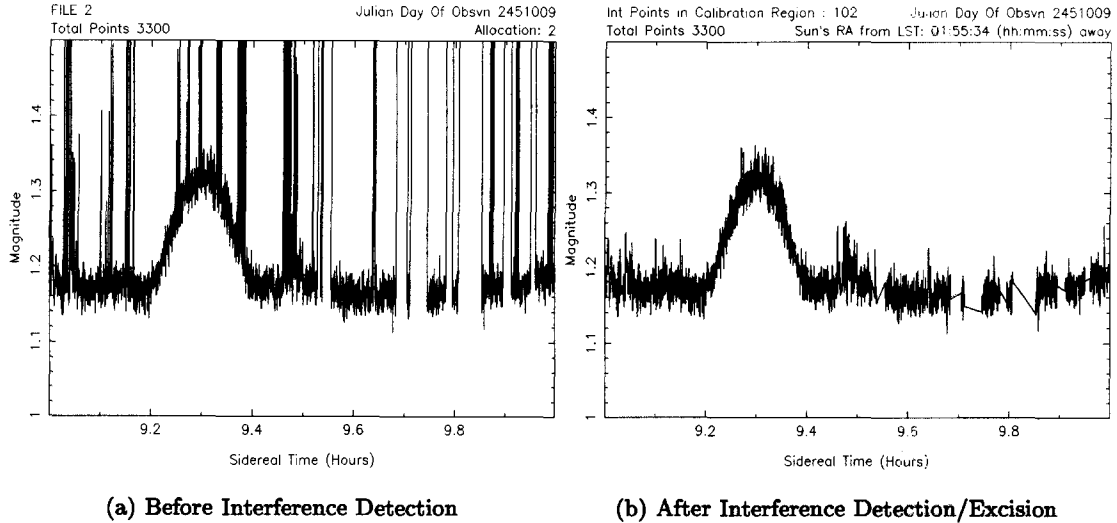


Fig. 3.— There are 700 interference points in this observation file. The interference points are many, and are of long duration. This is an example of an unsatisfactory data file for imaging.

To image one sidereal hour for the entire declination range we need good data in four delay zones. For selection of good data we assume that the interference affects the visibilities measured with four delay settings similarly. In other words the interference is narrow band and is correlated in the visibility measurements with all the four delay settings. So we use only one zone for data selection. We consider the declination zone which has the maximum number of sources as per the Molongolo Radio Catalogue (MRC) (Large *et al.* 1981), to select data for each sidereal hour.

- The first step while assigning a QF to the data file is to check for the completeness of the data. This checks for uninterrupted observation during the sidereal hour to be imaged. The interruption is generally due to mains power supply failures and occasionally due to instrumental failures. We give least priority to the data which is interrupted once or more.
- The interference detection program (Sachdev & Udaya Shankar 2001) sums the magnitude of visibilities on all the baselines and detects interference points in the sum of visibility domain. The program writes down the RA values at which the interference occurs. The number of interference points in this file is a first order indication of the quality of the data. Data with short duration interference stretches is preferred to data with long duration interference stretches. Figures 2 and 3 show the sum magnitudes of visibilities on all the baselines for a given allocation plotted versus Sidereal Time, before and after interference detection for two data files. Data shown in Figure 2 is considered as good data while data shown in Figure 3 is considered as bad data and is not satisfactory for imaging.
- At MRT generally night time observations are interference free and are most suitable for imaging. Data recorded when Sun's RA is 6 hours farther than Local Sidereal Time (LST) of observation is preferred over the data in which the Sun is closer.

Due to paucity of strong sources in the southern sky, we have very few calibration sources. At MRT we use MRC 0915-118 and MRC 1932-464 having flux densities of 252.5 Jy and 94.5 Jy respectively at 151.5 MHz as calibrators. For getting the QF of the calibration files the observations of these calibrators are passed through the above three stages of check. We use only 8 min of observations around the transit time of the calibrator for calibration. Thus only 8 min of data in these observations are passed through the quality checks. First we assign QF to all the calibration files. This information is later used to select good data. Calibrator which is closest to the sidereal hour imaged is preferred for calibration.

### 2.3. Assignment of Quality Factor (QF)

We have evolved a scheme to classify all the data files based on QF ranging from 1 to 10. QF 1 refers to best quality data while QF 10 refers to data of poor quality. We assign QF to a data file based on the following methodology. A QF of 1 is assigned to a file of Class-I category, which is complete and has no interference. An incomplete file is given a QF of 10. Generally a file having QF up to 5 is considered satisfactory for imaging. The assignment of QF shown in Table 2 is based on the experience of the distribution of quality of data in the MRT survey.

Quality Factor (QF)	Completeness of file (Y/N)	Number of Interference points	Maximum duration of Interference (secs)	Class (I-IV)
1	Y	0	0	I
2	Y	0	0	II
3	Y	<100	<16	I,II
4	Y	100-300	<16	I,II
5	Y	<300	<16	III
6	Y	300-600	<16	I,II,III
7	Y	<600	>16	I,II,III
8	Y	<600	-	IV
9	Y	>600	-	I,II,III,IV
10	N	-	-	I,II,III,IV

Table 2: Assignment of Quality Factor.

The data selection process at MRT is accomplished automatically with little manual intervention through a *Perl* program. Perl (Larry *et al.* 2000; Srinivasan 1997) is an Object Oriented and a cross platform language which is portable across various operating systems. Perl supports referencing but does not directly support addressable pointers. This enables easy construction of complex data structures without dangers inherent in pointer arithmetic. Structured Query Lan-

File Name	46a255r1.kr4
Date Of Observation	21:06:1996
Julian Day	2450255
Allocation	46
Sidereal Hour	17-18
Zone	4
Total No. Of Data Points	3306
Completeness	Y
Total No. Of Interference Points	120
Class	I
Maximum Duration Of Interference	9
QF Assigned To The Data File	4
QF Of Calibration File (MRC 1932-464)	2
QF Of Calibration File (MRC 0915-118)	5

Table 3: The details the data selection software outputs for all the observation files.

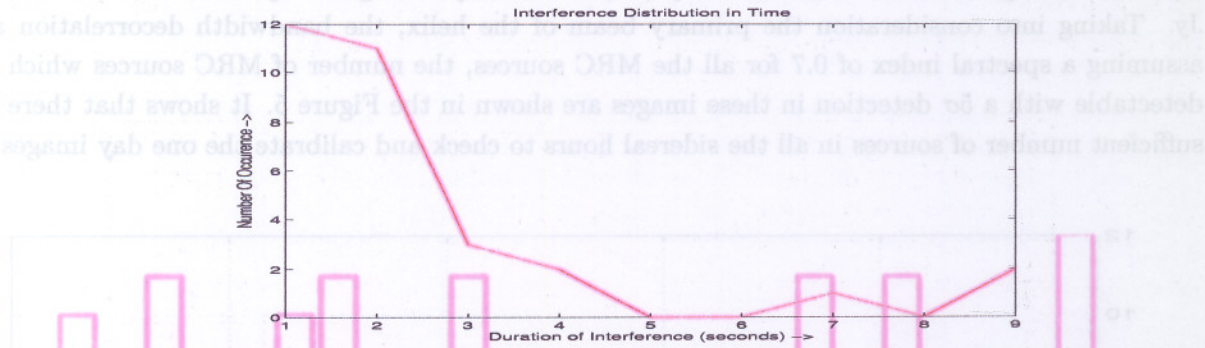


Fig. 4.— Plot shows the distribution of duration of interference. X axis shows the duration in secs for which interference is continuous and Y axis shows the number of occurrences of such an interference during the sidereal hour of observation.

guage (SQL) evaluation, and template driven code generation are its inherent features which make it a very powerful language. Also its standard library comes with comprehensive eXtensible Mark Language (XML) support and Graphical User Interface (GUI) apart from long list of support modules. Perl has provision for embedding C code inside a Perl program and one can also embed a Perl code inside a C program with support of modules, which makes it very useful for MRT where most of the software has been written in C. Perl provides excellent text support, is fast and is freely available. Due to these features Perl was a natural choice for writing the data selection software. The code for data selection program runs to  $\approx 3000$  lines.

This data selection software at MRT has made the data selection process objective, efficient and fast with little manual intervention and results in the best choice of data for imaging. The user has been assigning the quality factor manually for the data based on the above mentioned

criteria. The data selection program gets all the details required automatically and outputs a table (Table 3). In addition the program also displays a plot of sum of magnitudes of visibilities for all the baselines, versus sidereal time (as in Figures 2 and 3). The program also gives a plot of the graph of the number of times an interference of a given duration occurs (Figure 4) .

The data is prioritised based on the QF of the data file and of the Calibration file. Also in case more than one very good data file is available for the same allocation and sidereal hour one can use all of them for imaging to improve the Signal to Noise Ratio.

### 3. Analysis of Images.

As a first step towards the survey we made full resolution images covering the RA 18:00 to 19:00 hrs and the entire declination range  $-70^\circ$  to  $-10^\circ$ . Since the observations span almost a five year time period, after making images for different allocations (each day's image), the images are precessed to a common epoch (*Epoch 2000*) and regridded to a common grid. Then we analyse each day's image in detail. The sensitivity ( $1\sigma$ ) of each day's image is expected to be around 1.25 Jy. Taking into consideration the primary beam of the helix, the bandwidth decorrelation and assuming a spectral index of 0.7 for all the MRC sources, the number of MRC sources which are detectable with a  $5\sigma$  detection in these images are shown in the Figure 5. It shows that there are sufficient number of sources in all the sidereal hours to check and calibrate the one day images.

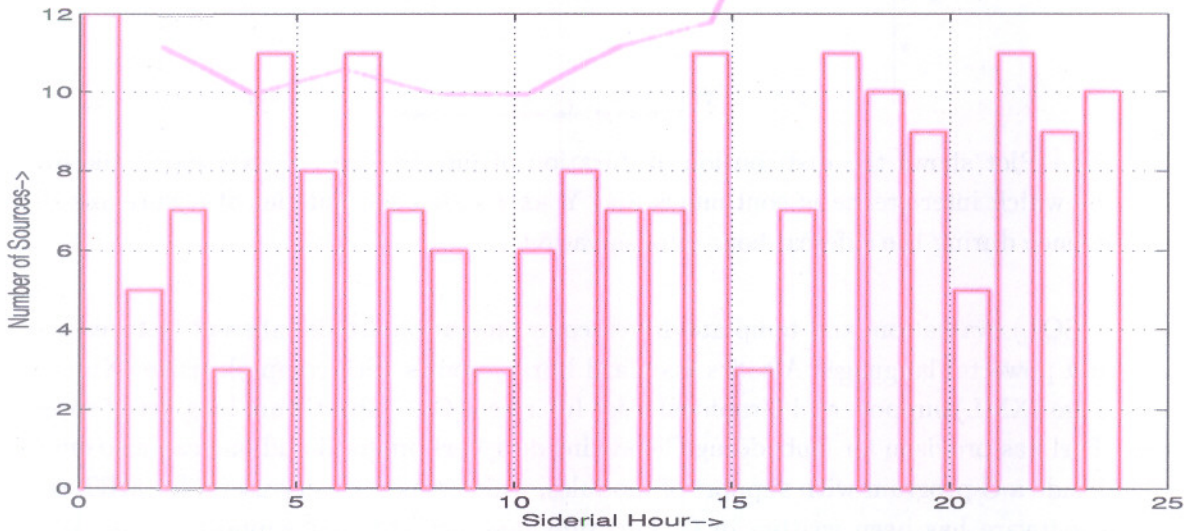


Fig. 5.— The figure shows the number of MRC sources in different sidereal hours which can be detected with a minimum Signal to Noise Ratio of 5 in each day's image.

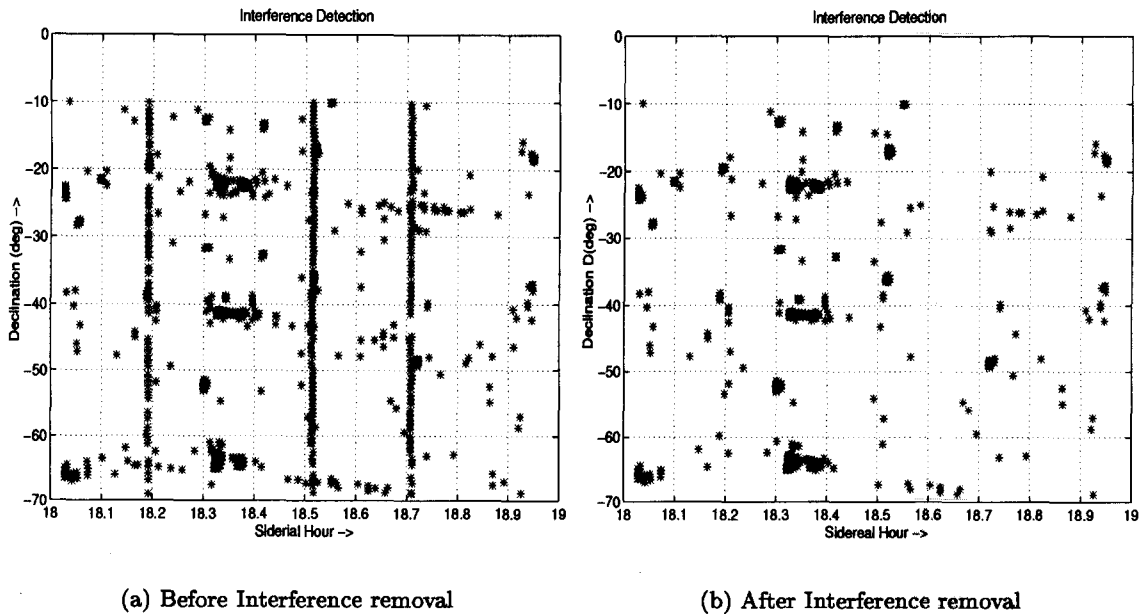


Fig. 6.—  $5\sigma$  points for a given allocation image before and after interference removal.

### 3.1. Interference Detection

Detection of man made interference and estimation of relative antennae gains on different days are two main steps in the analysis of the images.

We detect all the points above  $5\sigma$  ( $\sigma$  is RMS noise) in each day's image. We plot sidereal hour and declination of these points. Figure 6 shows such a plot for one of the images. Since the interference is generally correlated on all the baselines, it appears at a given RA in most of the points in declination. Thus interference appears as a strip running along declination in the plot. These points are noted and flagged in the images respectively. We regenerate these plots after flagging these interference points. We find the maximum value in the map and enclose a region around it. We find all the maximas above  $5\sigma$  in the map excluding the regions enclosed by the previous peaks found. Figures 6(a) and 6(b) show the  $5\sigma$  points before and after interference removal.

A single plot of all the  $5\sigma$  points after regeneration is made for all the 60 images. A sample plot is shown in the Figure 7. A source of sufficient strength which can be detected in each day's image appears as clusters in this plot. A source rather than appearing as a single cluster in this plot appears in more than one cluster along the declination due to the grating response. In each allocation the trolleys are spread out with a  $3\lambda$  ( $\lambda$  is wavelength) spacing along the S rail. This causes grating response. We use MRC catalogue and confirm each of these detections. We discard

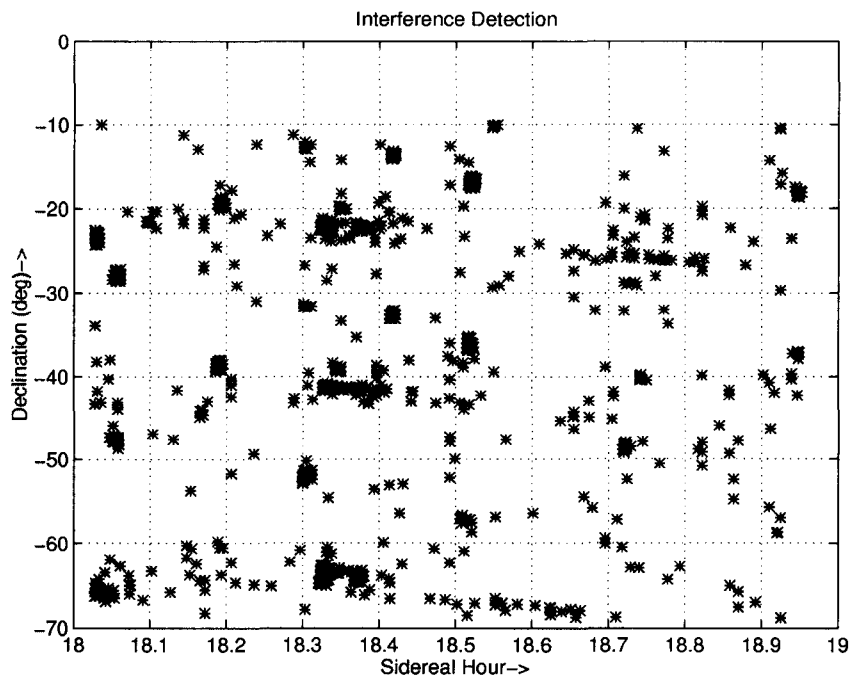


Fig. 7.—  $5\sigma$  points in all the 60 allocation images after interference removal. One Notes clusters at places of strong sources, as these sources show up above  $5\sigma$  in each of the images.

images which do not show the sources expected. We ensure that a data file is not rejected in case the expected source is flagged as an interference. We also notice that there are isolated individual points. If these points are found to be above a threshold value say  $10\sigma$  these are flagged.

At each RA and declination of the sources detected we do one dimensional fits along RA and Declination for the expected beam of the array in each allocation. This fit enables us to estimate the complex gain for the images on each day. This is taken into consideration while adding images of different days.

#### 4. Preliminary Analysis

A dirty image with the RA range 18h06m to 18h48m and the declination  $-56^\circ$  to  $-48^\circ$  is shown in Figure 8. This represents the zone four image. In this paper we have given only a small portion of the image made. The contour levels are 0.3, 1.4, 2.0, 2.8, 3.4, 4.3, 6.0, 8.4, 12.0, 17.0, 24.0, 35.0, 48.0 Jy/beam. We have been able to detect 17 out of 18 MRC sources present in this field with a  $5\sigma$  detection. The strongest source being MRC1814-519 (J2000-18:18:06,-51:58:09) and the weakest being MRC1802-535 (J2000-18:06:57,-53:32:41) having flux densities of 28.5 Jy and 1.6 Jy at 151 MHz respectively. Detailed analysis of the images to estimate the flux densities, positions, Signal to Noise Ratio of detection and number of sources in the field of view are under progress. The method developed at MRT to deconvolve these images are discussed in a separate paper in this conference entitled "Limitations Of Tangent Plane Approximation For Wide-Field Imaging Using The Mauritius Radio Telescope" by Oozeer & Udaya Shankar 2001.

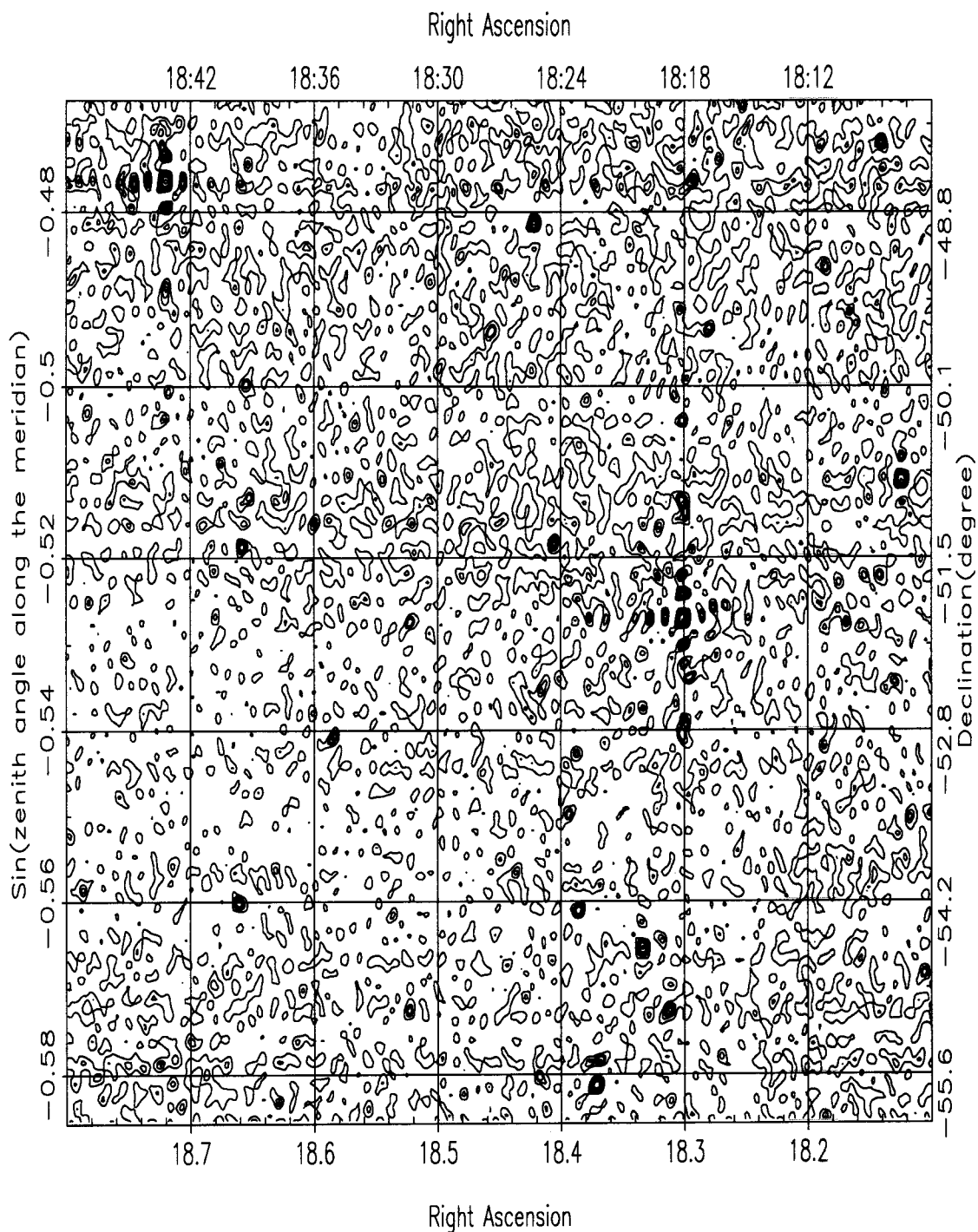


Fig. 8.— A full resolution dirty Image covering RA 18h06m to 18h48m and the declination  $-56^\circ$  to  $-48^\circ$ . The contour levels are 0.3, 1.4, 2.0, 2.8, 3.4, 4.3, 6.0, 8.4, 12.0, 17.0, 24.0, 35.0, 48.0 Jy/beam.

## 5. Conclusion

Selection of good data from a large data base which is the result of 20,000 hours of astronomical observations ( $\approx 1000$  Gigabyte) for the survey is a very important task. A new Perl program has made the selection of good data from this data base for imaging automatic and objective. The data selection time has been brought down by a few days to a few hours by this program. Each day's image is analysed to detect and remove interference which escaped excision in the first round. Complex gains for each day's image are estimated by fitting the RA and Dec beams for sources detected in each day's image. Images are added taking into account these complex gains. A sample of the Full resolution Image for RA range 18h06m to 18h48m and the declination  $-56^\circ$  to  $-48^\circ$  is shown in Figure 8. Detection of interference and its removal has resulted in a good quality image. The Full resolution image has a PSF very close to the PSF expected theoretically. The image presented in this paper and its preliminary analysis clearly demonstrate the success of the method developed.

## 6. Acknowledgments

We thank H. A. Ashwathappa, Srijan, N.V.Madhusudana, A. Atmacharan and S. Castroe for their invaluable contribution.

## REFERENCES

- Baldwin, J. E., Boysen, R. C., Hales, S. E. G., Jennings, J. E., Waggett, P. C., Warner, P. J., and Wilson, D. M. A., 1985, *MNRAS*, **217**, 717.
- Dodson, R.G., "*The Mauritius Radio Telescope And A Study Of Selected Supernova Remnants Associated With Pulsars*". PhD thesis, University of Durham, 1997.
- Golap, K., Udaya Shankar, N., Sachdev, S., Dodson, R., Sastry, Ch. V., 1998, *J. Astrophys. Astr.*, **19**, 35.
- Large, M. I., Mills, B. Y., Little, A. G., Crawford, D. F., and Sutton, J. M., 1981, *MNRAS*, **194**, 693.
- Larry Wall, Tom Christiansen & Jon Orwant "Programming Perl", O'Reilly publishers, 2000.
- Oozeer, N., Udaya Shankar, N., 2001. *Submitted to UN-ESA proceedings, 2001*.
- Sachdev, S., "Wide field Imaging with the Mauritius Radio Telescope". PhD thesis, University of Mauritius, 1999.
- Sachdev, S., Udaya Shankar, N., 2001. *J. Astrophys. Astr.*, **22**, 229.

Srinivasan Sriram "Advanced Perl Programming", O'Reilly publishers, 1997.

Udaya Shankar N., 2001. *Submitted to UN-ESA proceedings, 2001.*

"Astronomical Image Processing System." *NRAO, 31 Dec 2000.*

# Limitations Of The Tangent Plane Approximation For Wide-field Imaging Using The Mauritius Radio Telescope

N. Oozeer<sup>1</sup> and N. Udaya Shankar<sup>2</sup>

1-Department of Physics, University of Mauritius, Reduit, Mauritius

2- Raman Research Institute, Sadashivanagar, Bangalore 560080, India

## ABSTRACT

The Mauritius Radio Telescope (MRT) is a Fourier synthesis, non-coplanar T array. The primary objective of the telescope is to survey the southern sky at 151.5 MHz in the declination range  $-70^\circ$  to  $-10^\circ$ . Due to non-coplanarity, wide-field imaging and deconvolution of wide field images made using MRT are challenging problems in applications of radio interferometric techniques. This paper discusses the usefulness and limitations of the tangent plane approximation in transforming the measured visibilities to wide field images and in estimating the point spread function (PSF) required for the deconvolution.

*Subject headings:* Synthesis imaging, Deconvolution, Point Spread Function, Tangent Plane Approximation

## 1. Introduction

The Mauritius Radio Telescope (MRT) is an aperture synthesis non-coplanar T-array operating at 151.5 MHz. It consists of an East-West (EW) arm of length 2048m having 1024 helical antennas and a South (S) arm of length 880m consisting of 15 movable trolleys, each with four helical antennas. The main objective of the telescope is to make a survey of the southern sky with a resolution of  $4' \times 4.6'$   $\sec(\delta + 20.14^\circ)$  and a point source sensitivity of 200 mJy ( $3\sigma$ ) level. The local terrain is rocky and uneven, specially in the EW direction. Due to the uneven EW array and an almost planar S array, the visibilities at MRT can be thought of as being measured on a pleated sheet with discrete steps in height.

The Van Cittert-Zernike theorem describes the relationship between the visibility and the brightness distribution, of an incoherent planar source, (Thompson, Moran & Swenson 1986).

$$V(u, v, w) = \iint_{-\infty}^{+\infty} A(l, m)B(l, m)e^{-j2\pi(ul+vm+wn)} \frac{dldm}{\sqrt{1-l^2-m^2}} \quad (1)$$

$V(u, v, w)$  is the visibility function,  $A(l, m)$  is the primary beam pattern,  $B(l, m)$  is the sky brightness distribution,  $(l, m, n)$  are the direction cosines and  $(u, v, w)$  are the lengths of baselines measured along the West, South and towards the zenith respectively.

The above equation is **NOT** a Fourier transform relation between visibility and the brightness distribution. The visibility is a function of three variables ( $u, v, w$ ) whereas the brightness distribution is a function of only two variables, ( $l$  &  $m$ ). For a coplanar array, where a coordinate system can be chosen such that  $w=0$ , the above relation turns out to be a 2-D Fourier relation.

At MRT to obtain the brightness distribution from the measured visibilities we apply Direct Fourier Transform along the  $v$  and  $w$  axis and finally sum along  $u$  to obtain the images on the meridian, (Golap et al. 1998). This gives an image function  $I^d$ , generally called the dirty image which is the convolution of the true brightness distribution  $I$  and the Point Spread Function (PSF),  $B^d$ .

$$I^d = I * B^d$$

Due to the non-coplanarity of the MRT, the PSF even for meridian transit imaging, is a function of the zenith angle, ( $za$ ) of the source. This implies that for deconvolution of the array response from the 2-D dirty image we need PSFs which vary with the ( $za$ ) of the source being deconvolved (Golap & Udaya Shankar 2001).

In this paper we first discuss the limitations of the tangent plane approximation for making dirty images. The next section, § 3 discusses the possibility of using the tangent plane approximation for the calculation of the PSF. § 4, gives the results of applying the methods discussed here for deconvolving the MRT images.

## 2. Tangent plane approximation

Fig. 1 shows the the brightness distribution of the sky and sampling of the visibilities. The direction cosines ( $l, m, n$ ) denote a position on the celestial sphere defined by  $l^2 + m^2 + n^2 = 1$ . A tangent plane is a plane tangential to the celestial sphere at a given  $n$ . Let us consider the tangent plane defined by  $n = 1$ . On this plane, by using equation(1), we have the relation:

$$V(u, v, w) = \iint_{-\infty}^{+\infty} A(l, m) B(l, m) e^{-j2\pi(ul+vm+w(n-1))} \frac{dl dm}{\sqrt{1-l^2-m^2}} \quad (2)$$

For Small fields of view this equation can be simplified by the approximation that

$$\sqrt{1-l^2-m^2} \approx 1 \quad (3)$$

The relationship between the visibility and the brightness distribution then becomes a two-dimensional Fourier Transform:

$$V(u, v) \approx \iint B(l, m) e^{-j2\pi(ul+vm)} dl dm \quad (4)$$

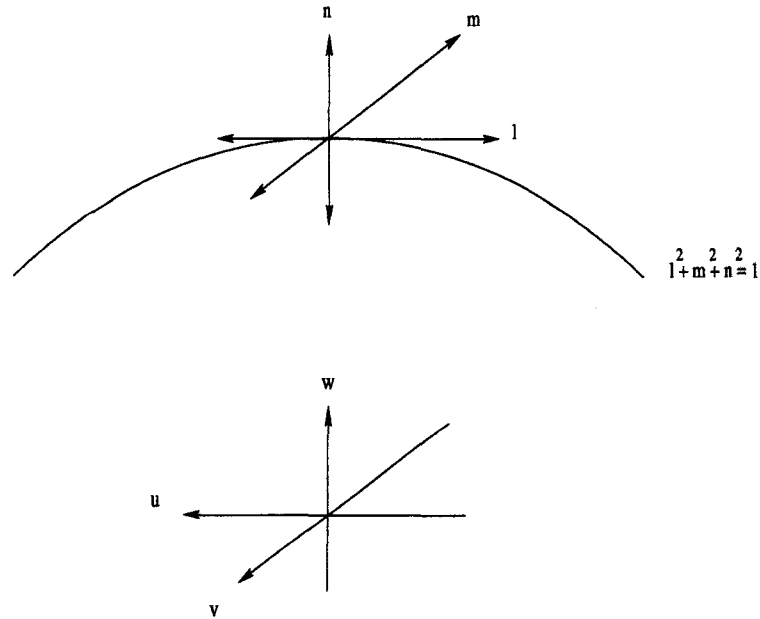


Fig. 1.— Geometry of the brightness distribution of the sky and sampling of the visibilities.

In general, this approximation will result in a phase error  $\phi_w \sim w\pi(l^2 + m^2)$ , (Cornwell & Perley 1992).

To estimate the errors specific to MRT we carried out the following simulation:

- Phase errors leading to amplitude errors.

To avoid the problems due to the grating response of the EW array, presently the imaging is done on the meridian only. Along the meridian,  $m = \sin(za)$  and  $n = \cos(za)$ . We considered tangents at various zenith angles and corrected for phases on the tangent due to heights as seen by a source at the tangent point.

By examining the source response on the tangent we calculated for sources away from the tangent point the ratio of the peak flux density measured to the true peak flux density. Fig. 2 shows plots of reduction in strengths of point sources as a function of the offset angle  $\Phi$  measured from the tangent point. We see from this plot that on the tangent at  $za = 0^\circ$ , the measured flux density of a source which is  $9^\circ$  away from the tangent point decreases by 10% of its true value. At higher zenith angles ( $\sim 50^\circ$ ), the offset angle (the zenith distance from the tangent point) at which the measured flux reduces by 10% decreases to  $1^\circ$ .

Fig. 3, shows the zenith distance from the tangent point at which the source strength falls to 90% of its true value as a function of the  $za$  of the tangent point.

- Phase errors leading to positional errors.

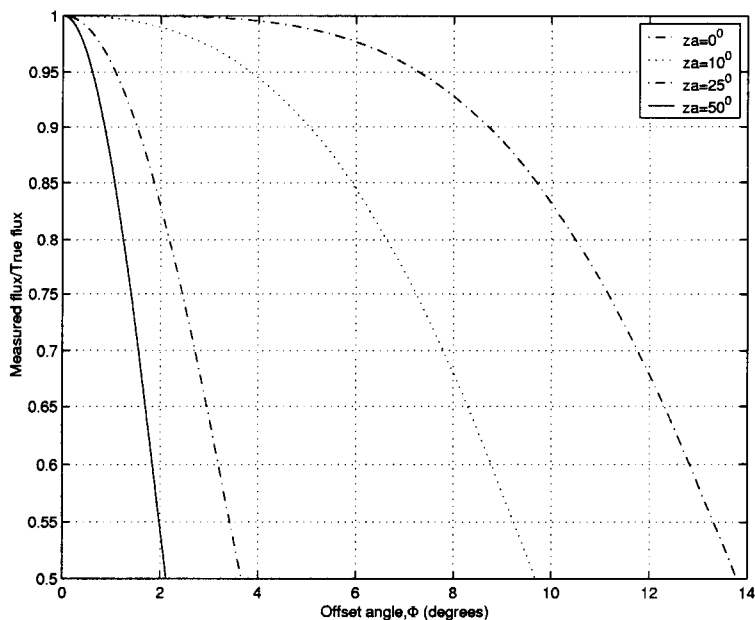


Fig. 2.— The above plots show the ratio of the measured flux density due to the Tangent Plane Approximation to the true flux density as a function of the offset angle  $\Phi$ , for various zenith angles.

As already mentioned, presently the imaging is restricted to making 1-D scans along the meridian. The 2-D image is time stacks of these 1-D scans. As a point source drifts across the meridian the 1-D stacks will give the point spread function. When we examined the 2-D PSF of a source, transiting the meridian at the tangent point, was as expected on the meridian. However for the sources which transited away from the tangent point, the peak of the 2-D PSF was away from the meridian. This shift is due to the geometry of the MRT array. The height distribution of the EW array is shown in Fig. 4. The W16 to W1 and E1 to E3 groups can be approximated by an array with a slope of about  $1.61^\circ$ . E4 to E16 can be approximated by a planar array, Fig. 5.1. While imaging a source at the tangent point the phases due to the heights are corrected properly at this point and both the planar array and the sloping array have their peaks pointing to the tangent point. While imaging a source away from the tangent point, since the phase errors due to the tangent plane approximation are proportional to the  $w$  component, there will be a linear phase gradient across the sloping array. This shifts its pattern away from the meridian. The peak of the pattern of the planar array continues to be directed towards the meridian. The resulting EW array pattern which can be thought of as the product of these two array patterns explains the shifting of the source away from the meridian. This is schematically shown in the Fig. 5.2.

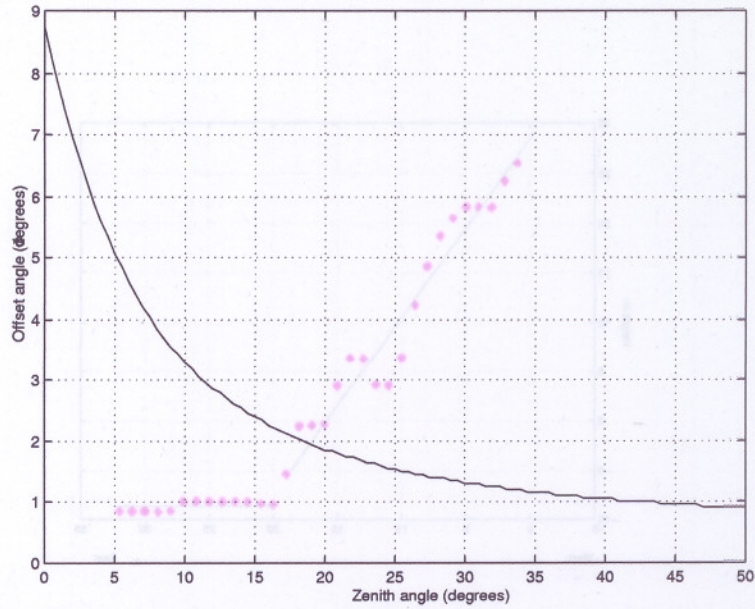


Fig. 3.— This figure shows the zenith distance from the tangent point for various zenith angles at which the strength of a source falls to 90% of its true value due to the tangent plane approximation.

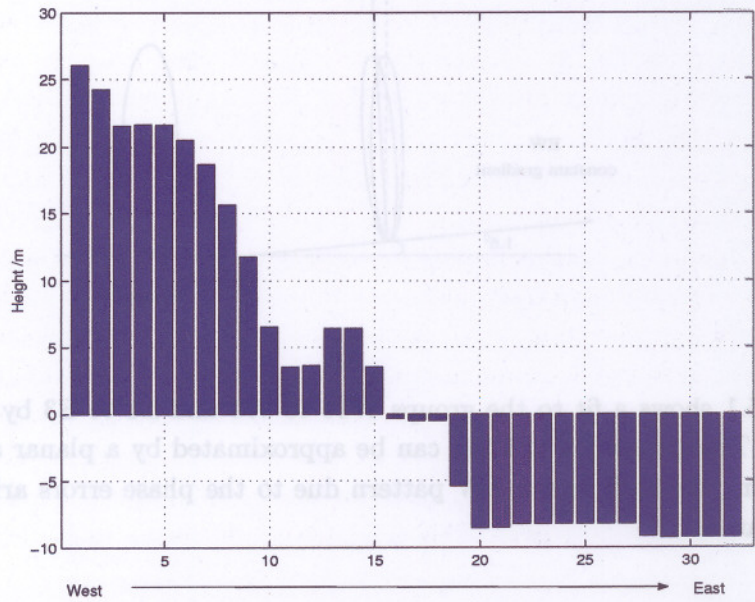
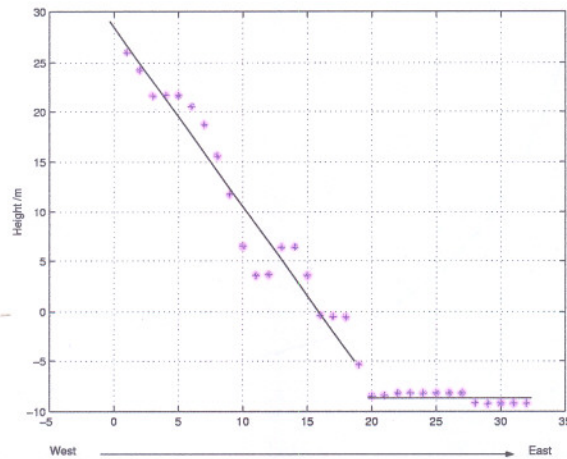
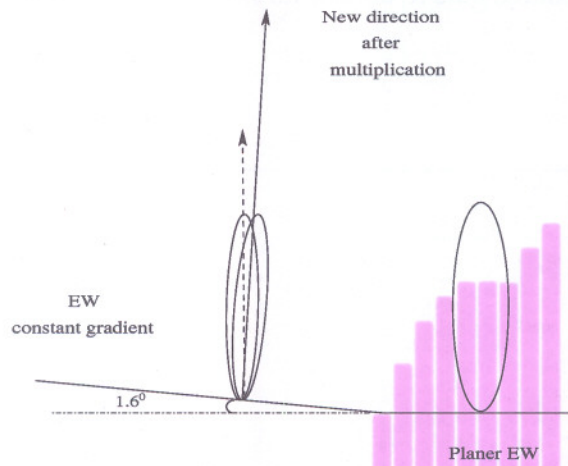


Fig. 4.— The EW height profile. The maximum height difference in the EW arm is 35m

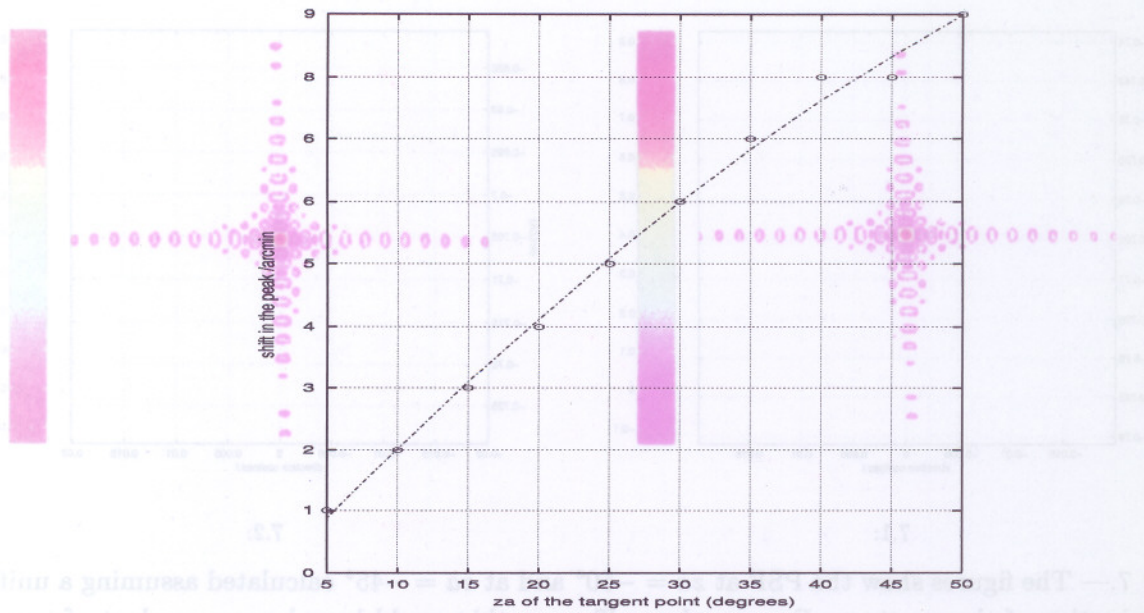


5.1:

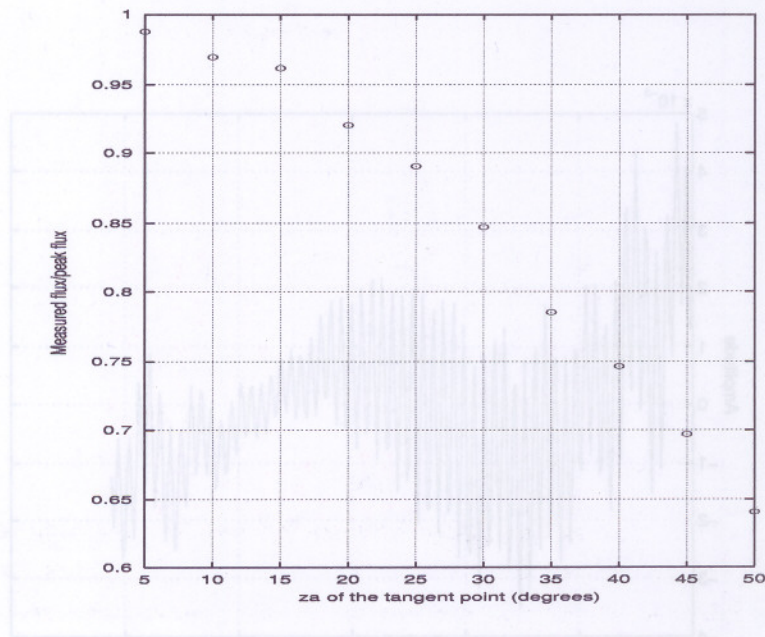


5.2:

Fig. 5.— Fig. 5.1 shows a fit to the groups W16 to W1 and E1 to E3 by an array with a slope of about  $1.61^\circ$ . The groups E4 to E16. can be approximated by a planar array. Fig. 5.2 gives a schematic showing the shift in the EW pattern due to the phase errors arising from the tangent plane approximation.

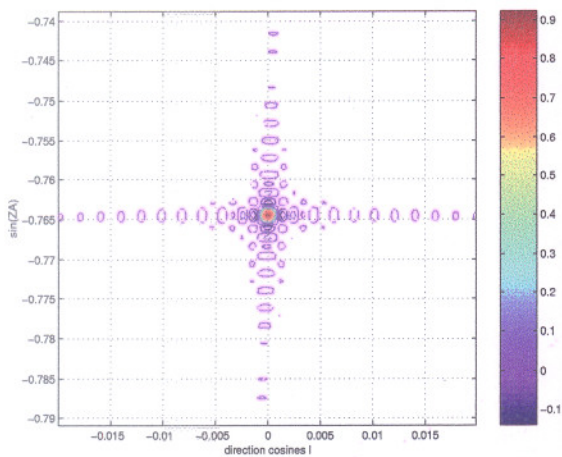


6.1:

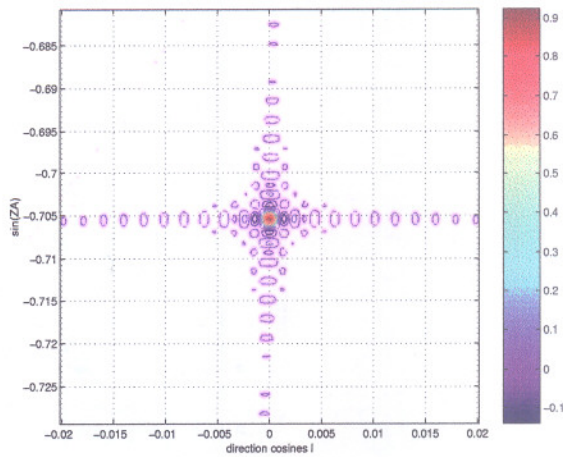


6.2:

Fig. 6.— Fig. 6.1, shows the shift of the source away from the meridian for an offset angle of  $5^\circ$  as a function of the zenith angle of the tangent point. Fig. 6.2, shows the peak value of the 2-D PSF for an offset angle of  $5^\circ$  as a function of various  $z_a$  of the tangent point .



7.1:



7.2:

Fig. 7.— The figures show the PSF at  $z\alpha = -50^\circ$  and at  $z\alpha = -45^\circ$  calculated assuming a uniform illumination of the aperture. For a coplanar T-array this would have been a product of two sinc functions along the two axes. The shift of the side lobes away from the meridian are clearly seen.

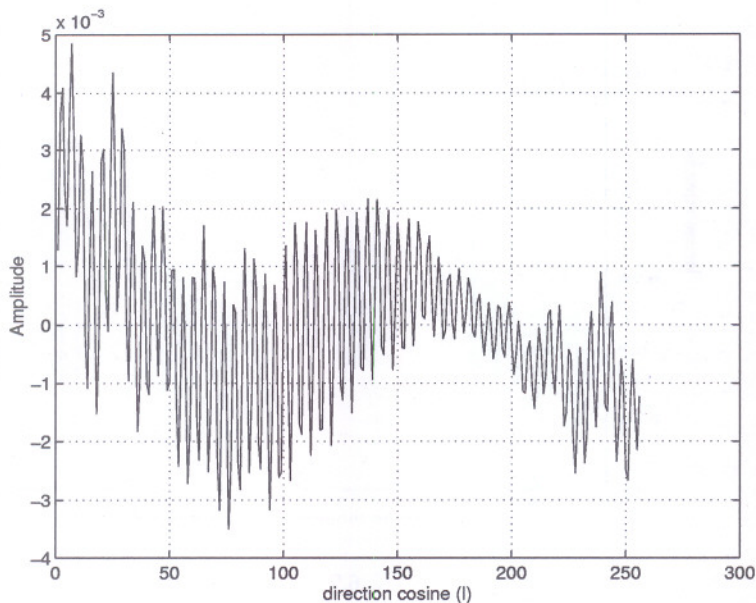


Fig. 8.— A one-dimensional slice of the difference between the PSFs at the tangent point  $z\alpha = -50^\circ$  and the PSF at  $z\alpha = -45^\circ$

3. Tangent plane approximation for getting the PSF

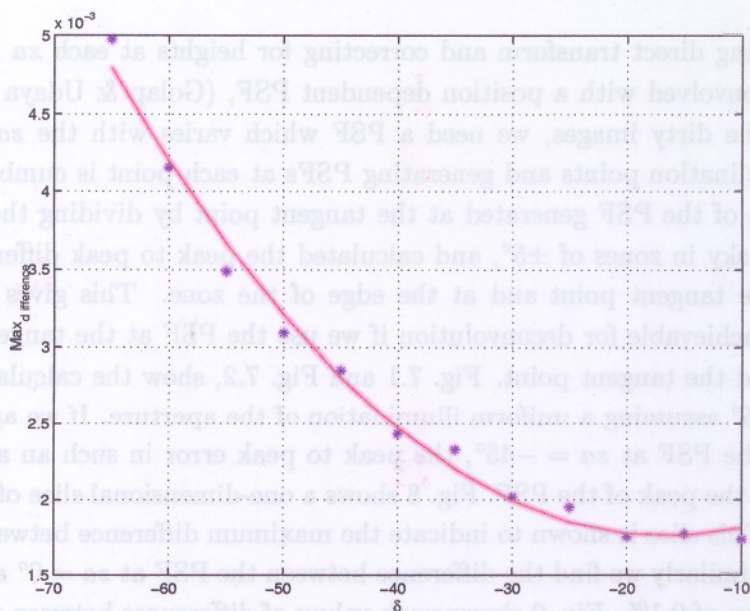


Fig. 9.— This figure shows the peak difference between the PSF at the tangent point and a PSF at the end of a 5° zone for various ZA of the tangent point.

Fig. 6.1, shows the shift of the source away from the meridian for an offset angle of 5° as a function of the zenith angle of the tangent point. When a source at  $za = 10^\circ$  is corrected for height phase at  $za = 5^\circ$ , the shift is 2'. It increases to as much as 9' when a source at  $za = 50^\circ$  is corrected for heights phase as seen by a source at  $za = 45^\circ$ . These shifts are not acceptable when compared to the resolution of MRT, ( $4' \times 4.6' \sec(\delta + 20.14^\circ)$ ). Thus even 14 tangent planes are not sufficient to ensure acceptable shifts in the position of sources.

The loss of amplitude and the shift in the position of the sources due to phase errors clearly show that the tangent plane approximation is not desirable for the inversion of visibilities at MRT. Hence the Direct Fourier Transform technique which compensated for heights at each point on the meridian, considered in the earlier works of MRT is indeed preferable, (Golap et al. 1998). This is equivalent of using as many tangent planes as many  $za$  points imaged. Such an approach ensures that all sources as expected peak on the meridian. However the sidelobes behave in a manner similar to the sources away from the tangent point in the tangent plane approximation. Thus they do not peak on the meridian and the shift from the meridian is a function of both the zenith angle of the source and zenith distance of the sidelobes from the source. This leads to a position dependent PSF.

### 3. Tangent plane approximation for getting the PSF

Imaging using direct transform and correcting for heights at each  $za$  in the image results in a dirty image convolved with a position dependent PSF, (Golap & Udaya Shankar 2001). Thus to deconvolve the dirty images, we need a PSF which varies with the  $za$ . We have about 800 independent declination points and generating PSFs at each point is cumbersome. So we studied the effectiveness of the PSF generated at the tangent point by dividing the sky into a few zones. We divided the sky in zones of  $\pm 5^\circ$ , and calculated the peak to peak difference between the PSF generated at the tangent point and at the edge of the zone. This gives us an estimate of the dynamic range achievable for deconvolution if we use the PSF at the tangent point for a range of  $za = \pm 5^\circ$  around the tangent point. Fig. 7.1 and Fig. 7.2, show the calculated PSF at  $za = -50^\circ$  and at  $za = -45^\circ$  assuming a uniform illumination of the aperture. If we approximate the PSF at  $za = -50^\circ$  by the PSF at  $za = -45^\circ$ , the peak to peak error in such an approximation is of the order of 0.5% of the peak of the PSF. Fig. 8 shows a one-dimensional slice of the difference between the two PSFs. This slice is shown to indicate the maximum difference between the two PSFs under consideration. Similarly we find the difference between the PSF at  $za = 0^\circ$  and the PSF at  $za = 5^\circ$  to have maximum of 0.1%. Fig. 9 shows peak values of differences between the PSF at the tangent point and the PSF at the end of a  $5^\circ$  zone.

This figure clearly indicates that the dynamic range achievable by using a single PSF for deconvolving zones of  $10^\circ$  is of the order of 200. Our estimated  $1 \sigma$  noise in MRT images is 200 mJy. Thus we will be dynamic range limited only for sources of strengths greater than 40 Jy. In the southern sky there are not many strong sources. According to the Molongolo Radio Catalog (MRC), there are 23 sources above 20 Jy at 408 MHz, (Large et al. 1981). Assuming a spectral index of -0.7 they will have flux densities above 40 Jy at 151.5 MHz. Thus a dynamic range of 200 seems to be a good target. However there are many other reasons for the dynamic range to get limited to values lesser than 200. At MRT correlation of signals from groups of helices are performed. There are 32 helices in each of the EW groups and 4 helices in each of the NS groups. The calibration procedure used, (Golap et al. 1998), gives the phases and amplitudes of a group. The illumination pattern within each group is not estimated. This sets a limit to the extent of the PSF that can be estimated from the illumination pattern. With 32 groups, we can estimate the PSF up to 16 sidelobes on each side of the main beam along RA. Assuming a sinc function for the PSF, the image will have a dynamic range of only  $\sim 50$  if such a PSF is used for deconvolution. Golap & Udaya Shankar (2001) have discussed the estimation of the PSF from the dirty image to improve the dynamic range. Their paper deals with the deconvolution of low resolution images ( $17' \times 13^\circ \text{sec}(\delta + 20.14^\circ)$ ) made using the MRT. However most of their discussions are valid for deconvolution of full resolution images discussed in this paper.

#### 4. Deconvolution

The first Full resolution ( $4' \times 4.6' \sec(\delta + 20.14^\circ)$ ) images have been made using the Mauritius Radio Telescope for the Right Ascension (RA) range 18:00 to 19:00 hrs, (Pandey, Udaya Shankar & Somanah 2001). For demonstrating the method discussed here, we chose the region 18:18:00 hrs to 18:45:00 hrs in RA and  $-45^\circ$  to  $-35^\circ$  in declination. The dirty and the deconvolved images are shown in Fig. 10 and Fig. 11 respectively. Deconvolution was carried out using the PSF appropriate for a source at the centre of the image. We have been able to identify 23 MRC sources out of total 25 MRC sources in this field. The strongest being MRC1827-360, having a flux density of 51.66 Jy at 151.5 MHz, if one assumes a spectral index of -0.7, (Large et al. 1981). Detailed analyses of the CLEANed images to estimate the dynamic range achieved, the noise in the maps, positional accuracy of the point sources detected are under progress.

#### 5. Conclusion

The tangent plane approximation is not a viable method for inverting the measured visibilities at MRT. At a zenith angle of around  $50^\circ$  the tangent plane approximation for a zone of  $\pm 5^\circ$  leads to a shift in the source away from the meridian by almost  $9'$ . Thus the Direct Fourier Transform technique which compensates for heights at each  $z\alpha$  on the meridian is more appropriate for inverting the measured visibilities at MRT. This technique causes the sidelobes to shift away from the meridian in the dirty image and needs a position dependent PSF for deconvolution. Our simulations indicate that such a dirty image can be deconvolved with a dynamic range of the order of 200 by using 6-7 PSFs for the entire declination range of the MRT. However the method used for antenna calibration may limit the achievable dynamic range. In this paper we have presented images deconvolved by the methods discussed here. Detailed analyses of the CLEANed images to estimate the dynamic range achieved, the noise in the maps, positional accuracy of the point sources detected are under progress.

#### 6. Acknowledgments

N. Oozeer is grateful to the Tertiary Education Commission (TEC), Reunion, Mauritius, who has financially sponsored the research and the University of Mauritius for all other facilities given. He is also indebted to the Raman Research Institute for the facilities and support they provided during his stay.

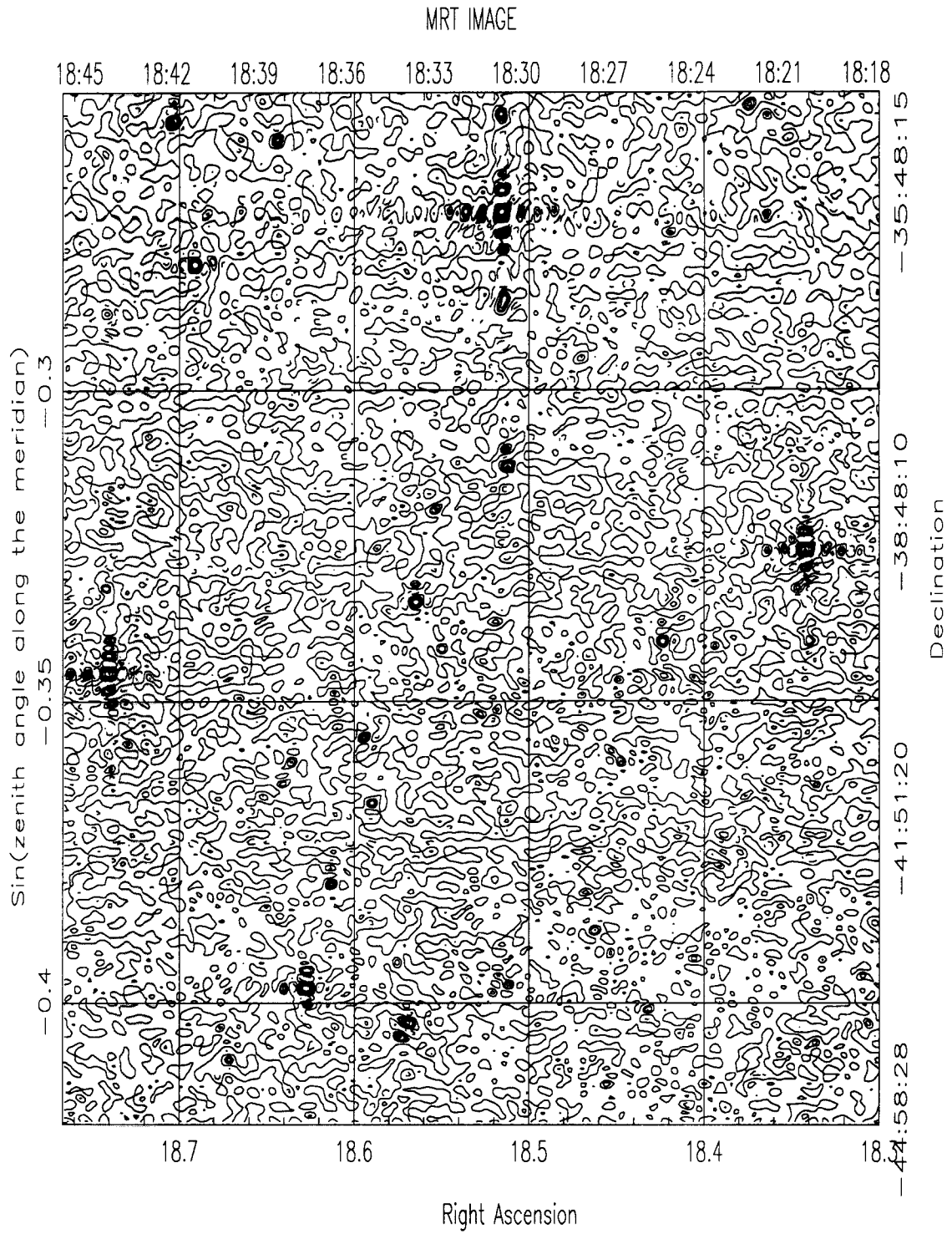


Fig. 10.— A “Dirty” image in the right ascension range 18h18m to 18h45m and declination range  $-45^\circ$  to  $-35^\circ$ . The contour levels are: -2, 0.1, 2, 3, 4, 5, 7, 10, 14, 24, 33, 42, 55 Jy/beam

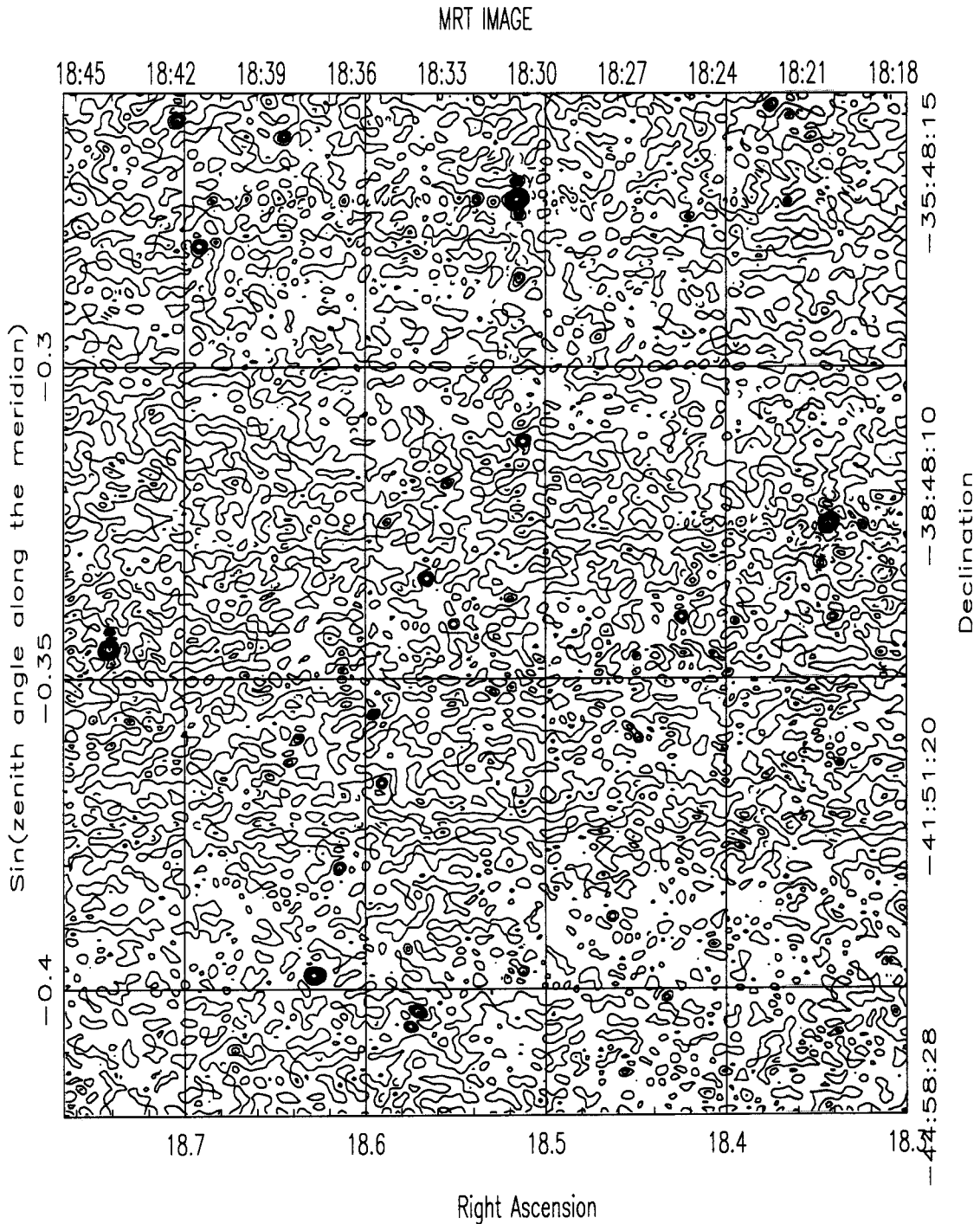


Fig. 11.— A CLEANed image obtained after the deconvolution of the dirty image seen in 10, by a PSF appropriate to the centre of the image. The contour levels are: -2, 0.1, 2, 3, 4, 5, 7,10, 14, 24, 33, 42, 55 Jy/beam

## REFERENCES

- Thompson A. R., Moran J. M., & Swenson G. W. Jr. *"Interferometry and Synthesis in Radio Astronomy"*. John Wiley and Sons, 1986.
- Golap K., Udaya Shankar N., 2001. *"Deconvolution of Wide-field Images from a Non-Coplanar T-Array"*. *J. Astrophys. Astr.*, **22**, 251.
- Cornwell T. J., and Perley R. A. *"Radio-interferometric imaging of very large fields: The problem of non-coplanar arrays"*. *Astron. Astrophys.* 261:353-364, 1992.
- Golap K., Udaya Shankar N., Sachdev S., Dodson R., Sastry Ch. V., 1998. *"A Low Frequency Radio Telescope at Mauritius for a Southern Sky Survey"* *J. Astrophys. Astr.*, **19**, 35.
- Golap K. *"Synthesis Imaging at 151.5 MHz using the Mauritius Radio Telescope"*. PhD thesis, University of Mauritius, 1998.
- Large, M. I., Mills, B. Y., Little, A. G., Crawford D. F., and Sutton, J. M., 1981. *MNRAS*, **194**, 693.
- Pandey V. N., Udaya Shankar N., Somanah R., 2001. *"The full resolution images from the Mauritius Radio Telescope survey."* submitted to *UN-ESA proceedings, 2001*

# Study of Extended Radio Galaxies at 151.6 MHz using the Mauritius Radio Telescope

Radhakrishna Somanah<sup>1</sup> and N. Udaya Shankar<sup>2</sup>

1- Faculty of Science, University of Mauritius, Reduit, Mauritius

2- Raman Research Institute, Sadashivanagar, Bangalore 560080, India

## ABSTRACT

The MRT survey will be by far one of the most extensive survey at low frequencies. This survey will provide a moderately deep radio catalog reaching a source density of about  $2 \times 10^4 \text{ sr}^{-1}$  over the southern sky with an angular resolution of  $4' \times 4'$  and a limiting flux density of 70 mJy ( $1\sigma$ ) at 151 MHz. The availability of zero spacing and short baselines in the MRT array will make it sensitive to the background temperature and to large scale features in the sky. A study of continuum emission from large radio sources at low frequencies has several interesting and important implications to the study of radio galaxies. This paper discusses the parameter space of radio galaxies which can be explored using the MRT. Images of a few extended radio galaxies are also presented.

## 1. Introduction

It is estimated that there are over 100 billions of galaxies in the universe. Only a small percentage of them are radio galaxies. The optical counterparts of most strong radio galaxies have been identified and are found to be ellipticals. The optical counterpart identification is important to estimate the redshifts and hence to calculate the intrinsic properties of the radio galaxies, like radio luminosity, energy density, pressure and magnetic field.

Since the identification of strong radio sources with the galaxies M87 and NGC5128 as early as 1949 by Bolton and Stanley, much progress has been made in the understanding of different classes of radio galaxies. But still a study of continuum emission from large radio sources at low frequencies has several interesting and important implications to the study of radio galaxies. These include the studies of large-scale diffuse structures such as lobes, plumes and bridges which are due to the 'old' electrons and hence more prominent at low frequencies. The MRT survey can make interesting contributions in the areas like studies of the aging of the radiating electrons and re-acceleration processes by combining the low-frequency images with similar data at higher frequencies, identification of giant radio sources which are in the last stages of evolution, constraining models of evolution of radio sources, identifying dead or relic radio sources and possibly probing the external environment on different scales and redshifts.

## 1.1. The Mauritius radio Telescope

The Mauritius Radio-Telescope (MRT) is a T-shaped array with an East-West (EW) arm of length 2048 m having 1024 helical antennas and a South (S) arm of length 880 m consisting of a rail line on which 15 movable trolleys, each with four helical antennas are placed. The EW arm is divided into 32 groups of 32 helices each. Each trolley in the S arm constitutes one S group. In the receiver room the 32 EW and 16 S group outputs are fed into a  $32 \times 16$  complex, 2-bit 3-level digital correlator. The 512 complex visibilities are integrated and recorded at intervals of 1 second. At the end of 24 hours of observation the trolleys are moved to a different position and new visibilities are recorded. A minimum of 60 days of observing are needed to obtain the visibilities up to the 880 m spacing. The Fourier transform of the phase corrected visibilities obtained after the complete observing schedule, produces a map of the area of the sky under observation with a synthesized beam of width  $4' \times 4.6' \sec(\delta + 20.14^\circ)$ . More technical details about the MRT array can be obtained in Dodson 1997; Golap 1998; Golap *et al.* 1998; Sachdev 1999; Sachdev & Udaya Shankar 2001.

The next section discusses the limiting values of the surface brightness, the energy densities of the radio galaxies that MRT can explore. The linear size and the redshift of the resolved sources and the limiting value of the redshift for a given luminosity range of the ExtraGalactic Radio Sources (EGRS) in the MRT survey are also discussed. Section 3 discusses different types of EGRS that may dominate the future investigations using the MRT survey. Section 4 gives the present status of the study at MRT. Images of a few extended radio galaxies are also shown.

## 2. Radio Galaxies And The MRT Survey

### 2.1. Surface Brightness Sensitivity

The expected root mean squared (RMS) values of the background in the synthesized images, arising from the system noise with a 1 MHz bandwidth and an integration time of 8 seconds is expected to be around 200 mJy ( $3\sigma$ ). With this sensitivity and resolution of approximately  $4' \times 4'$  the expected surface brightness sensitivity is

$$B = \frac{S}{\Omega} = \frac{200 \times 10^{-29}}{\left(\frac{\pi}{4ln2}\right)\left[\frac{4}{60} \times \frac{\pi}{180}\right]^2}$$

$$\approx 10^{-21} W m^{-2} Hz^{-1} Sr^{-1}$$

This is a good limit to investigate low surface brightness features in the radio galaxies.

### 3. Minimum Energy density of Radio Galaxies in the MRT survey

The energetics of radio sources are important not only because of their relation to the source-production mechanism but because they also play an important role in all considerations of how radio sources are held together or confined. Total intensity distributions provide information about the minimum energies involved. A good discussion of source energetics is given by Moffet (1975). The minimum energy condition corresponds almost to equipartition of the energy between the relativistic particles and the magnetic field. The minimum energy density,  $U_{me}$  is given by

$$U_{me} = .0928 B_{me}^2 \text{ ergs cm}^{-3}$$

Miley (1980).

The magnetic field in the radio source can be written as follows.

$$B_{me} = 5.69 \times 10^{-5} \left[ \frac{(1+K)(1+z)^{3-\alpha}}{\eta} \times \frac{1}{S\theta_x\theta_y \text{Sin}^{\frac{3}{2}}\phi} \times \frac{S_0}{\nu_0^\alpha} \times \frac{\nu_2^{\alpha+\frac{1}{2}} - \nu_1^{\alpha+\frac{1}{2}}}{\alpha + \frac{1}{2}} \right]^{2/7} \text{ gauss}$$

- K = Ratio of energy in the heavy particles to that in electrons.
- $\eta$  = Filling factor for emitting regions.
- $\phi$  = angle between uniform magnetic field and line of sight.
- $S_0 \rightarrow$  Jy per beam.
- S = size in Kpc
- $\nu_1, \nu_2 \rightarrow$  lower and upper cut off frequencies in GHz.

Apart from the basic assumption that the radiation is synchrotron emission, there are several uncertainties inherent in these formulas. Using the values generally quoted in the literature and the parameters of MRT, one gets for

$$K = 1, \eta = 1, \phi = 90^\circ,$$

$$S_0 = 0.2 \text{ Jy, (The minimum detectable flux of the MRT)}$$

$$\theta_x, \theta_y \rightarrow \text{Half Power Beam Width of the MRT array,}$$

$$\Rightarrow \theta_x \approx \theta_y = 240''$$

$$\nu_1 = .01 \text{ GHz, } \nu_2 = 100 \text{ GHz,}$$

$$\alpha = -0.7$$

$$U_{me} \approx 4.08 \times 10^{-13} (S)^{-4/7} (1+z)^{2.3}$$

Considering the local neighborhood  $z \approx 0$  and  $S = 200$  Kpc which is the typical size of FRIs,

$$U_{me}(MRT) \approx 2 \times 10^{-14} \text{ ergscm}^{-3} = 2 \times 10^{-15} \text{ Jm}^{-3}$$

Energy densities in radio galaxies are typically of the order  $10^{-15}$  to  $10^{-12} \text{ Jm}^{-3}$ . Thus we will be able to sample a fair number of close by radio galaxies. It is also obvious from above that if we go to higher redshifts, the limit for the calculated value of  $U_{me}$  will go up and we'll see lesser number of sources.

#### 4. Linear dimension and Redshift of Resolved Sources in the MRT survey

The properties of radio sources change with luminosity. This is especially true of radio galaxies whose structures seem to undergo an abrupt transition at  $P_{178MHz} \approx 5 \times 10^{25} \text{ WHz}^{-1}$ . This was first noted by Fanaroff and Riley in 1974 ( Fanaroff 1974 ). They introduced a simple classification scheme around this critical luminosity. Sources below this critical luminosity are known as FRI type objects and those above as FRII type objects. FRI sources tend to have prominent, smooth continuous two-sided jets running into large-scale lobe structures (plumes) which are edge-darkened and whose steepest radio spectra, which by implication the most radiatively aged material, lie in the outermost extended regions farthest from the host galaxy. FRII sources tend to have large-scale structures which are edge brightened with bright outer hotspots. The steepest radio spectra are found in the inner extended regions of the lobes or bridges nearest to the optical identification.

A good surface brightness sensitivity of MRT yields itself conveniently for the study of plumes in low luminosity FRI sources. The low frequency of operation will be an added advantage to look at the the most radiatively aged material due to its steep spectra.

The angular extent  $\theta$  is related to the linear dimension  $l$  and the effective distance  $D$  by the relation

$$\theta = \frac{l(1+z)}{D}$$

Using the Friedmann equation and the definition for  $D$  and taking the cosmological constant to be zero.

$$D = \frac{2c}{H_0 \Omega_0^2 (1+z)} \{ \Omega_0 Z + (\Omega_0 - 2) [(\Omega_0 Z + 1)^{\frac{1}{2}} - 1] \}$$

(Silk 1994).

For  $\Omega_0 = 1$ ,

$$D = \frac{2c}{H_0} \{1 - (1+z)^{-\frac{1}{2}}\}$$

Assuming  $H_0 = 50$  Km/s/Mpc and using the resolution of the MRT,  $\theta = 4' = \frac{\pi}{2700} rad$ , the linear dimension  $l$  is given by:

$$l = \frac{D\theta}{(1+z)} = \frac{\pi}{2700} \times \frac{D}{1+z}$$

Thus if we fix  $\theta$ , it can be easily seen from above that for a given value of  $\Omega_0$ , there will be a value of  $z$  for which  $l$  will be maximum. For  $\Omega_0 = 1$ , the maximum  $l$  is around  $z = 1.5$ .

For  $\theta = 4'$ , Table 1 shows the variation of  $l$  with  $z$ .

$z$	.001	.01	.1	.5	1.0	1.5	2.0	3	4	5
D Mpc	6	60	600	2200	3500	4400	5070	6000	6633	7100
l Kpc	1.75	17.5	175	1700	2000	2050	2000	1700	1500	1400

Table 1: The table shows the variation of  $l$  with  $z$  for  $\Omega_0=1$  and  $\theta = 4'$

Most FR II sources have linear dimensions in the range  $100 \text{ Kpc} < l < 250 \text{ Kpc}$ . Thus for  $Z \leq .1$ , many FR II sources may be resolved in the MRT survey. Detailed analysis of these sources by comparing them with high frequency images may provide interesting results.

For  $z > .1$ , most FR II sources will be seen as point sources and MRT survey will be able to get only the flux densities of these sources and get an estimate of the spectral index by comparing them with images at other frequencies.

#### 4.1. Limiting Redshift of the survey for a given luminosity

It is also interesting to investigate the red-shift up to which we will be able to see FRIs and FRIIs.

The observed flux density is related to the actual luminosity of a source by the equation:

$$S_\nu(\nu_{obs}) = \frac{L_\nu(\nu_{obs})}{4\pi D^2(1+z)^{1+\alpha}}$$

For  $\Omega_0 \approx 1$ ,

$$D = \frac{2c}{H_0} \left(1 - (1+z)^{-1/2}\right)$$

(Silk 1994).

FRIIs have been found in the luminosity range ( $L_\nu$ ) :  $10^{23} \rightarrow 10^{25} W/Hz$  and FRIIs in the the range:  $10^{25} \rightarrow 10^{28} W/Hz$ . Equating the observed flux density to the minimum detectable flux density of the MRT array, one gets:

$$S_\nu(\nu_{obs}) = \text{sensitivity limit of MRT} = 200 \text{ mJy}$$

$$(1+z)^\alpha S_\nu 4\pi \times \frac{4c^2}{H_0^2 \{1 - (1+z)^{-1/2}\}^2} = L_\nu$$

$$\Rightarrow f(z) = 2.91 \times 10^{-28} L_\nu$$

By taking the spectral index  $\alpha$  as -0.7, we can find the limiting  $Z$  up to which the MRT can see for a given luminosity. Table 2 shows the limiting  $z$  for different luminosities.

	x where $L_\nu = 10^x$	$L_\nu \times 2.91 \times 10^{-28}$	z
FRIIs	23	.000029	.010
FRIIs	23.5	.00010	.02
FRIIs	24	.00029	.035
FRI and FRII break	25	.0029	.1
FRIIs	26	.029	.4
FRIIs	27	.29	1.5
FRIIs	28	2.9	11

Table 2: The limiting  $z$  up to which sources of different luminosities can be seen in the MRT survey

## 5. A Few Types Of Interesting EGRS In The MRT Survey

The following types of EGRS are likely to dominate the future investigations using the MRT survey:

### 5.1. Giant Radio Sources

Giant radio sources are defined as those with a projected linear size greater than 1 Mpc. With this linear dimension, MRT survey will be able to get detailed images of many giant radio sources.

Almost tens of giant sources were discovered in 4C and 8C surveys, which are low frequency surveys. New ones are still being found in low frequency surveys like the WENNS (Westerbork Northern Sky Survey) survey <sup>1</sup>. Thus the MRT survey has a potential to discover many new giant

---

<sup>1</sup>WENNS is a low frequency survey carried out by the Westerbork Synthesis Radio Telescope at a wavelength of

radio sources since we are imaging regions hitherto not imaged at low frequencies.

### 5.2. High Redshift Radio Galaxies

Similar to giant radio sources many high redshift radio galaxies were discovered in low frequency radio surveys due to their steep spectral index. Thus the MRT database will be a powerful tool to look for High Redshift Radio Galaxies also. One may ask the question why should it be interesting to find these distant radio galaxies when quasars are much easier to detect? Because radio galaxies appear extended in the optical/near-infrared band. This provides an opportunity to separate the stellar component from the AGN where as in QSO the AGN outshine every thing else. This also allows one to study the kinematics and the ionisation structure of the, often very extended-emission line gas. Thus radio galaxies are crown witness to early galaxy formation and evolution .

### 5.3. Diffuse Cluster Radio Sources

Diffuse radio sources in clusters remain a poorly understood phenomenon. They are very extended sources (0.4-0.6 Mpc), of low surface brightness and steep spectrum, which cannot be identified with any active radio galaxy. They are a rare phenomenon, as they have been found so far in a few clusters of galaxies. Two important classes of diffuse cluster radio sources are cluster-wide halos and relics. Cluster-wide halos include sources located at the cluster centres, while relics are those diffuse extended sources located at the cluster peripheries. The surface brightness sensitivity of MRT and its low frequency operation which enables it to probe radiatively aged regions of clusters may lead to possible detections of new diffuse cluster radio sources .

## 6. Present Status of the study at MRT

We have chosen 25 EGRS with angular sizes  $> 8'$ , south of declination  $-30^\circ$  for imaging with the MRT. This list was made using the Molonglo Radio Catalogue (MRC) (Large *et al.* 1981) and is given in the table 3.

Most of the above sources in table 3, have been imaged at 408, 843 and 5000 MHz with the Molonglo, MOST and Parkes telescopes due to the overlapping sky regions Mills *et al.* 1981. A study of these sources at a lower frequency by MRT will enable detailed investigations of these sources.

---

92 cm that covers the whole sky north of declination  $30^\circ$ . It will have a sensitivity of 18 mJy and a resolution of  $54'' \times 54'' \text{ cosec}(dec.)$ .

	MRC	RA(2000)	DEC(2000)	Size in'	S(843) Jy	
1	0114-476	01 14 12	-47 38 13	9.5	3.8	FRII*
2	0131-367A	01 31 41	-36 44 29	10.2	10.3	FRII*
3	0319-453	03 19 26	-45 23 34	25.6	4.8	FRII**
4	0320-453	03 20 48	-37 22 19	48	169	FRI/FRII*
5	0511-305	05 11 39	-30 31 50	10.6	4.6	FRII*
6	0546-330	05 46 39	-32 59 27	8	1.85	FRI/FRII**
7	0707-359A	07 07 35	-35 57 16	8.1	3.26	FRII*
8	1056-360	10 56 31	-36 03 40	8	2.4	FRI**
9	1234-723	12 34 06	-72 18 25	14	1.86	FRI**
10	1302-491	13 02 33	-49 12 02	8.5	8.3	Spiral
11	1308-441	13 08 30	-44 07 35	14.4	1.76	FRI/FRII**
12	1318-434B	13 18 15	-43 26 58	17	7.16	FRI**
13	1322-427	13 22 36	-42 44 29	6.8	392	FRI/FRII**
14	1333-337	13 33 47	-33 43 45	32	14.9	FRI/FRII*
15	1452-517	14 52 28	-51 47 39	19	2.87	FRI/FRII*
16	1610-605	16 10 31	-60 30 39	25	6.01	FRI*
17	1610-608	16 10 40	-60 48 28	16	90	HT
18	1749-508	17 49 54	-50 49 03	8	0.39	C
19	1750-508	17 50 45	-50 48 18	8	0.89	C
20	2006-566	20 06 20	-56 35 55	28	1.89	Complex
21	2013-557	20 14 06	-55 48 51	20	2.43	FRI*
22	2026-413	20 26 05	-41 20 53	8	0.45	FRI/FRII*
23	2147-555	21 48 09	-55 34 37	13	2.45	FRI*
24	2331-493	23 31 48	-49 23 03	8	0.43	C
25	2331-492	23 31 58	-49 15 14	8	0.51	C

Table 3: Sources of size  $\geq 8'$  and south of declination for  $-30^\circ$ .

(\* = without core    \*\* = with core    HT = Head-Tail    \*\*C = Compact)

Figures 1, 2 and 3 show  $4' \times 4'$  images of a few extended radio galaxies. These have not yet been deconvolved.

Figure 1 shows the inner lobes of Cen A (MRC1322-427) which is associated with the elliptical galaxy NGC 5128. The size of the inner lobes in our image is around  $10'$ . The diffuse external lobes of Cen A extend up to  $10^\circ$  and are not shown here. It is one of the most widely studied radio galaxy mainly because of its large size and flux density. It is the nearest galaxy having both a very active nucleus and extended radio lobes, thus making possible an exceptionally detailed investigation of its intrinsically faint and small emission feature. Cen A could be a double-double radio galaxy which is classified as edge-darkened complex FRI source with core component (Jones *et al.* 1981).

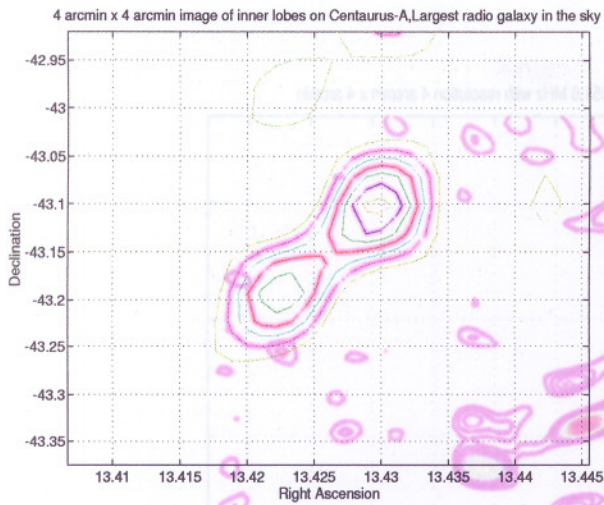


Fig. 1.— 151.6 MHz image of inner lobes on Centaurus-A, MRC1322-427

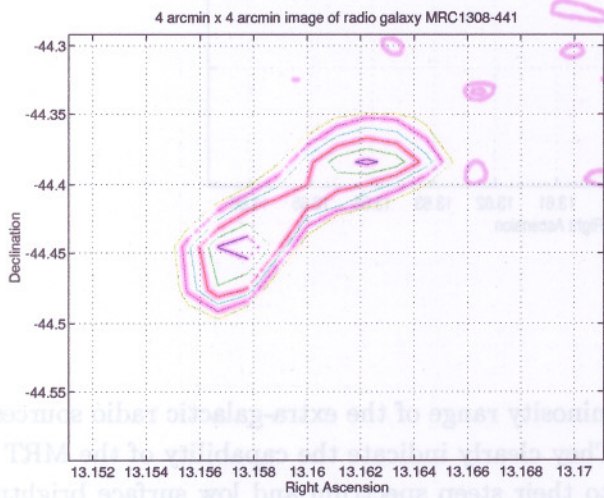


Fig. 2.— 151.6 MHz image of MRC1308-441

Figure 2 shows MRC1308-441 which is a giant complex source which is an asymmetric double with diffuse lobes. It is classified as a FRI/FRII with core (Jones *et al.* 1981).

Figure 3 shows MRC1333-337 which is a complex triple source. This is one of the largest known extragalactic source found in the MRT images (33'). One can easily see the three components of the source in the MRT image. It is classified as FRI/FRII without core (Jones *et al.* 1981).

## 7. Conclusion

We have calculated the limiting values of the surface brightness and the energy density of radio galaxies that can be explored using MRT. The linear size and the redshift of resolved sources and

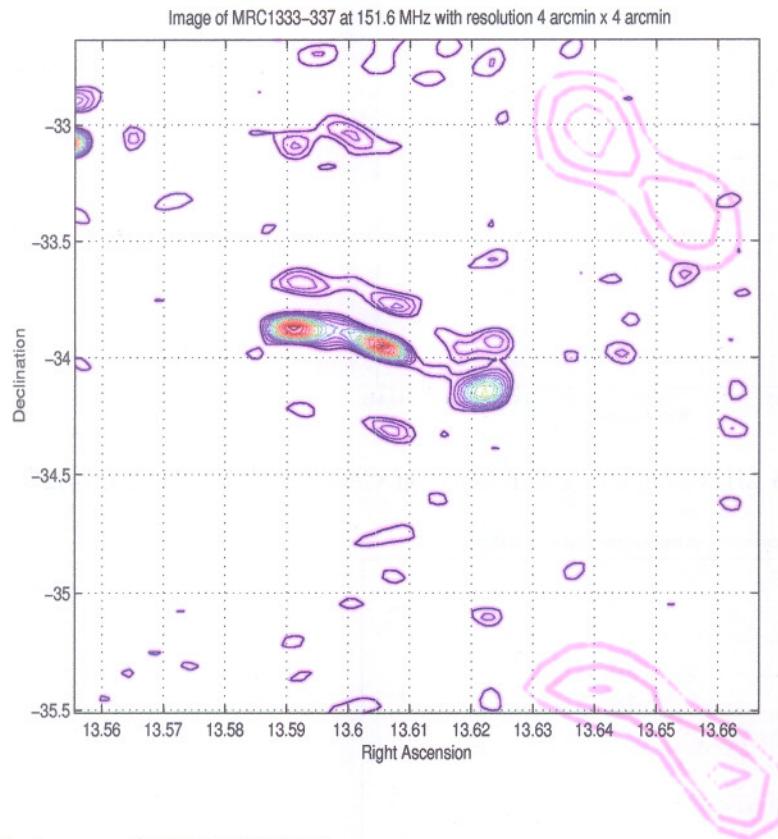


Fig. 3.— 151.6 MHz image of MRC1333-337

the limiting value of the redshift for a given luminosity range of the extra-galactic radio sources in the MRT survey have also been investigated. They clearly indicate the capability of the MRT for detailed investigations of radio galaxies. Due to their steep spectrum and low surface brightness features, giant radio sources, high redshift galaxies and diffused cluster halo sources will dominate the future investigations of EGRS by the MRT. Images of a few extended radio galaxies shown are very encouraging.

### Acknowledgement

MRT is an Indo-Mauritian facility operated by the University of Mauritius (UOM) and the Raman Research Institute (RRI) and the Indian Institute Of Astrophysics (IIA). We would like to thank the University of Mauritius and the Mauritius Research Council for providing the facilities for this work. We would also like to thank Ravi Subrahmanian from the Australia Telescope National Facility (ATNF) who has been very supportive of our efforts. Our thanks also go to our colleagues K Golap, R Dodson and S Sachdev for their support in the image processing work.

## REFERENCES

- Dodson, R.G., "*The Mauritius Radio Telescope And A Study Of Selected Supernova Remnants Associated With Pulsars*". PhD thesis, University of Durham, 1997.
- Fanaroff, B.L., Riley, J.M., 1974 *MNRAS* **167**, 31.
- Golap, K., "*Synthesis Imaging at 151.5 MHz using the Mauritius Radio Telescope*". PhD thesis, University of Mauritius, 1998.
- Golap, K., Udaya Shankar, N., Sachdev, S., Dodson, R., Sastry, Ch. V., 1998, *J. Astrophys. Astr.*, **19**, 35.
- Jones, P.A., McAdam, W.B., *Astrophys. J. Suppl. Ser.* 1981. **80**, 137.
- Large, M. I., Mills, B. Y., Little, A. G., Crawford, D. F., and Sutton, J. M., 1981, *MNRAS*, **194**, 693.
- Miley, G., *Ann. Rev. Astron. Astrophys.*, 1980. **18**, 165.
- Mills, B.Y., *Proc. Astron. Soc. Australia.* 1981. **4**, 156.
- Moffet, A.T., *Strong Nonthermal Radio Emission from Galaxies* , 1975.
- Sachdev, S., "*Wide field Imaging with the Mauritius Radio Telescope*". PhD thesis, University of Mauritius, 1999.
- Sachdev, S., Udaya Shankar, N., 2001. *J. Astrophys. Astr.*, **22**, 229.
- Scott., D., Silk., J., Kolb, E.W., Turner, M.S., *Astrophysical quantities* A.N. Cox publishers, 1974.

